國 立 交 通 大 學

電 子 物 理 學 系

碩 士 論 文

破壞塊材反轉對稱在CdTe/HgTe/CdTe結構的量子自旋霍爾物理的影響

EFFECT OF BREAKING BULK-INVERSION SYMMETRY ON THE QUANTUM SPIN HALL PHYSICS OF CdTe/HgTe/CdTe STRUCTURES

研 究 生：林儀玹

指導教授：朱仲夏 教授

中 華 民 國 一 ○ 二 年 四 月

破壞塊材反轉對稱在CdTe/HgTe/CdTe結構的量子自旋霍爾物理的影響

EFFECT OF BREAKING BULK-INVERSION SYMMETRY ON THE QUANTUM SPIN HALL PHYSICS OF CdTe/HgTe/CdTe STRUCTURES

研 究 生：林儀玹　　　　　Student: Yi-Shiuan Lin

指導教授：朱仲夏 教授　　　Advisor: Prof. Chon-Saar Chu

國 立 交 通 大 學

電 子 物 理 學 系

碩 士 論 文

A Thesis
Submitted to Department of ElectroPhysics
College of Science
National Chiao Tung University
in Partial Fulfillment of the Requirements
for the Degree of
Master
in
ElectroPhysics

April 2013
Hsinchu, Taiwan, Republic of China

中華民國一〇二年四月

破壞塊材反轉對稱在CdTe/HgTe/CdTe結構的量子自旋霍爾物理的影響

研 究 生 ： 林儀玹　　　　　　　　指 導 教 授 ： 朱仲夏　教授

國立交通大學

電子物理研究所

摘要

在本篇論文中，我們探討Dresselhaus自旋軌道作用對CdTe/HgTe/CdTe量子井的拓樸物理之影響，此Dresselhaus自旋軌道作用來自於塊材反轉不對稱。我們也研究以此量子井結構所建構的量子通道的拓樸物理現象。我們研究的出發點為三維的Kane模型，在加上Dresselhaus自旋軌道作用後推導出二維(量子井)及一維(量子通道)的等效哈密頓算符。我們發現系統的拓樸現象並未因Dresselhaus自旋軌道作用的引進而消失，但卻對邊緣態的特性有微妙的影響。具體的影響表現在邊緣態在量子通道中行進的同時發生邊緣態橫向來回移動的現象，是為邊緣切換的現象。此外，在引進位能障後，量子通道的傳輸能譜有Fano共振的結構，且發現可用位能障的高低來調控此結構，Fano結構的出現的同時也驅使邊緣態在穿越位能障的同時完成邊緣切換。本研究詳細分析上述所提之Fano共振的相關物理機制，並獲得一致的結論。

Effect of breaking bulk-Inversion symmetry on the quantum spin Hall physics of CdTe/HgTe/CdTe structures

Student: Yi-Shiuan Lin   Advisor: Prof. Chon-Saar Chu

Department of Electrophysics

National Chiao-Tung University

Abstract

In this thesis, we consider the effects of the Dresselhaus spin orbital interaction (DSOI), a form of breaking inversion symmetry, on the topological physics of a well known topological structure, namely, the CdTe/HgTe/CdTe quantum well. Related system such as a quantum channel formed out of the above quantum well is also considered. Instead of using model 2D Hamiltonian, and quasi-1D Hamiltonian, for the quantum well and quantum channel, respectively, we have calculated these Hamiltonians from the 3D Kane model. This includes our introduction of the DSOI at the 3D Kane model. Our finding is that the DSOI does not destroy the topological physics (the edge states) but has caused intricate effect on the edge states. This is most evident in the case of a quantum channel, when the edge state, under the effect of the DSOI, is caused to exhibit an edge-switching behavior. Furthermore, in the presence of a potential barrier, the transmission exhibits Fano-type characteristics that can be fine-tuned by the barrier height. There is also a feature of forcing the edge-switching to occur in the immediate vicinity of the transmission region. A detail Fano-type process analysis has been performed to confirm the above finding.

誌謝

感謝朱老師的指引，讓我的兩年多來的研究可以順利完成，也從研究中學習到很多。 感謝 Roland Winkler教授幫忙確認二維能帶結構的計算結果，以及研究上的指導。 並感謝吳玉書教授、林志忠教授和陳永富教授抽空為學生口試以及指導。 感謝呂智國教授、王律堯學長、張力學長、邱志宣學長和張榮興學長給我許多研究上的意見和課業上的幫助。 感謝其他學長江吉偉、劉悌鐳、蘇韋綾、陳文長，同學余韋均、張永業、魏銘佐，以及學弟徐豪、吳雨柔、曾哲銘給我愉快的研究生時光。 最後感謝我父母的提支持，讓我能完成研究生學位。

Contents

List of Figures

Chapter 1

Introduction

The quantum spin Hall effect (QSHE) has been theoretically predicted and experimentally observed in a HgCdTe/HgTe/HgCdTe quantum well system.[1-2] The band structure of the HgCdTe is normal and the band structure of the HgTe is inverted. Changing the width d of the HgTe layer will change the two dimension (2D) electronic structure of the quantum well between normal and inverted region. Specifically, the eigenenergy of the conduction and heavy hole bands at the Γ points exhibit an energy crossing at a critical well width d_c ($d_c = 6.3nm$[1]). The 2D band structure is topologically non-trivial in the $d > d_c$ region.

In the topologically non-trivial region, the system supports edge states which is helical, namely, the spin polarization is connected with its propagation direction. Furthermore, time reversal symmetry requires that edge states at the same sample edge exist in a pair: consisting of opposite propagation directions. This is the so called quantum spin Hall effect. These edge states are robust against weak non-magnetic impurities or potential profile.[3] As such, the edge states are expected to have high (almost perfect) transmission through a potential barrier. Even though the gapless spectra of the edge states, in a quantum channel, could open up a gap due to edge state wave function overlapping[4], the back scattering of the edge states remain small as long as the energy of interest is far away from the small energy gap. Here the quantum channel is formed out of the quantum well. Recently, transport characteristics through such a quantum channel in the presence of a potential barrier was studied.[5] They speculate that that transport dip structures are orginated from Fano-type resonance. No analysis has been performed to support this

speculation.

On the other hand, the fact that bulk inversion asymmetry (BIA) exists, where the Dresselhaus spin orbital interaction (DSOI) comes into play, has not been seriously considered.[6] An earlier study along this line claimed that BIA effects has no significant bearing on the electronic property of the system.[7] However, the DSOI term do cause mixing in the conduction and heavy hole bands, removing the energy crossing at the Γ point.[8] Would this level anti-crossing destroy the QSHE completely? Or, if the QSHE is to survive, how would the electronic states adjust to maintain the topological nature of the system? We feel that this issue has far from being fully explored.

Still there are a number of recent works that have included DSOI into their effective 2D Hamiltonian for the exploration of the quantum transport of the system.[9-11] Disorder in a quantum channel is found to back scatter the edge states if the impurity is strong enough and the channel is narrow enough, or if bulk states exist at the Fermi energy.[9] Furthermore, back scattering of the edge states can occur in a quantum channel that has abrupt change in the channel width even though there is no impurity.[10] On the other hand, the DSOI is found to provide a scheme monitoring the transmission or reflection of an incoming edge state by the monitering og the Fermi energy.[11] This is due to the interplay of the DSOI and the finite channel width effect, causing the spin of the edge state to precess and the simultaneous switching of its location from one sample edge to the other. This work has not included bulk states of the channel into their consideration. A major focus of our work is to study inticate processes made possible by the presence of both bulk and edge states in a quantum channel.

In this thesis, we perform a careful and detail calculation, both numerically and semi-analytically, on the effects of the DSOI on the effective 2D Hamiltonian in a CdTe/HgTe/CdTe quantum well system, the electronic states in the corresponding semi-infinite system or quantum channel, and the transport characteristic through a potential barrier in the quantum channel. Furthermore, we have discussed in depth on the topological nature (in terms of topological number) of the edge states; and we have explicitly demonstrated the Fano-type mechanism that leads to the transport spectra in the transmission. Our finding is that the DSOI provides us a handle to tune the Fano-spectra. We also demonstrate that by fine tuning the potential barrier in the vicinity of a Fano-spectra, we can switch

the transmitted edge state from one edge to the other of the quantum channel. This scheme of invoking the Fano-physics is more sensitive and less restrictive upon the structure requirement than that proposed in ref[11]. This noval feature could find application in furture spintronic devices.

This thesis contains 7 chapters, including this Introduction chapter. In chapter 2, we show our result of the the effective 2D Hamiltonian for the quantum well with DSOI which we have derived from a 3D Kane model. The detail of the derivation is presented in Appendix A. In chapter 3, we solve for the edge states in the semi-infinite 2D system is formed out by the quantum well. Our methods of approach include both semi-analytical and numerical methods. In chapter 4, we explore the topological origin of the edge state in sight of topological quantities such as Chern number, winding number and the spin Chern number. In chapter 5, we derive Hamiltonian for a quantum channel that is formed out of the quantem well system. The electronic states for the quantum channel is obtained and discussed. In chapter 6, we consider the transport through the quantum channel that consists of the a potnetial barrier. Both full numerical and semi-analytical approaches are used to obtain and to analyze the transprot characteristics. Dip structures in the transmission are found and are shown to originate from Fano physics. This Fano-type process is made possible by the coexistance of edge state and bulk like resonance state in the barrier region. Finally, we present a summery of our work (a majonity of it is in chapters 5 and 6), and a suggestion to possible future work.

Chapter 2

From basic band formulation to effective 2D Hamiltonian

In this chapter, we show the effective 2D Hamiltonian of the CdTe/HgTe/CdTe quantum well system with DSOI. And, we also show how DSOI removes the energy-crossing of the conduction and beavy hole bands in the quantum well.

The lattice structures of HgTe and CdTe are zinc blende structure so they do not have center of inversion.[6] It makes those materials be BIA. This symmetry broken makes a spin orbital interaction well known as DSOI. Kane Hamiltonian describes the 3D bulk electronic structure of the HgTe and CdTe (with DSOI) so we use it to start our analysis on the quantum well. How the DSOI comes in the 3D Kane Hamiltonian and the detail derivation of the effective 2D Hamiltonian are presented in Appendix A.

In the resent study[1], the non-trivial edge bands is observed in the energy gap between the conduction and heavy hole bands of the quantum well. We do the derivation presented in Appendix A to obtain the effective 2D 4×4 Hamiltonian which describes the bands structure at the energy range of the conduction and heavy hole bands. In the set of basis $(|E1, +\rangle, |H1, +\rangle, |E1, -\rangle, |H1, -\rangle)$, the effective Hamiltonian H_{eff} is of the form:

$$H_{eff} = Dk^2 + \begin{pmatrix} -M + Bk^2 & Ak_+ & 0 & \delta \\ Ak_- & M - Bk^2 & \delta & 0 \\ 0 & \delta & -M + Bk^2 & Ak_- \\ \delta & 0 & Ak_+ & M - Bk^2 \end{pmatrix}. \tag{2.1}$$

Table 2.1: The band structure parameter of H_{eff}

	$M(meV)$	$B(meV/nm^2)$	$D(meV/nm^2)$	$A(meV/nm)$	$\delta(meV)$
ours	4.83	753	578	376	1.68
S.C. Zhang[1]	6.86	169	5.14	346	
Markus König[7]	10	686	512	364	1.6

[a] This band parameter is for $d = 7nm$.
[b] In ref[1], they didn't include the DSOI so there are no δ terms.

The value of the band parameters in H_{eff} is showed at Table 2.1. The from of the effective Hamiltonian is as the same as the other's result.[7] (By applying an unitary transformation, we can obtain the same effective Hamiltonian as their result.) Our value of parameters A, B, D and δ are similar to theirs result. Only the value of M is much different. The difference is because they replace the CdTe layers by the HgCdTe layers. The band parameters of the bulk material aren't equal so that we have a different set of band parameters. The topological properties of the two set of band parameters are the same. We will show it in chpater 3.

The DSOI only adds the δ terms into the effective Hamiltonian. The other terms are independent of the DSOI. The δ terms are constant and couple the conduction ($E1$) and the heavy hole ($H1$) band. The value of δ isn't zero in this system so the crossing of eigenenergy at the Γ point is removed. The energy spectrum becomes anti-crossing.

Chapter 3

Edge-state at an open boundary

In this chapter, we calculate the energy dispersion of edge bands in the corresponded semi-infinite system showed in Fig.3.1. The condition of the edge state existence both with DSOI and without DSOI is derived. We also discuss the transmission property of the edge states with DSOI.

The gapless edge state exists in the system described by H_{eff} (equation (2.1)) with $\Delta = MB - (B\delta/A)^2 > 0$ and $|B| > |D|$. (In the system without DSOI, the condition is $\Delta = MB > 0$, $A \neq 0$ and $|B| > |D|$.) The gapless property of the edge states is due to time reversal symmetry. For semi-infinity boundary, there are only two edge bands in the system whether we include DSOI or not. Time reversal symmetry makes system have a two level degeneracy at Γ point. This energy degeneracy makes the edge bands be crossing. Therefore, the edge bands are gapless and the system is topologically non-trivial if $\Delta > 0$. On the other hand, the DSOI only makes some systems that are topologically non-tirival without DSOI become topologically trivial. The DSOI does effect the topological phase of the 2D electronic system.

In the end of this chapter, we derive the form of effective 1D Hamiltonian consists of edge branches by time reversal symmetry and the form of the edge states. The edge band gap is zero and the pseudo-spin is only dependent on the k linear terms. Those properties are due to time reversal symmetry. The form of edge states make the k^2 terms be zero so the edge band aren't scattered by non-magnetic potential or impurities. Only magnetic impurities or field scatter the edge bands so DSOI doesn't weak the edge bands.
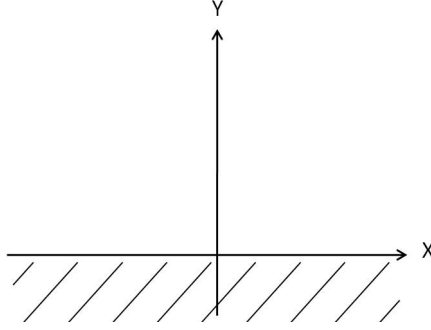
Figure 3.1: It shows the structure of a open boundary system. The wave function is zero when $y \leq 0$ and $y = \infty$.

3.1   Edge-state branch

In this section, we analytically solve the edge branches without DSOI for semi-infinity boundary. (Here we assume we can tune all parameter in H_{eff} so that we can see what is condition that edge state exists.) We consider the effective Hamiltonian H_{eff} with $\delta = 0$ (equation (2.1)),

$$H_{eff} = \begin{pmatrix} h_+ & 0 \\ 0 & h_- \end{pmatrix}. \tag{3.1}$$

$$h_\tau = \begin{pmatrix} -M + D_+ k^2 & Ak_\tau \\ Ak_{-\tau} & M + D_- k^2 \end{pmatrix}.$$

Where $D_\pm = D \pm B$. The spin up part is decoupled to the spin down part. We can divide H_{eff} into two 2×2 Hamiltonian h_+ and h_-.

The open boundary is along x-direction so the k_x is the quantum number of the wave function. The wave function is of the form:

$$\Psi(x, y) = e^{ik_x x} \sum_j C_j e^{ik_{y,j} y} \xi_j. \tag{3.2}$$

Where ξ is the pesudo-spin of Ψ. To form an edge state, we need at least two different decay k_ys. When A is zero, the $E1$ and $H1$ subband are decoupled. We can't find two of k_y for each band so the value of A must be non-zero.

We assume that Ψ is edge state like form which consists of two of k_y. For given k_x

7

and energy E, k_y^2 is of the form:

$$k_{y,\nu}^2 = \frac{\alpha + \nu\beta}{D_+D_-} - k_x^2. \tag{3.3}$$

Where $\alpha = ED + \frac{A^2}{2} - MB$, $\beta = \sqrt{\alpha^2 - D_+D_-E_+E_-}$ and $E_\pm = E \pm M$. According to the form of h_τ, there are only four k_ys. Two k_ys are minus times of the others. To form an edge state, we need two different k_ys whose decay directions are the same. So only when all k_ys are complex, the edge state exists in this system.

Form the Schrödinger eqaution, we have two ways to define the pesudo-spin ξ corresponding to $k_{y,\nu}$.

$$\xi_\nu^\dagger = N_\nu \left(\begin{array}{cc} E_- - \frac{\alpha + \nu\beta}{D_+} & A\left[k_x + \tau i k_{y,\nu}^*\right] \end{array} \right). \tag{3.4}$$

$$(\xi_\nu')^\dagger = N_\nu' \left(\begin{array}{cc} A\left[k_x - \tau i k_{y,\nu}^*\right] & E_+ - \frac{\alpha + \nu\beta}{D_-} \end{array} \right). \tag{3.5}$$

At the edge, $y = 0$, the wave function msut be zero. It means that the pseudo-spins of two k_ys must be parallel. From the definition of k_y^2, $\xi_+ = \xi_-'$ and $\xi_- = \xi_+'$, we obtain

$$k_{y,+} + k_{y,-} = \frac{2\beta}{D_+D_-}\frac{1}{k_{y,+} - k_{y,-}} = -i\frac{\tau A^2 k_x}{EB - MD}. \tag{3.6}$$

From the equation (3.6) and $\xi_-' = \xi_+'$, we have

$$\frac{\beta}{D_-}\left(2BE - 2DM + A^2\right)\left(\frac{k_x}{EB - MD} + \frac{EB - MD}{A^2D_+D_-k_x}\right) = 0. \tag{3.7}$$

If β is zero, there are only two kinds of k_y, so β must be non-zero. For $2BE - 2DM + A^2 = 0$, its energy dispersion is not gapless. Here we focus upon the gapless edge bands so we drop this solution.

We obtain the form of the energy dispersion:

$$E = M\frac{D}{B} + \rho\frac{1}{B}\sqrt{A^2\left(B^2 - D^2\right)}k_x. \tag{3.8}$$

Where $\rho = \pm 1$. The k_x, A, B, D and M, are real and k_y must be well defined (equation (3.3)). Therefore, the edge state exists if the amplitude of B is larger than D. If $|B| \leq |D|$,
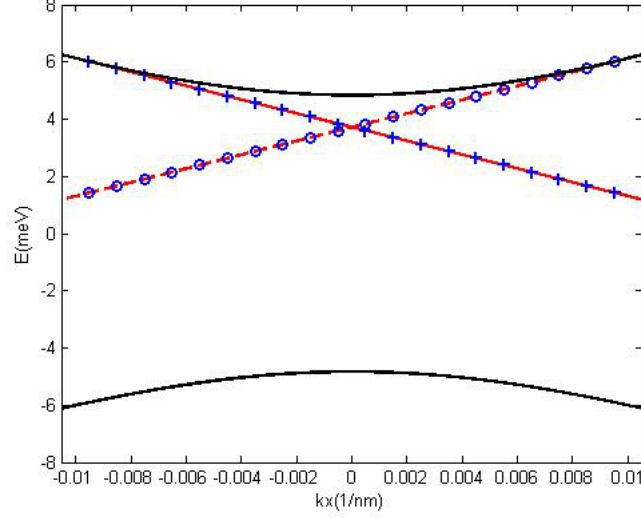
Figure 3.2: It shows the eigenenergy of edge state for H_{eff} with $d = 7nm$. The black line is the bulk band. The red solid line is spin-up edge band and the red dash line is spin-down edge band. The blue circle is numerical result for spin-up edge band and blue plus sign is numerical result for spin-down edge band.

the global energy band gap will be closed. There are at least two of pure real k_y for given energy and k_x, so no eigenstate has two different decay k_ys. But two decay k_ys is the condition for existence of edge states. So, only if $|B| > |D|$, the edge states may exist.

From equations (3.6), (3.8) and definition of α and β, we find out that k_y is of the form:

$$k_{y,\nu} = -i\tau\rho\frac{A^2 + 2\nu\beta}{2\sqrt{A^2\left(B^2 - D^2\right)}}. \tag{3.9}$$

Let $\Lambda = \tau\rho\frac{A^2}{2\sqrt{A^2(B^2-D^2)}}$ and $\lambda = \tau\rho\frac{\beta}{\sqrt{A^2(B^2-D^2)}}$. The wave function is of the form:

$$\Psi\left(x, y\right) = N\left(k_x\right)e^{ik_x x}e^{\Lambda y}\left(e^{\lambda y} - e^{-\lambda y}\right)\xi. \tag{3.10}$$

$$\xi^\dagger = \frac{1}{\sqrt{2B}}\left(\begin{array}{cc} \sqrt{B - D} & -\tau\mathrm{sgn}\left(A\right)\sqrt{B + D} \end{array}\right). \tag{3.11}$$

The $e^{\lambda y} - e^{-\lambda y}$ part can be sin or sinh function so this part doesn't make the wave function decay. Only the $e^{\Lambda y}$ part makes the wave function be an edge state. The wave function Ψ must be zero at $y = \infty$ so ρ must be $-\tau$. (For $\Psi\left(y = -\infty\right) = 0$, $\rho = \tau$.)

Λ is always real if $|B| > |D|$. λ may be pure imaginary or pure imaginary. If λ is real, the amplitude of λ and Λ will determine the existence of edge states. Only when

$\lambda^2 < \Lambda^2$, the wave function will be 0 at $y = \infty$. (If λ is imaginary, λ^2 is also smaller than Λ^2.) Form the definition of Λ and λ, we have

$$\Lambda^2 - \lambda^2 < \frac{M}{B}. \tag{3.12}$$

If $MB < 0$, there is no edge state solution. So far, we only assume that the value of A is non-zero. It is the difference between ref[4] and our result. Our result shows that if $A \neq 0$, $MB > 0$ and $|B| > |D|$, the edge state exists for this Hamiltonian. (Our result is similar to ref[14].)

For H_{eff} with $d = 7nm$, we have $MB > 0$ so we can find gapless edge bands. In Fig. 3.2, we show the analytical and numerical result of the edge branches. Because the two results are the same, our analtyical result works.

3.2   Edge-state branch in the presence of DSOI

In this section, we numerically calculate the energy dispersion of edge state with DSOI. And we also prove the edge bands are gapless.

We consider the effective Hamiltonian H_{eff} (equation (2.1)),

$$H_{eff} = Dk_x^2 + \begin{pmatrix} h_+ & \delta\sigma_x \\ \delta\sigma_x & h_- \end{pmatrix}. \tag{3.13}$$

$$h_\tau = \begin{pmatrix} -M + Bk^2 & Ak_\tau \\ Ak_{-\tau} & M - Bk^2 \end{pmatrix}.$$

Because the root of k_y is difficult to analytically solve, we numerically solve eigenenergy of edge bands. The open boundary is along x-direction so k_x is the quantum number of the wave function. The wave function is of the form:

$$\tilde{\Psi}(x, y) = e^{ik_x x} \sum_j \tilde{C}_j e^{ik_{y,j}y} \tilde{\xi}_j. \tag{3.14}$$

Where $\tilde{\xi}$ is a 4×1 column vector.

The Schrödinger equation is

$$H_{eff}(k_x, k_{y,j})e^{ik_x x + ik_{y,j}y}\tilde{\xi}_j = \tilde{E}e^{ik_x x + ik_{y,j}y}\tilde{\xi}_j. \tag{3.15}$$

Where $\tilde{E}$ is the eigenenergy. To compute the k_y for given E and k_x, we define H'_0, H'_1 and H'_2 as the following forms.

$$H'_0 = \begin{pmatrix} N(k_x) & \delta\sigma_x \\ \delta\sigma_x & N(k_x) \end{pmatrix}.H'_1 = \begin{pmatrix} -A\sigma_y & 0 \\ 0 & A\sigma_y \end{pmatrix}.H'_2 = \begin{pmatrix} D+B\sigma_z & 0 \\ 0 & D+B\sigma_z \end{pmatrix}.$$

Where $N(k_x) = -\tilde{E} - M\sigma_z + A\sigma_x k_x + (D+B\sigma_z)k_x^2$ and σ_i is Pauli matrix. We rewrite the Schrödinger equation in this form:

$$H'_0\tilde{\xi} + H'_1(k_y\tilde{\xi}) = -k_y H'_2(k_y\tilde{\xi}). \tag{3.16}$$

Combining equation (3.16) and $(k_y\tilde{\xi}) = k_y(\tilde{\xi})$, we have

$$\begin{pmatrix} 1 & 0 \\ 0 & -H'_2 \end{pmatrix}^{-1} \begin{pmatrix} 0 & 1 \\ H'_0 & H'_1 \end{pmatrix} \xi' = k_y\xi'. \tag{3.17}$$

Where $\tilde{\xi}'^{\dagger} = \begin{pmatrix} \tilde{\xi}^{\dagger} & k_y^*\tilde{\xi}^{\dagger} \end{pmatrix}$. In this form, we can get the value of k_y and the corresponded eigenvector by the numerical diagonalization.

Because $\tilde{\xi}$ is a 4×1 column vector, we need at least four decay k_ys to match the boundary condition at the edge. However there are only 8 k_ys for given k_x and E. (See equation (3.17).) The edge state only exists at the energy range that all k_ys are complex. We can only seek the edge states at the energy range where no bulk state with given k_x.

At energy range where all k_ys are complex, we can find a wave function $\tilde{\Psi}$ that consists of four complex k_ys and satisfies $\tilde{\Psi}(y=\infty) = 0$. At $y=0$, we derive an equation that determines the eigenenergy of the edge states:

$$\sum_j \tilde{C}_j\tilde{\xi}_j = 0. \tag{3.18}$$

The eigenenergy is showed at Fig. 3.3.
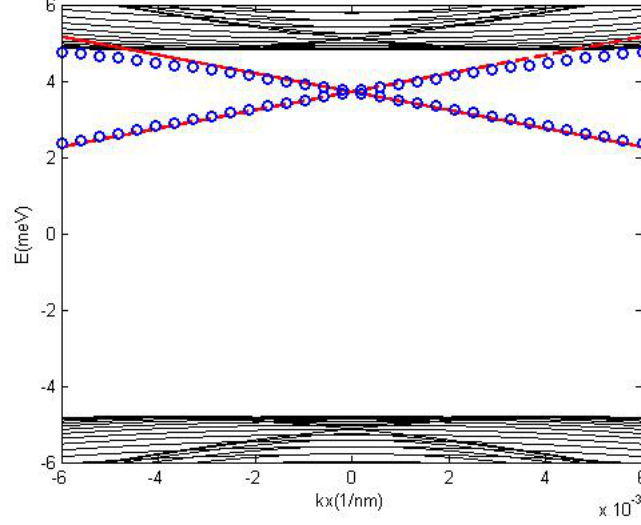
Figure 3.3: It shows the eigenenergy of edge state for H_{eff} with $d = 7nm$. The black line is the bulk bands with DSOI. The red lines are edge bands without DSOI. The blue circle is numerical result for edge band with DSOI.

From the numerical result, we find out that there only two edge bands in the system. The edge bands touch the conduction and heavy hole bulk bands. If the edge band gap is zero, the edge bands are still gapless with DSOI.

Let Ψ' be one of the edge states with $k_x = 0$. The time reversed state $\Theta\Psi'$ is also an edge state with $k_x = 0$. The Ψ' and $\Theta\Psi'$ are different states. (The form of time reversal operator is listed in Appendix D.)

$$\langle \Psi' | \Theta\Psi' \rangle = \int \left[\begin{array}{c} -\Psi'_1(x,y)^*\Psi'_3(x,y)^* + \Psi'_2(x,y)^*\Psi'_4(x,y)^* \\ +\Psi'_1(x,y)^*\Psi'_3(x,y)^* - \Psi'_2(x,y)^*\Psi'_4(x,y)^* \end{array} \right] dxdy = 0. \qquad (3.19)$$

The Hamiltonian is time reversal invariant so both Ψ' and $\Theta\Psi'$ are the eigenstates of the system. At Γ point, there is a two level degeneracy protected by time reversal symmetry. In the global bulk energy gap, we only find two edge bands so those edge bands are gapless.

3.3 Analytic analysis for k=0 edge state

In this section, we first try to obtain the condition that edge bands exist for the effective Hamiltonian with DSOI. In the end of this section, we discuss the transport property of the edge bands with DSOI.

The effective 4×4 Hamiltonian H_{eff} with $k_x = 0$ is of this form(equation (2.1)):

$$H_{eff}(0, k_y) = \begin{pmatrix} h_+(k_y) & \delta\sigma_x \\ \delta\sigma_x & h_-(k_y) \end{pmatrix}. \tag{3.20}$$

$$h_\tau(k_y) = Dk_y^2 + \begin{pmatrix} -M + Bk_y^2 & i\tau Ak_y \\ -i\tau Ak_y & M - Bk_y^2 \end{pmatrix}.$$

The eigenenergy of edge state is at the energy range where all k_y is complex. Only when $|B| > |D|$, all the k_ys are complex at the energy band gap. For case $A = 0$, we can divide the H_{eff} into two 2×2 Hamiltonian. For each 2×2 Hamiltonian, we can find four complex k_ys and two of different k_ys have the same decay direction. However, the pseudo-spins of those two k_ys aren't the same. The wave function can't be zero at $y = 0$ so there is no edge state solution. Therefore, A must be non-zero and $|B| > |D|$.

We define a new set of basis $((|E, +\rangle - i|E, -\rangle)/\sqrt{2}, (|H1, +\rangle + i|H1, -\rangle)/\sqrt{2}, (|E, +\rangle - i|E, -\rangle)/\sqrt{2}, (|H1, +\rangle + i|H1, -\rangle)/\sqrt{2})$. In this representation, the effective 4×4 Hamiltonian will becomes block diagonal form.

$$\tilde{H}_{eff}(0, k_y) = \begin{pmatrix} \tilde{h}_+(k_y) & 0 \\ 0 & \tilde{h}_-(k_y) \end{pmatrix}. \tag{3.21}$$

$$\tilde{h}_\mu(k_y) = Dk_y^2 + \begin{pmatrix} -M + Bk_y^2 & i(Ak_y + \mu\delta) \\ -i(Ak_y + \mu\delta) & M - Bk_y^2 \end{pmatrix}.$$

In this representation, there are some k_x dependent terms at the off-block diagonal part. The $\tilde{H}_{eff}$ is block diagonal form only if $k_x = 0$. The following analysis only works with $k_x = 0$.

From numerical result, we obtain the eigenenergy and the form of the edge states:

$$\tilde{E} = M\frac{D}{B}. \tag{3.22a}$$

$$\tilde{\Psi}_\mu = \tilde{N}_\mu \left(e^{i\tilde{k}^\mu_{y,1}y} + e^{i\tilde{k}^\mu_{y,2}y} \right) \tilde{\xi}. \tag{3.22b}$$

$$\tilde{\xi}^\dagger = \frac{1}{\sqrt{2B}} \left(\ \sqrt{B-D} \ \ -sgn\left(A\right)\sqrt{B+D} \ \right). \tag{3.22c}$$

Here we have found a pair of k_y and a pair of corresponded pseudo-spins that are parallel to each other. The wave function, $\tilde{\Psi}_\mu$, are zero at $y = 0$. Next step, we try to find the condition that both k_ys decay at the same direction, y-direction. (The set of equation (3.22) also works when the edge states aren't the real state of the system.)

Taking equation (3.22a), (3.22b) and (3.22c) into equation (3.21), we have

$$\sqrt{B^2 - D^2} \left(M - B\left[k^\mu_y\right]^2 \right) = -isgn\left(A\right)B\left(Ak^\mu_y - \mu\delta\right). \tag{3.23}$$

From equation (3.23), k_y is of the form

$$k^{\nu s}_y = i\left|\frac{A}{2b}\right| + s\sqrt{\frac{\Delta}{B^2} + \left(\nu\frac{\delta}{A} + i\left|\frac{A}{2b}\right|\right)^2}. \tag{3.24}$$

Where $b = \sqrt{B^2 - D^2}$ and $\nu = \mu sgn\left(A\right)$. The edge state doesn't exist when one of k_y is real or the imaginary parts of k_ys aren't both positive. For the form of k_y, one of k_y will be real only if $\Delta = 0$. The region at where the k_y is real is the boundary between the regions at where k_ys have opposite sign of imaginary part. There is no other condition makes the imaginary part of k_y change sign. (If the imaginary part of wave vector can't be zero, the sign of the imaginary part is unchanged for whole parameter space.) Let $|\Delta| << 1$ and $s = -1$, we have

$$k^\mu_y \approx i\left|\frac{A}{2b}\right|\frac{\Delta}{2B^2\kappa^2} - \mu\frac{\delta}{|A|}\left[1 - \frac{\Delta}{2B^2\kappa^2}\right]. \tag{3.25}$$

Where $\kappa = \sqrt{\frac{\delta^2}{A^2} + \left|\frac{A}{2b}\right|^2}$. We obtain that the edge state exist when $\Delta > 0$.

According to the form of Δ, the DSOI only makes some systems that are topologically non-tirival without DSOI become topologically trivial. (It doesn't change the topological

phase of the topological trivial region.) There is still a clear boundary between topologically trivial and non-trivial in the topological phase diagram. The DSOI just shifts the boundary of the topological phase.

Finally, we want to discuss the transmission property of edge bands in the semi-infinite system. We compose an effective 1D Hamiltonian H^{edge} consisting of the edge bands.

$$H^{edge} = \sum_{i=0}^{2} \sum_{j=0}^{3} h_i n_j^i \sigma_j k_x^i. \tag{3.26}$$

Where h_i and n_j are parameter and σ_0 is 2×2 identity matrix. We set the basis vector as the edge states with $k_x = 0$. The edge subbands are time reversal pair so the time reversal operator is of the form:$\Theta = i\sigma_y K$. The time reversal property of k vector operator is $\Theta k_x^i = (-1)^i k_x^i \Theta$. The 1D Hamiltonian H^{edge} is time reversal invariant so we have $[H^{edge}, \Theta] = 0$. Therefore, time reversal symmetry leads the following condition.

$$\Theta h_i n_j^i \sigma_j = (-1)^i h_i n_j^i \sigma_j \Theta. \tag{3.27}$$

By the symmetry argument, we derive the general form of H^{edge}.

$$H^{edge} = h_0 + \left(\sum_{j=1}^{3} n_j \sigma_j \right) h_1 k_x + h_2 k_x^2. \tag{3.28}$$

The direction of pseudo-spin is independent of k_x. The back scattering induced by pseudo-spin changing is suppressed. Though the pseudo-spin doesn't change, the propagation direction may change by k_x. However, the form of the basis vector makes h_2 zero whether we include DSOI or not. The scattering process with edge band only is weak. The edge state is robust against a normal impurity and a small potential. (In contrast, we doesn't imply that edge state is robust to large potential. A large potential that makes bulk bands and edge bands coupled may scatter the edge state.)

Chapter 4

Topological origin of the edge states

In this chapter, we try to obtain the topological number by chern number, winding number and spin chern number method. The chen number in this chapter is the Berry's phase of a energy band.

In chern number consideration, we can't tell the topological phase changing. The chern number is always zero for the eigenvectors of the effective Hamiltonian with DSOI. The form of the eigenvectors makes this result so the chern number of the eigenvector we maintained above is zero even if $\delta = 0$. On the other hand, we can obtain the non-trivial topological number by another kind of eigenvectors for the effective Hamiltonian without DSOI. The two kinds of eigenfunction both characterize the system, effective Hamiltonian with $\delta = 0$. The chern number of the different kinds of eigenvectors aren't the same so the chern number isn't invariant under guage transformation.

In winding number consideration, we can obtain the condition of the topological phase changing that we obtained in chapter 3. But it only works for 2×2 Hamiltonian and we must drop the small wave vector region of the 2D k space to obtain this result.

In spin chern number consideration, we can obtain the topological non-trivial condition which we obtained at chapter 3. However, the phase diagram is dependent on the generator that generates the eigenvectors to calculate the spin chern number. It means that we need a proper way to obtain the generator.

4.1 Chern number consideration

The definition of Berry's curvature is of the form[18]:

$$\vec{B}_j\left(\vec{R}\right) = \nabla_{\vec{R}} \times \left\langle j\left(\vec{R}\right) \middle| \nabla_{\vec{R}} \middle| j\left(\vec{R}\right) \right\rangle = \left\langle \nabla_{\vec{R}} j\left(\vec{R}\right) \middle| \times \middle| \nabla_{\vec{R}} j\left(\vec{R}\right) \right\rangle. \tag{4.1}$$

This is the Berry's curvature of state j represented by vector of parameters $\vec{R}$. Substituting k vector and eigenvectors of the system with DSOI for $\vec{R}$ and state j, we obtain the Berry's curvature of the system with DSOI. The chern number is equal to integrate the Berry's curvature for whole k space.

The effective 4×4 Hamiltonian H_{eff} (equation (2.1)) is

$$H_{eff} = Dk_x^2 + \begin{pmatrix} h_+ & \delta\sigma_x \\ \delta\sigma_x & h_- \end{pmatrix}. \tag{4.2}$$

$$h_\tau = \begin{pmatrix} -M + Bk^2 & Ak_\tau \\ Ak_{-\tau} & M - Bk^2 \end{pmatrix}.$$

The eigenenergy $E_{\rho\mu}$ and eigenvector of H_{eff} are (See Appendix E.)

$$E_{\rho\mu} = Dk^2 + \rho\sqrt{\left(M - Bk^2\right)^2 + \left(Ak + \mu\delta\right)^2}, \tag{4.3}$$

$$\varphi_{\rho\mu}^\dagger = \frac{1}{\sqrt{2}} \begin{pmatrix} \alpha_1^{\rho\mu}(k)\,e^{-i\phi} & \alpha_2^{\rho\mu}(k) & \mu\alpha_1^{\rho\mu}(k) & \mu\alpha_2^{\rho\mu}(k)\,e^{-i\phi} \end{pmatrix}, \tag{4.4}$$

where $\alpha_1^{\rho\mu}(k) = N_{\rho\mu}(Ak + \mu\delta)$, $\alpha_2^{\rho\mu}(k) = N_{\rho\mu}(k)\left(E_{\rho\mu} - Dk^2 + M - Bk^2\right)$ and $N_{\rho\mu}(k) = \left[(\alpha_1^{\rho\mu})^2 + (\alpha_1^{\rho\mu})^2\right]^{-1/2}$.

The Berry's curvature of the $\varphi_{\rho\mu}$ is always zero even if $\delta = 0$. It is because the spin up and spin down parts of the eigenvector are equal weighting. The Berry's curvatures from the spin up and spin down parts for a given k are totally canceled.

Actually, the Berry's curvature is only zero for non-zero k and diverges at Γ point. It is because there is a two level degeneracy protected by time reversal symmetry. From an another formula of Berry's curvature, this degeneracy makes the Berry's curvature diverge at Γ point.

$$\vec{B}_m = \mathrm{Im}\left[\sum_{n\neq m} \frac{\langle m|\,\nabla H\,|n\rangle \times \langle n|\,\nabla H\,|m\rangle}{\left(E_m - E_n\right)^2}\right]. \tag{4.5}$$

Where E_i is the eigenenergy of the wave function.

Obtaining the chern number in this case is similar to calculate the total electric flux on a plane from an electric charge that is on that plane. The electric flux is zero except of the location of the charge and is undefined at the location of the charge. If we want to calculate the flux from the charge, we need to shift that charge slightly out of the plane. It is similar to add some terms that remove the time reversal protected degeneracy at Γ point in this case.

We have tried to compute the chern number by adding some term breaking time reversal symmetry. Taking those terms very small, we can obtain the chern number that decribes the original system. However, the chern number is only dependent on the terms we adding. We can't calculate the chern number in this way so we can't tell the topological phase change by the chern number consideration.

On the other hand, we have two set of eigenvectors which are the eigenatates of the effective Hamiltonian without DSOI. We have another set of the eigenvectors $\tilde{\varphi}_{\rho\mu}$ that are this form:

$$\tilde{\varphi}_{\rho+}\left(\vec{k}\right) = \frac{1}{\sqrt{2\varepsilon\left(\varepsilon + \rho\left[M - Bk^2\right]\right)}}\begin{pmatrix} \chi_{\rho+} \\ 0 \end{pmatrix}. \tag{4.6a}$$

$$\tilde{\varphi}_{\rho-}\left(\vec{k}\right) = \frac{1}{\sqrt{2\varepsilon\left(\varepsilon + \rho\left[M - Bk^2\right]\right)}}\begin{pmatrix} 0 \\ \chi_{\rho-} \end{pmatrix}. \tag{4.6b}$$

Where $\varepsilon = \sqrt{A^2k^2 + \left(M - Bk^2\right)^2}$, $\chi_{\rho\mu}^{\dagger} = \begin{pmatrix} Ake^{-i\mu\phi} & \rho\varepsilon + M - Bk^2 \end{pmatrix}$ and μ indicates the spin. The Berry's curvature of $\tilde{\varphi}_{\rho\mu}$ is not zero for all k. The corresponded chern number is of ther form:

$$C_{\rho\mu} = \frac{\rho\mu}{2}\left[\text{sgn}\left(M\right) + \text{sgn}\left(B\right)\right]. \tag{4.7}$$

But, the chern number of $\varphi_{\rho\mu}$ is always zero. This form of wave function also describes the right state, even if DSOI disappears, because the Hamiltonian is invariant under gauge transformation. We obtain two very different chern numbers from two different set of eigenvectors that are all eigenfunctions of the same effective Hamiltonian. It shows the chern number depends on the wave function form we choosing. The chern number isn't invariant under gauge transformation so it may not be a good topological number. (The

Chern number for the Chern class is the summation of chern number for all occupied bands.[15] The Chern number is invariant under gauge transformation.)

4.2 Winding number consideration

Consider a 2×2 Hamiltonian h as this form:

$$h = g_0 \left(\vec{k} \right) + \sum_i g_i \left(\vec{k} \right) \sigma_i. \tag{4.8}$$

The chern number is also determined by the winding number of $\vec{g} \left(\vec{k} \right)$.[15]

$$C = \frac{1}{4\pi} \int dk d\phi \sum_{lmn} \varepsilon_{lmn} (\hat{g})_l (\partial_k \hat{g})_m (\partial_\phi \hat{g})_n. \tag{4.9}$$

If we have a 2×2 Hamiltonian characterizing the system, we can derive the chern number from the winding number of this Hamiltonian.

From the form of the eigenvector of H_{eff}, we have the unitary transformation V that can transform the H_{eff} (equation (2.1)) to the block diagonal form.

$$\tilde{H}_{eff} = V H_{eff} V^\dagger = \begin{pmatrix} \tilde{h}_+ & 0 \\ 0 & \tilde{h}_- \end{pmatrix}. \tag{4.10}$$

$$\tilde{h}_\mu = Dk^2 + \begin{pmatrix} -M + Bk^2 & (Ak + \mu\delta) e^{i\phi} \\ (Ak + \mu\delta) e^{-i\phi} & M - Bk^2 \end{pmatrix}. \tag{4.11}$$

The $\tilde{h}_\mu$ describes the same eigenenergy and eigenvector as H_{eff} so we can obtain the topological number by $\tilde{h}_\mu$.

For $\tilde{h}_\mu$, $\vec{g}^\mu \left(\vec{k} \right)$ is of the form:

$$\vec{g}^\mu \left(\vec{k} \right) = \left([Ak + \mu\delta] \cos\phi, -[Ak + \mu\delta] \sin\phi, -M + Bk^2 \right). \tag{4.12}$$

The corresponded chern number C_μ is

$$C_\mu = -\frac{1}{2} \left[\frac{M - Bk^2}{E_\mu} \right]_{k_i}^{k_f}. \qquad (4.13)$$

Where $E_\mu = \sqrt{(Ak + \mu\delta)^2 + (M - Bk^2)^2}$.

If we integral whole k space, the chern number is always not an integer.

$$C_\mu = \frac{1}{2} \left[\frac{B}{|B|} + \frac{M}{\sqrt{M^2 + \delta^2}} \right]. \qquad (4.14)$$

For $\mu = -sgn(\delta A)$, we can find the special $k'_c = |\delta/A|$ where $\frac{\partial}{\partial k} \frac{M - Bk^2}{E_\mu} \Big|_{k=k'_c} = 0$. If we only integral between k'_c and $k = \infty$, the chern number is zero for $\Delta \left(= MB - [B\delta/A]^2 \right) < 0$ and the chern number is ± 1 for $\Delta > 0$. It is the same result that we obtained in the Chapter 3.

It seems that we can exactly find the topological number by this method. However we may need to choose the range of integration. Here we must drop the contribution of the region $k < \delta/A$. The H_{eff} works for small k so the winding number mainly depends on the the region where H_{eff} can't characterize. In addition, we can only calculate the chern number for a 2×2 Hamiltonian. The winding number can't be a topological number for general systems.

4.3 Spin chern number consideration

The Berry's curvature in presence of DSOI is zero for $k \neq 0$ and diverge at Γ point. We can't defined a proper topological number from the chern number of the eigenvector of H_{eff} (equation (2.1)). To obtain the topological number, we need a way to redefined the eigenvector. The new set of vector must be smooth and unique at the whole k space.

In recent years, a new definition of topological number that is called spin chern number has been established.[16][17] The spin chern number is the chern number of the vector φ'.

Where φ' is the linear superposition of the valence bands of the system.

$$\varphi'_i = \sum_j^{\text{valence band}} C'^i_j \varphi_j. \tag{4.15}$$

φ'_i is the eigenvector of a spin operator S with eigenvalue m'_i. If the direct bulk energy gap and spin gap $\Delta m = m_1 - m_2$ are both non-zero, we have a well defined spin chern number.

Consider a spin operator I_z[17] is of the form:

$$I_z = \begin{pmatrix} I_{2\times2} & 0 \\ 0 & -I_{2\times2} \end{pmatrix}. \tag{4.16}$$

For H_{eff} without DSOI, we can distinguish the spin up and the spin down by I_z. Therefore, we use I_z to calculate the spin chern number of H_{eff} with DSOI.

To derive φ', we project I'_z onto the eigenstates of H_{eff} and drop the conduction bands.

$$I'_z = \left\langle \varphi_{-+}\left(\vec{k}\right) \middle| \varphi_{--}\left(\vec{k}\right) \right\rangle \sigma_x. \tag{4.17}$$

The eigenvector of I'_z is of the form:

$$\varphi'_\nu = \frac{1}{\sqrt{2}} \left(sgn\left[\left\langle \varphi_{-+}\left(\vec{k}\right) \middle| \varphi_{--}\left(\vec{k}\right) \right\rangle \right] \left| \varphi_{-+}\left(\vec{k}\right) \right\rangle + \nu \left| \varphi_{--}\left(\vec{k}\right) \right\rangle \right). \tag{4.18}$$

The value of direct spin gap $\Delta m'$ is $2\left| \left\langle \varphi_{-+}\left(\vec{k}\right) \middle| \varphi_{--}\left(\vec{k}\right) \right\rangle \right|$.

The spin gap is zero if $\varphi_{-+}\left(\vec{k}\right)$ and $\varphi_{--}\left(\vec{k}\right)$ are orthogonal. If the $\varphi_{-+}\left(\vec{k}\right)$ and $\varphi_{--}\left(\vec{k}\right)$ are different spin state of n̂, they are orthogonal. Therefore, the spin gap is zero if the vector $\vec{g}^+\left(\vec{k}\right)$(equation (4.12)) is equal to $-\vec{g}^-\left(\vec{k}\right)$ at $\vec{k}$. The two vectors are anti-parallel only when the z component of $\vec{g}^\mu\left(\vec{k}\right)$ is zero and $k < |\delta/A|$ so the spin chern number is undefined when $MB > 0$ and $MB - B^2\delta^2/A^2 < 0$. At the well defined region, the spin chern number C_ν is

$$C_\nu = -\frac{\nu}{2}\left[sign\left(B\right) + sign\left(M\right)\right]. \tag{4.19}$$

The Fig. 4.1 shows the topological phase diagram. The topological non-trivial region is equal to what we proved in chapter 3.

We have proved the spin chern number can describe the topological property of system. However, there is still a problem because we find out that the topological phase diagram is dependent of the generator.

We use the operator J_z to obtain spin chern number. The J_z is of the form:

$$J_z = \frac{1}{2} \begin{pmatrix} 1 & 0 & 0 & 0 \\ 0 & 3 & 0 & 0 \\ 0 & 0 & -1 & 0 \\ 0 & 0 & 0 & -3 \end{pmatrix}. \tag{4.20}$$

For H_{eff} without DSOI, we can also distinguish the spin up and the spin down by J_z. The basis vector of H_{eff} is the eigenvector of J_z. J_z is also a reasonable operator for spin chern number. We numerically calculate the topological phase diagram of J_z showed in Fig. 4.2.

With different spin operator, the undefined region is not the same. The undefined region of one operator may be the topologically non-trivial region of another. It needs to know how to find the proper spin operator that indicate all topologically non-trivial region.
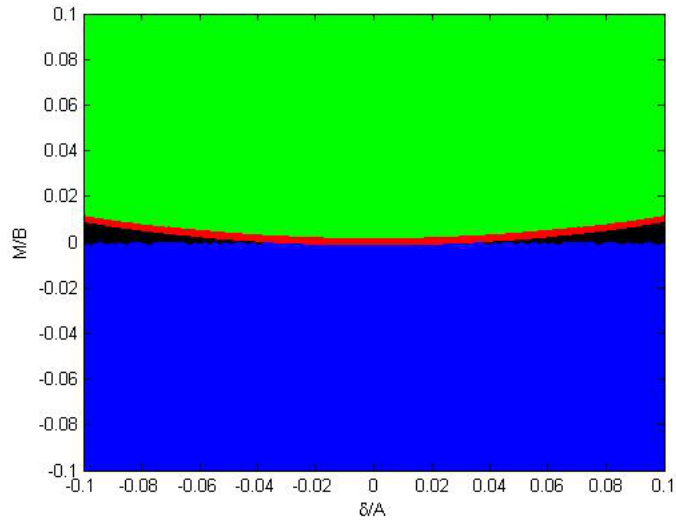
Figure 4.1: It shows the topological phase diagram with I_z. The x axis is δ/A and the y axis is M/B. The red line is $MB - B^2\delta^2/A^2 = 0$. The black region is undefined. The blue region is topological trivial. The green region is topological non-trivial.
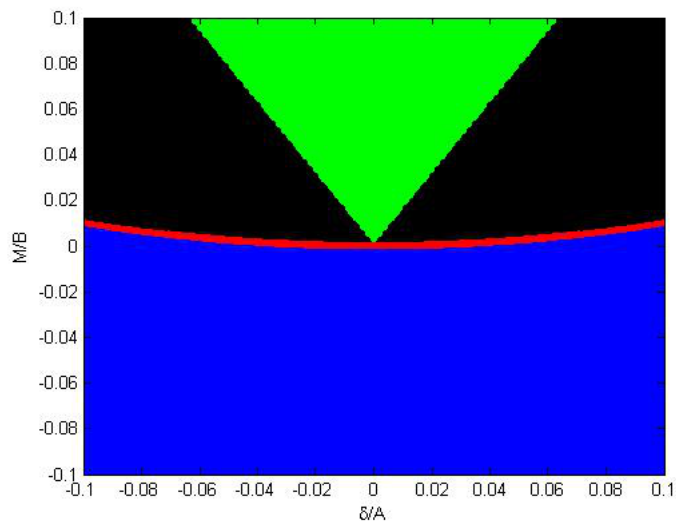
Figure 4.2: It shows the topological phase diagram with J_z. The x axis is δ/A and the y axis is M/B. The red line is $MB - B^2\delta^2/A^2 = 0$. The black region is undefined. The blue region is topological trivial. The green region is topological non-trivial.

Chapter 5

Edge-state branch in a quantum bar

In section 5.1, we derive the effective 1D Hamiltonian of the width W quantum bar (quantum channel). We find out that the effective 1D Hamiltonian has a symmetry that we call pseudo-parity. Because the operator y, the transverse direction, mixes the states with different pseudo-parity, it only simplifies the system in some cases. In chapter 6, we consider a system without y-dependent potential. Therefore, we use the pseudo-parity to simplifiy the calculations.

In section 5.2, we discuss the property of the edge states and the edge channels. Where the edge channels are the eigenstates of the 1D Hamiltonian with specific wave vector. The edge states are the linear combination of the edge channels. The DSOI terms mix spin so the edge channels isn't a pure spin state. The edge channels are localized at the two edges so the magnetic impurity near any edges of the sample will effect all of edge channels.

On the other hand, by the edge injection, we can generate an edge state that is a pure spin state and localized at an edge of the sample Where the edge state is linear superposition of the edge channels that have the same energy and propagation direction. The location of the edge state is determined by the relative phase between the edge channels. The finite size effect[4] and DSOI make relative phase vary in x, the longitudinal direction. The location of the edge state will change when it is propagating. The spin polarization of the edge state changes with the location so the spin polarization will automatically precess.

5.1 Effective Hamiltonian

In this section, we derive the effective 1D Hamiltonian of the quantum bar. Then, we define the pseudo-parity operator and prove that it is a symmetry of the effective 1D Hamiltonian.

We consider a quantum bar showed in Fig. 5.1. The boundary is along x-direction. The wave function Φ is zero when $y \geq W/2$ or $y \leq -W/2$. Where W is the width of the quantum bar. We derive an effective 1D Hamiltonian H_W to describe the band structrue with this boundary condition. We seperate H_{eff} (equation (2.1)) into two parts, H_0 and H'. H_0 contains all k_y dependent terms and M. H' contains the δ and all k_x dependent terms. We use H_0 to derive the basis vectors of H_W.
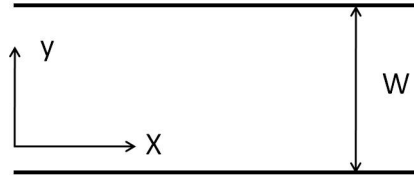
Figure 5.1: It shows the structure of a quantum bar system. We set the origin of y-axis at the middle of the bar. The wave function is zero when $y \leq -W/2$ and $y \geq W/2$.

In the set of basis $(|E1, +\rangle, |H1, +\rangle, |E1, -\rangle, |H1, -\rangle)$, H_0 is of the form:

$$
H_0 = \begin{pmatrix} Dk_y^2 - (M - Bk_y^2)\sigma_z - Ak_y\sigma_y & 0 \\ 0 & Dk_y^2 - (M - Bk_y^2)\sigma_z + Ak_y\sigma_y \end{pmatrix}.
\qquad (5.1)
$$

$|E1, +\rangle$ and $|H1, +\rangle$ subbands are decoupled to $|E1, -\rangle$ and $|H1, -\rangle$ subbands. $|E1, \pm\rangle$ and $|H1, \pm\rangle$ subbands are coupled by Ak_y terms and form $|S; i, \pm\rangle$ and $|A; i, \pm\rangle$ subbands. The $E1$ component of $|S; i, \pm\rangle$ subbands is even function. The $E1$ component of $|A; i, \pm\rangle$ subbands is odd function.

For H_{eff} with $d = 7nm$, the value of MB and Δ $(\Delta = MB - (B\delta/A)^2)$ is positive. There are four edge subbands in the system. The higher two subband is $|S; i, \pm\rangle$ subbands and the others are $|A; i, \pm\rangle$ subbands. In addition, the lowest conduction bulk subbands are $|A; i, \pm\rangle$ subbands and the highest valence bulk subbands are $|S; i, \pm\rangle$ subbands. (For the case $MB < 0$, the lowest conduction bulk subbands are $|S; i, \pm\rangle$ subbands and

the highest valence bulk subbands are $|A; \ i, \pm\rangle$ subbands.) The basis vectoers are of the form:

$$\langle S; \ i, +| = (\ \langle S; \ i| \quad 0_{1\times 2} \ ), \langle S; \ i, -| = (\ 0_{1\times 2} \quad \langle S; \ i| \ \sigma_z \ ),$$

$$\langle A; \ i, +| = (\ \langle A; \ i| \quad 0_{1\times 2} \ ), \langle A; \ i, -| = (\ 0_{1\times 2} \quad \langle A; \ i| \ \sigma_z \ ).$$

Where $|S; \ i\rangle$ is the pseudo-spin of $|S; \ i, +\rangle$ and $|A; \ i\rangle$ is the pseudo-spin of $|A; \ i, +\rangle$. (The detail definition of basis is listed in Appendix F.)

We define the set of basis vector ($|S; \ i, +\rangle$, $|A; \ i, +\rangle$, $|S; \ i, -\rangle$, $|A; \ i, -\rangle$). In this set of basis vector, the effective Hamiltonian H_W is defined as this form:

$$[H_W (k_x)]_{ij} = \langle i| (H_0 + H') |j\rangle = E_i \delta_{ij} + \langle i| H' |j\rangle . \tag{5.2}$$

Where $|i\rangle$ is the ith basis vector. The H' is of the form:

$$H' = Dk_x^2 + \begin{pmatrix} Bk_x^2\sigma_z + Ak_x\sigma_x & \delta\sigma_x \\ \delta\sigma_x & Bk_x^2\sigma_z + Ak_x\sigma_x \end{pmatrix} . \tag{5.3}$$

The σ_z doesn't couple $E1$ and $H1$ component so it does not couple $|S; \ i, \pm\rangle$ and $|A; \ i, \pm\rangle$ subbands. The σ_x couples $E1$ and $H1$ component so it only couples $|S; \ i, \pm\rangle$ and $|A; \ i, \pm\rangle$ subbands. (The same kind of subbands aren't coupled by the σ_x.)

The analytical form of H_W is

$$H_W (k_x) = \begin{pmatrix} E' + B'k_x^2 + A'k_x & \delta' \\ -\delta' & E' + B'k_x^2 - A'k_x \end{pmatrix} . \tag{5.4}$$

Where E' contain the eigenenergy of all basis vectors.

$$E' = \sum_i \left(E_i^S |S; \ i\rangle \langle S; \ i| + E_i^A |A; \ i\rangle \langle A; \ i| \right). \tag{5.5}$$

Where E_i^S is the eigenenergy of the $|S; \ i\rangle$ subband and E_i^A is the eigenenergy of the $|A; \ i\rangle$
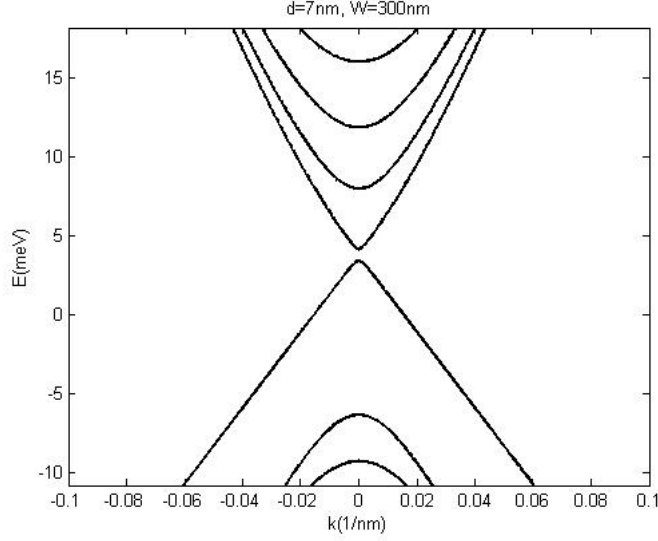
Figure 5.2: It shows the band structure of H_W for $W = 300nm$ with $\delta' = 0$.

subband. The other terms are of the form.

$$B' = D + B \sum_{ij} (|S; \ i\rangle \langle S; \ i| \sigma_z |S; \ j\rangle \langle S; \ j| + |A; \ i\rangle \langle A; \ i| \sigma_z |A; \ j\rangle \langle A; \ j|). \quad (5.6)$$

$$A' = A \sum_{ij} \langle S; \ i| \sigma_x |A; \ j\rangle (|Si\rangle \langle A; \ j| + |A; \ j\rangle \langle S; \ i|). \quad (5.7)$$

$$\delta' = -\delta \sum_{ij} \langle S; \ i| i\sigma_y |A; \ j\rangle (|Si\rangle \langle A; \ j| - |A; \ j\rangle \langle S; \ i|). \quad (5.8)$$

The band structure of H_W is showed in Fig. 5.2 and Fig. 5.3.

The effective Hamiltonian H_W has a symmetry we call pseudo-parity. The pseudo-parity operator π_p is of the form:

$$\pi_p = \begin{pmatrix} 0 & n_z \\ n_z & 0 \end{pmatrix}. \quad (5.9)$$

Where $n_z = \sum_i (|S; \ i\rangle \langle S; \ i| - |A; \ i\rangle \langle A; \ i|)$. We have $[E', n_z] = 0$, $[B', n_z] = 0$, $n_z A' n_z = -A'$ and $n_z \delta' n_z = -\delta'$. According to those equations above, we have $[\pi_p, H_W] = 0$. The H_W and π_p have simultaneous eigenvectors so we can obtain a more simple form of effective 1D Hamiltonian by projecting H_{eff} onto the eigenvectors of π_p.

We define a new set of basis vector($|S'; \ i, +\rangle$, $|A'; \ i, +\rangle$, $|S'; \ i, -\rangle$, $|A'; \ i, -\rangle$). Where
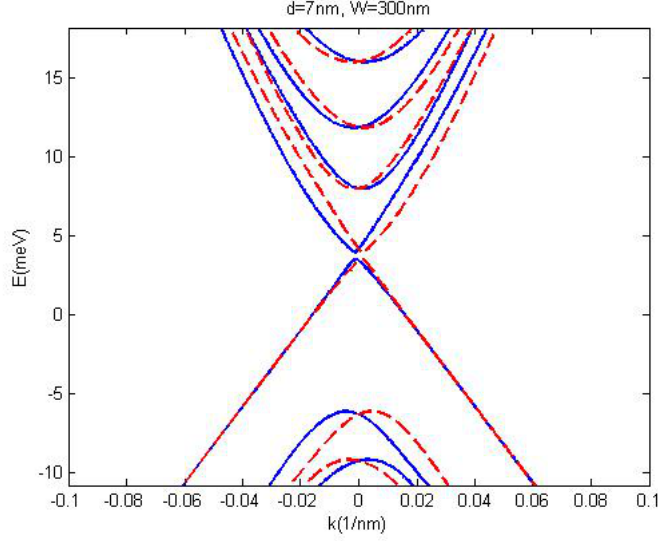
Figure 5.3: It shows the band structure of $\tilde{H}_W$ for $W = 300nm$. The blue solid line is $\mu = 1$ subbands. The red dash line is $\mu = -1$ subbands.

$|S'; i, \mu\rangle = (|S; i, +\rangle + \mu |S; i, -\rangle)/\sqrt{2}$ and $|A'; i, \mu\rangle = (|A; i, +\rangle - \mu |A; i, -\rangle)/\sqrt{2}$. $|S'; i, \mu\rangle$ and $|A'; i, \mu\rangle$ are eigenvectors of π_p with the eigenvalue μ. In this representation, the effective Hamiltonian $\tilde{H}_W$ is of the form:

$$\tilde{H}_W(k_x) = \begin{pmatrix} h'^W_+(k_x) & 0 \\ 0 & h'^W_-(k_x) \end{pmatrix}. \tag{5.10}$$

Where $h'^W_\mu(k_x) = \tilde{E} + \tilde{B}k_x^2 + \tilde{A}k_x + \mu\tilde{\delta}$. Here μ also indicates the quantum number of pseudo-parity. The other terms are of the forms:

$$\tilde{E} = \sum_i \left(E_i^S |S'; i\rangle \langle S'; i| + E_i^A |A'; i\rangle \langle A'; i| \right). \tag{5.11}$$

$$\tilde{B} = D + B \sum_{ij} \left(|S'; i\rangle \langle S; i| \sigma_z |S; j\rangle \langle S'; j| + |A'; i\rangle \langle A; i| \sigma_z |A; j\rangle \langle A'; j| \right). \tag{5.12}$$

$$\tilde{A} = A \sum_{ij} \langle S; i| \sigma_x |A; j\rangle \left(|S'; i\rangle \langle A'; j| + |A'; j\rangle \langle S'; i| \right). \tag{5.13}$$

$$\tilde{\delta} = \delta \sum_{ij} \langle S; i| i\sigma_y |A; j\rangle \left(|S'; i\rangle \langle A'; j| - |A'; j\rangle \langle S'; i| \right). \tag{5.14}$$

According to the definition of the basis vector $(|S'; i, \mu\rangle, |A'; i, \mu\rangle)$ and time reversal

operater (See Appendix D), we derive the time reversed state of basis vector.

$$\Theta \left| S'; \ i, \mu \right\rangle = -\mu \left| S'; \ i, -\mu \right\rangle . \tag{5.15a}$$

$$\Theta \left| A'; \ i, \mu \right\rangle = \mu \left| A'; \ i, -\mu \right\rangle . \tag{5.15b}$$

The time reversal operator in this representantion is of the form:

$$\Theta = \begin{pmatrix} 0 & \tilde{n}_z \\ -\tilde{n}_z & 0 \end{pmatrix} K. \tag{5.16}$$

Where $\tilde{n}_z = \sum_i \left(\left| S'; \ i \right\rangle \left\langle S'; \ i \right| - \left| A'; \ i \right\rangle \left\langle A'; \ i \right| \right)$. The time reversed states of $\left| S'; \ i, + \right\rangle$ and $\left| A'; \ i, + \right\rangle$ are $\left| S'; \ i, - \right\rangle$ and $\left| A'; \ i, - \right\rangle$. The eigenstates of h'^W_+ and h'^W_- are time reversal pair. It seems that the eignstates of h'^W_+ aren't coupled with the eigenstates of h'^W_- by the normal impurity or potential. But the operator y can couple the basis vectors with different pseudo-parity symmetry. According to the symmetry of the basis vector, we can obtain the form of operator y.

$$y = \begin{pmatrix} 0 & y' \\ y' & 0 \end{pmatrix} . \tag{5.17}$$

Where $y' = \sum_{ij} \left\langle S; \ i \right| y \left| A; \ j \right\rangle \left(\left| S'; \ i \right\rangle \left\langle A'; \ j \right| + \left| A'; \ j \right\rangle \left\langle S'; \ i \right| \right)$. In this set of basis vector, the π_p is of the form :

$$\pi_p = \begin{pmatrix} 1 & 0 \\ 0 & -1 \end{pmatrix} . \tag{5.18}$$

The operator y doesn't commute with π_p so the potential in terms of odd power of operator y can mix the states with different pseudo-parity.

5.2 Wave function for bulk like and edge like states

In this section, we discuss property of the edge channels and the edge states in the quantum bar. Where the edge channels are the eigenstates of the effective 1D Hamiltonian. The edge state is the superposition of the edge channels with the same energy and propagation direction.

For H_W without DSOI, the solution of edge channels with certain k_x can be of the
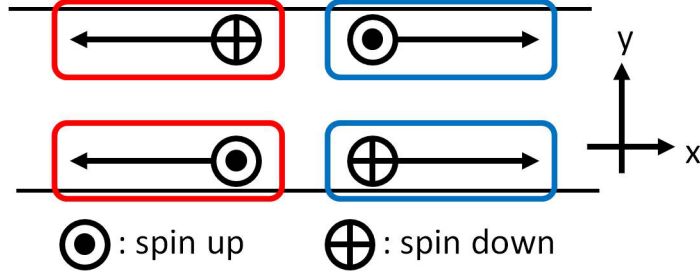
Figure 5.4: It shows the edge states with certain k_x and spin in absence of DSOI.

form that contains only one spin (Fig. 5.4). At the lower edge, $y = -W/2$, the spin up state is left going and the spin down state is right going. At the upper edge, $y = W/2$, the spin of the right and left going state is opposite to the edge states at the lower edge. The edge channels aren't robust against the magnetic impurity. However the magnetic impurity near the upper edge hardly scatters the edge channels at the lower edge. The edge channel only scattered by the impurities at the same edge.

For H_W with DSOI, the DSOI and finite size effect couple the two edge channels that are the eigenstates of H_W without DSOI and have the same propagation direction. Those two edge channels are mixed together to form two edge channelss $\psi_{\mu p}^{edge}$ with the same p but different μ (Fig. 5.5 and Fig. 5.6). Where μ is the quantum number of pseudo-parity and p is the propagation direction ($p = +$ is right going.). The edge channel has specific wave vector $k_{\mu p}^{edge}$ but it can't be the form that contains only one spin component. And it is localized at both two edges so the magnetic impurity near any edges scatters the edge channels. The DSOI terms makes the edge channel become weaker to magnetic impurity.

If we inject charge current at an edge of the sample, we predict that we can generate an edge state Φ_p^{edge} which is at the edge. The Φ_p^{edge} is the linear combination of the $\psi_{\mu p}^{edge}$ with same p and energy.

$$
\begin{aligned}
\Phi_p^{edge}(x, y) &= \frac{1}{\sqrt{2}} \left[\psi_{+p}^{edge}(x, y) + e^{i\Delta_0'} \psi_{-p}^{edge}(x, y) \right] \\
&= \frac{1}{\sqrt{2}} e^{ik_{+p}^{edge} x} \left[f_{+p}^{edge}(y) + e^{i\Delta'(x)} f_{-p}^{edge}(y) \right].
\end{aligned}
\tag{5.19}
$$

Where $f_{\mu p}^{edge}(y)$ is the column vector part of $\psi_{\mu p}^{edge}(x, y)$ and $\Delta'(x) = \Delta_0' + \left(k_{-p}^{edge} - k_{+p}^{edge} \right) x$. The location of the edge state depends on the phase difference Δ'. We choose the guage
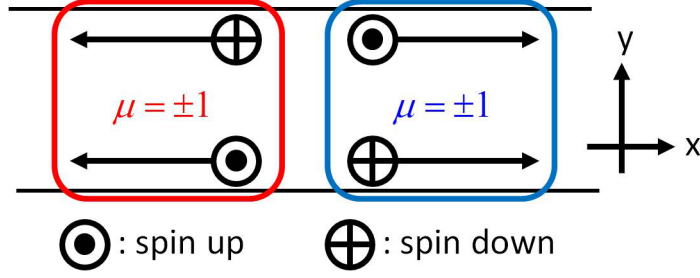
Figure 5.5: It shows the edge states with certain k_x in the presence of DSOI.

that spin up part of $f_{\mu p}^{edge}$ is the same sign such that the edge state is at one of the sample edges if $\Delta'(x) = 0$ or $\Delta'(x) = \pi$.

In the system without DSOI, the $k_{\mu p}^{edge}$ is equal to each other. The Δ' is constant so the location of the edge state doesn't change. On the other hand, the DSOI and finite size effect make $k_{\mu p}^{edge}$ different. The Δ' becomes a function of x and the edge state isn't always localized at one edge. (Fig. 5.8 and Fig. 5.9) When the edge state propagates, the location of the edge state is from a edge of the quantum bar to the other. After propagating a length L_c we call edge-switching length, the edge state will becomes localized at the other edge. (The value of L_c can be larger than $100um$. At that case, the edge state performs like the edge channel without DSOI.) The spin polarization of the edge state depends on the location and the propagation direction of the edge state. Therefore, the spin polarization of the edge state will automatically changes. (This property is also showed in ref[11].)

For the bulk like states, the DSOI makes the bulk states with certain k_x isn't a pure spin state too (Fig. 5.7). We also can define a set of bulk state that is a pure spin state initially. The spin of those state also varies like edge state we showed in Fig. 5.9. In contrast, the density of the bulk states are localized at the middle of the ribbon.
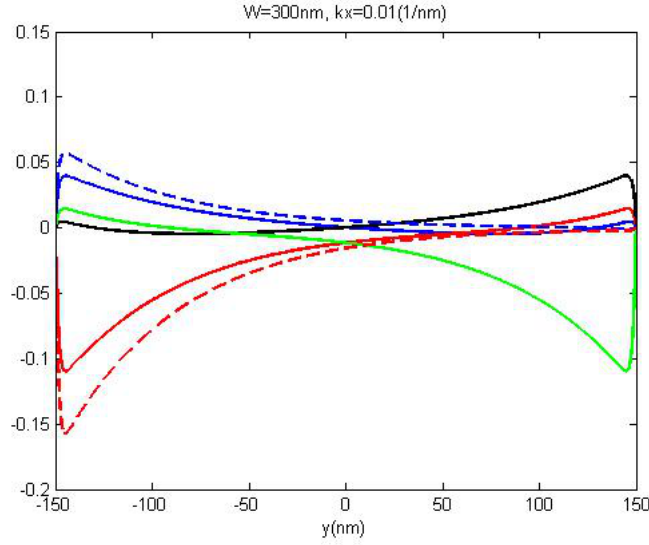
Figure 5.6: It shows the column vector part of the two edge states of H_W with $W = 300nm$. The solid line is the $\mu = +1$ state with DSOI and the dash line is the state without DSOI. Those two state are the upper edge bands and their k value is $0.01nm^{-1}$. The blue line is $|E1, +\rangle$ component. The red line is $|H1, +\rangle$ component. The black line is $|E1, -\rangle$ component. The green line is $|H1, -\rangle$ component.
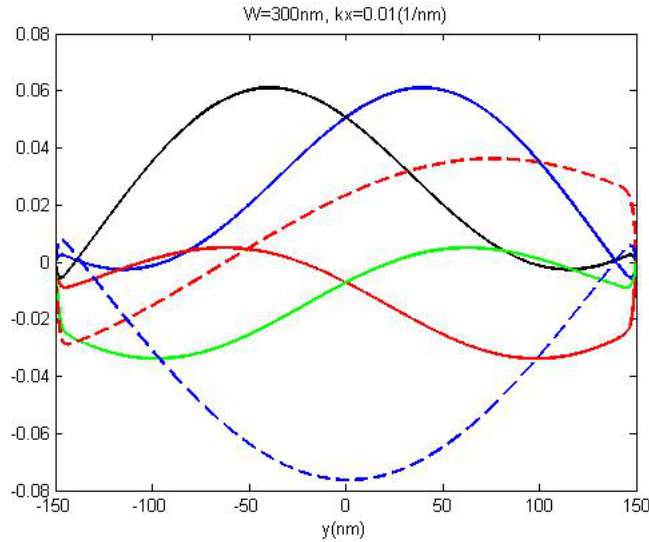
Figure 5.7: It shows the column vector part of the two bulk states of H_W with $W = 300nm$. The solid line is the $\mu = +1$ state with DSOI and the dash line is the state without DSOI. Those two state are the lowest conduction subbands and their k value is $0.01nm^{-1}$. The blue line is $|E1, +\rangle$ component. The red line is $|H1, +\rangle$ component. The black line is $|E1, -\rangle$ component. The green line is $|H1, -\rangle$ component.
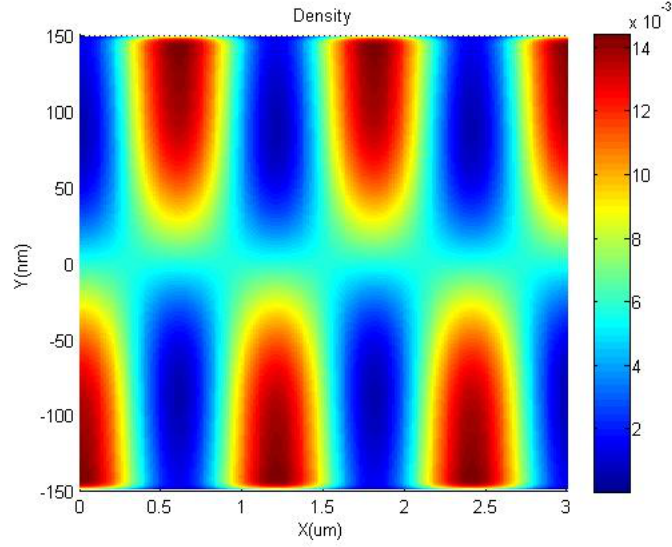
Figure 5.8: It shows the density of edge states Φ_+^{edge} with $W = 300nm$, $\Delta_0' = -1$ and $E = 6.4meV$. (Note: the dimension of y-axis is different to x-axis)
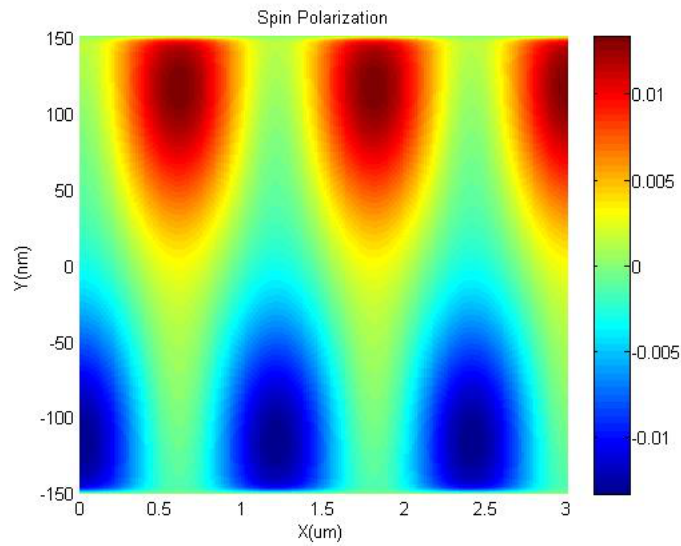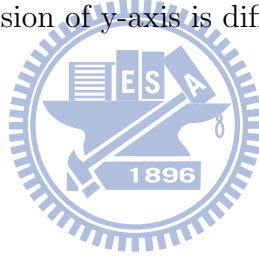
Figure 5.9: It shows the spin polarizationf edge states Φ_+^{edge} with $W = 300nm$, $\Delta_0' = -1$ and $E = 6.4meV$. (Note: the dimension of y-axis is different to x-axis)

Chapter 6

Quantum transport in a quantum bar

In this chapter, we fully numerically and semi-analytically calculate the transport of the edge channels and edge states in a quantum bar consisting of a potential barrier. Where the edge channels are the eigenstates of the effective 1D Hamiltonian. The edge state is the superposition of the edge channels with the same energy and propagation direction.

First, we discuss the transmission structure through a square potential in the quantum bar without DSOI. The edge band gap is not zero in a quantum bar because of finite size effect.[4] We show that the edge channels are back scattered by a potential at the energy range near the energy gap. The pseudo-spin of the edge channel at that energy range becomes energy dependent so the reflection is not zero. Though the non-zero edge band gap makes the edge channels scattered by the potential, the edge channel still totally transmits at the energy range not near the energy gap.

On the other hand, we show the transmission dips at the energy range not near the edge band gap is due to the Fano resonance. The edge channel forms the continuum spectrum and the resonance bulk channel forms the discrete state (quasi-bound state). Because the life time of the quasi-bound state are very long (the quasi-bound state is very well), we need to change the representation channel to calculate the Fano factor and life time of quasi-bound state. For the system without DSOI, the Fano factors are unique and the edge channels are totally back scattered at the dip energy.

Finally, we discuss the transmission structure through a square potential in the presence of DSOI. The edge channels are more robust against a potential because the edge energy gap is smaller to the no DSOI case. The edge energy gap reduction is mainly due to the coupling between edge and bulk subbands. On the other hand, the transmission dips at the energy range not near the edge band gap are still characterized by the Fano resonance. The Fano factors now depend on the potential energy (or the length of the potential). The edge channels aren't totally back scattered at the dip energy. The additional phase from the Fano resonance is dependent on the pseudo-parity. We can use this to change the spin polarization and the location of the edge state. The length of the potential barrier can be much shorter than the edge-switching length L_c so we can change the spin without a very long (large) device.

6.1   The transport property of the effective 1D system

In this section, we first derive the formulas of the transmission spectrum, full numerical result and multiple scattering result, of the quantum bar consists of a potential barrier. Second, we calculate the transport of the quantum bar without DSOI. We will point out which dip structrues in the transport are originated from Fano physics. Finally, we discuss the reflection of edge channels at the energy near the edge band gap

The L nm long square potential V is of the form: (It is also showed in Fig.6.1.)

$$V\left(x\right) = \begin{cases} U_0 & 0 < x < L \\ 0 & otherwise \end{cases} \text{for} \quad . \tag{6.1}$$

Where U_0 is the potential energy. The potential V commutes with π_p so the effective 1D Hamiltonian can be a block-diagonalized form even if we include DSOI terms.

First we study the quantum transport of the system without DSOI. The effective 1D
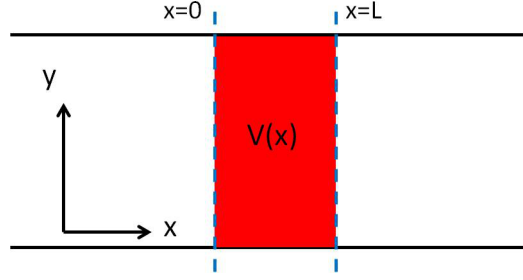
Figure 6.1: It is the structure of a quantum channel system we want to study. An uniform potential U_0 is imposed at the red area between $x = 0$ and $x = L$.

Hamiltonian H_W (equation (5.4)) is of the form.

$$H_W = \begin{pmatrix} h_+^W(k_x) & 0 \\ 0 & h_-^W(k_x) \end{pmatrix}. \tag{6.2}$$

Where $h_\eta^W = E' + \eta A' k_x + B' k_x^2$ and the η indicates the spin of eigenstates. The operator E', A' and B' are defined in equations (5.5)-(5.8). The spin up and spin down parts are decoupled so we can compute the scattering state only with the spin up part. According to equation (3.17), we can calculate the eigenstate of h_+^W for given energy E by diagonalizing this matrix h_+.

$$h_+(E) = \begin{pmatrix} 1 & 0 \\ 0 & -B' \end{pmatrix}^{-1} \begin{pmatrix} 0 & 1 \\ -E + E' & A' \end{pmatrix}. \tag{6.3}$$

Then we obtain the eigenstate ψ_{pm}^E as this form.

$$\psi_{pm}^E(x) = e^{ik_{pm}^E x} f_{pm}^E. \tag{6.4}$$

Where f_{pm}^E is the column vector of mth eigenstate with $k_x = k_{pm}^E$. The p is the propagation diection or decay diection of ψ_{pm}^E. ($p = +1$ is right going or decay in right direction.)

In this chapter, we focus upon the erengy range at where only edge channels are the incident channel. For given energy E, the scattering state $\Phi_{p=+}^E$, which is for the incident

channel ψ_{+m}^E, is of the form.

$$\Phi_+^E(x) = \begin{cases} \psi_{+m}^E(x) + \sum_{m'} r_{m'}\psi_{-m'}^E(x) & x < 0 \\ \sum_{m'} \left[a_{m'}\psi_{+m'}^{E-U_0}(x) + b_{m'}\psi_{-m'}^{E-U_0}(x) \right] & \text{for} \quad 0 \leq x \leq L \\ \sum_{m'} t_{m'}\psi_{+m'}^E(x) & L < x \end{cases} \quad . \tag{6.5}$$

The wave function and the Schrödinger equation are continuous at the boundaries so we obtain the set of equations that determine the coefficients r_m', t_m', a_m' and b_m'.

$$\sum_{m'} \left[r_{m'} f_{-m',n}^E - a_{m'} f_{+m',n}^{E-U_0} - b_{m'} f_{-m',n}^{E-U_0} \right] = -f_{+m,n}^E. \tag{6.6a}$$

$$\sum_{m'} \left[r_{m'} k_{-m'}^E f_{-m',n}^E - a_{m'} k_{+m'}^{E-U_0} f_{+m',n}^{E-U_0} - b_{m'} k_{-m'}^{E-U_0} f_{-m',n}^{E-U_0} \right] = -k_{+m}^E f_{+m,n}^E. \tag{6.6b}$$

$$\sum_{m'} \left[a_{m'} e^{ik_{+m'}^{E-U_0}L} f_{+m',n}^{E-U_0} + b_{m'} e^{ik_{-m'}^{E-U_0}L} f_{-m',n}^{E-U_0} - t_{m'} e^{ik_{+m'}^E L} f_{+m',n}^E \right] = 0. \tag{6.6c}$$

$$\sum_{m'} \left[a_{m'} k_{+m'}^{E-U_0} e^{ik_{+m'}^{E-U_0}L} f_{+m',n}^{E-U_0} + b_{m'} k_{-m'}^{E-U_0} e^{ik_{-m'}^{E-U_0}L} f_{-m',n}^{E-U_0} - t_{m'} k_{+m'}^E e^{ik_{+m'}^E L} f_{+m',n}^E \right] = 0. \tag{6.6d}$$

Where $f_{pm,n}^E$ is the nth component of f_{pm}^E.

Next we derive the current density of Φ_+^E. Form the continuty equation, we have the relation between the probability density $\rho_{p=+}^E$ and the current density $J_{p=+}^E$. The probability density is the magnitude square of the scattering function. Substitute the sacttering function and $-i\partial_x$ for the probability density and k_x by the Schrödinger equation, we obtain the current density.

$$J_+^E = \frac{1}{\hbar} \left[\left(\Phi_+^E\right)^+ A'\Phi_+^E - i\left(\Phi_+^E\right)^+ (D+B') \partial_x \Phi_+^E + i\left(\partial_x \Phi_+^E\right)^+ (D+B') \Phi_+^E \right]. \tag{6.7}$$

The possible incident state is unique so we can define the transmission as this form.

$$|T|^2 = \frac{J_{scattering\ state}}{J_{incident\ channel}}. \tag{6.8}$$

We call the transmission from this definition as full numerical result (FN).

We also use the multiple scattering method to semi-analytically study the transport
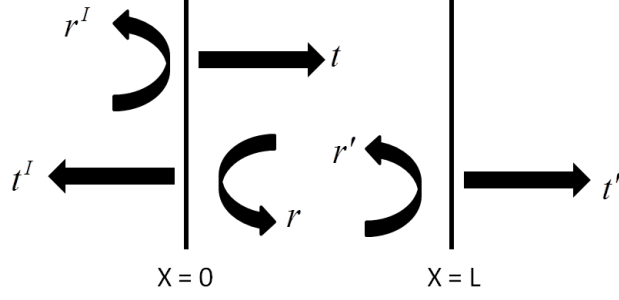
Figure 6.2: This figure shows the definition of the t, r, t', r', t^I and r^I. The t, t' and t^I are the transmission coefficients and the others are the reflection coefficients. The t and r are at the right boundary, $x = L$, and the t' and r' are at the left boundary, $x = 0$.

property. For derive the transmission by multiple scattering method, we need to obtain the transmission and reflection coefficients at each boundary first. At boundary $x = 0$, the scattering state $\Phi_m^{E,I}$, that is for the incident channel ψ_{+m}^E, is of the form.

$$\Phi_m^{E,I}(x) = \begin{cases} \psi_{+m}^E(x) + \sum_{m'} r_{m'}^I \psi_{-m'}^E(x) & \\ \sum_{m'} t_{m'} \psi_{+m'}^{E-U_0}(x) & \end{cases} \text{for} \begin{array}{l} x < 0 \\ x \geq 0 \end{array}. \tag{6.9}$$

The scattering state $\Phi_m^{E,II}$ for the incident channel $\psi_{-m}^{E-U_0}$ is of the form.

$$\Phi_m^{E,II}(x) = \begin{cases} \sum_{m'} t_{m'}^I \psi_{-m'}^E(x) & \\ \psi_{-m}^{E-U_0}(x) + \sum_{m'} r_{m'm} \psi_{+m'}^{E-U_0}(x) & \end{cases} \text{for} \begin{array}{l} x < 0 \\ x \geq 0 \end{array}. \tag{6.10}$$

At boundary $x = L$, the scattering state $\Phi_m^{E,III}$ for the incident state $\psi_{+m}^{E-U_0}$ is of the form.

$$\Phi_m^{E,III}(x) = \begin{cases} \psi_{+m}^{E-U_0}(x) + \sum_{m'} r'_{m'm} \psi_{-m'}^{E-U_0}(x) & \\ \sum_{m'} t'_{m'} \psi_{+m'}^E(x) & \end{cases} \text{for} \begin{array}{l} x < L \\ x \geq L \end{array}. \tag{6.11}$$

The definition of the coefficients is showed in Fig. 6.2. From the continuity of wave function and Schrödinger equation, we obtain the coefficients $t_{m'}^I$, $r_{m'm}^I$, $t'_{m'}$, $r'_{m'm}$, $t_{m'}$ and $r_{m'm}$ (by the set of equations similar to equation(6.6)). Here we focus on the energy range where only edge channel is incident channel. Only the edge channel are propagating mode at $x \geq L$. We can just calculate the coefficient of this channel because the
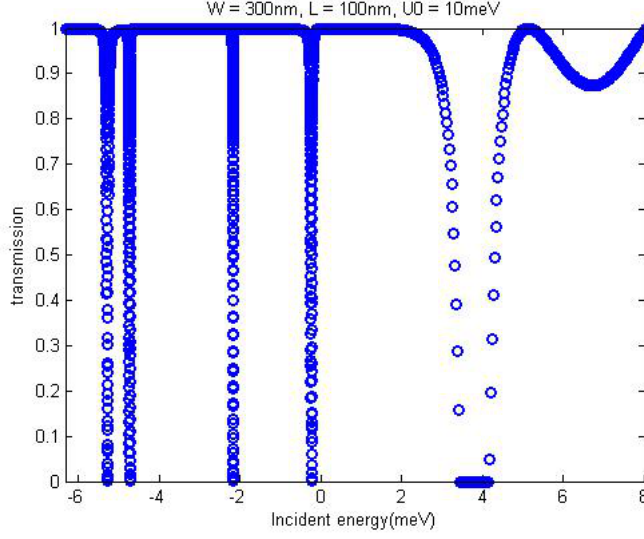
Figure 6.3: It is the transmission from FN versus the incident energy for H_W without DSOI. The width W of the quantum channel is $300nm$. The length L of the potential $V(x)$ is $100nm$ and the value of potential energy U_0 is $10meV$.

others contribute nothing to the total current. (This is only valid for total current in the propagation direction. If we want to know the current at the transverse direction, we must include all the terms of the scattering state.) The transmission coefficient T^{MS} from multi-scattering method is of the form.

$$
\begin{aligned}
T^{MS} &= \sum_{m'} t'_{m'} t_{m'} + \sum_{m'''m''m'} t'_{m'''} r_{m'''m''} r'_{m''m'} t_{m'} + \dots \\
&= \sum_{m''m'} t'_{m''} \left[\frac{1}{1 - \gamma_{MS}} \right]_{m''m'} t_{m'}.
\end{aligned} \tag{6.12}
$$

Where $[\gamma_{MS}]_{m'm} = [rr']_{m'm}$ and m in equation (6.12) indicates the incident channel. The transmission is $\left| T^{MS} \right|^2$ and we call this as multiple scattering result (MS).

For fixed U_0, the transmission is showed in Fig. 6.3. At this energy range, one of eigenstates is the edge channel in the potential area. The transmission dip near $4meV$ is the edge band gap for the incident channel. The minimum of the dips lower than the edge gap is zero. At the energy range of the dips, some of bulk channels are propagating mode. The edge and bulk channels couple together to form the dip structure. The energy of dips is determined by the resonant energy of the bulk channels. At the next section,
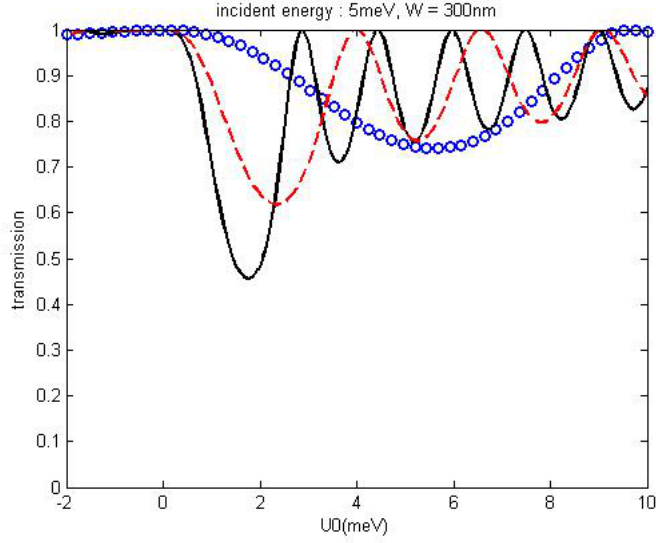
Figure 6.4: It is the transmission from FN versus U_0 for H_W without DSOI. The width W of the quantum channel is $300nm$ and the incident energy is $5meV$. The blue circle is for $L = 100nm$. The red dash line is for $L = 300nm$. The black solid line is for $L = 500nm$.

we will proof that the dips are described by Fano physics.

For fixed incident energy which near the edge band gap region, the transmission structure is showed in Fig. 6.4. There is an oscillation spectrum due to the Fabry-Pérot resonance and the transport spectrums shows that the edge channels could be scattered by the potential barrier. To study the origin of this reflection, we consider an effective 1D Hamiltonian H_W^{edge} only containing spin-up edge bands.

$$H_W^{edge} = E_0^{edge} + M^{edge}\sigma_z + A^{edge}k_x\sigma_x. \tag{6.13}$$

Where $E_0^{edge} = 3.8meV$, $M^{edge} = 0.37meV$ and $A^{edge} = 256meV/nm$ for $W = 300nm$. In Fig. 6.5, it shows the transmission for H_W and H_W^{edge} with fixed incident energy. The transmission structures of the two Hamiltonians are similar. Therefore, the reflection is mainly determined by the edge subbands and the bulk subbands only enhance the reflection.

The transmission dip near $U_0 = 2meV$ is due to the edge band gap in the potential region. The tunneling length λ^{edge} of the edge channel is propertional to $\left|A^{edge}/M^{edge}\right|$. The value of A^{edge} is very large becuase the system has strong spin-orbital coupling. The
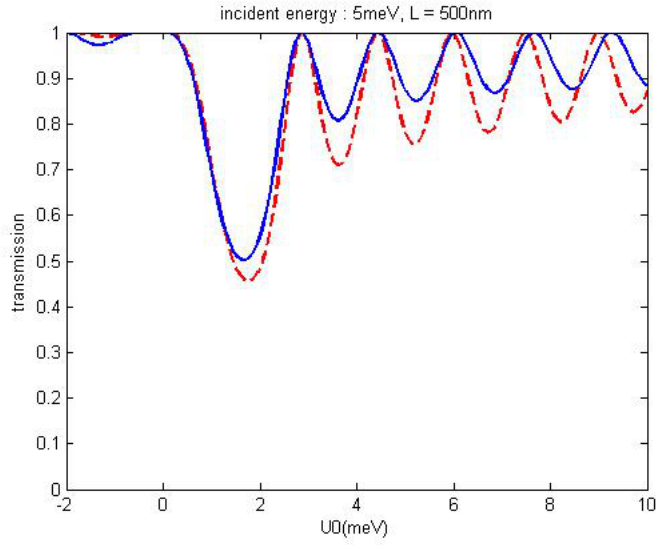
Figure 6.5: It is the transmission from FN versus U_0 for H_W and H_W^{edge}. The width W of the quantum channel is $300nm$ and the incident energy is $5meV$. The length L of the potential area is $500nm$. The red dash line is for H_W. The blue solid line is for H_W^{edge}.
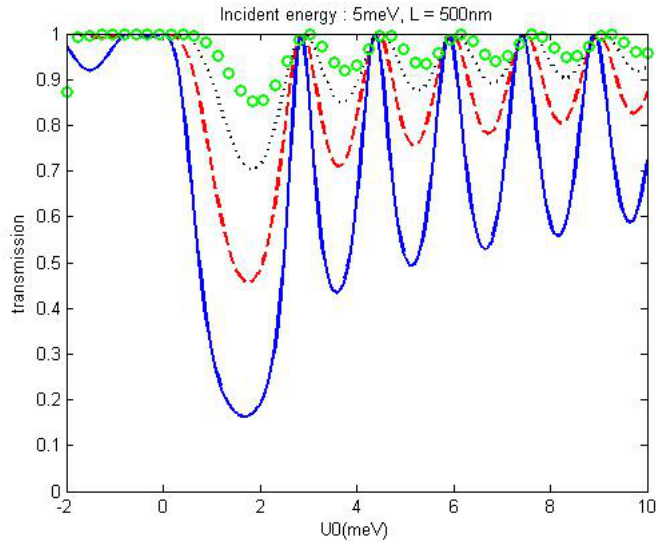
Figure 6.6: It is the transmission from FN versus U_0 for H_W without DSOI. The length of the potential L is $500nm$ and the incident energy is $5meV$. The blue solid line is for $W = 2500nm$. The red dash line is for $W = 300nm$. The black dot line is for $W = 350nm$. The green circle is for $W = 400nm$.

41

width of the quantum channel is large enough so the energy gap of the edge bands is small. It cause that the tunnel length of the edge channels is larger than $700nm$ (for $W = 300nm$) so the transmission at that energy range is not small.

At the potential range except for the edge band gap region, the reflection is induced by the pseudo-spin mismatch. If the edge bands is gapless, the pseudo-spins of the opposite propagation direction edge channels are orthogonal. The pseudo-spin is determined by the propagation direction of the k_x and it is independent of the energy. The reflection of edge channel is forbidden because of the Klein paradox.

On the other hand, the wave function overlapping of the edge channels at opposite edge sides opens up the edge band gap in the quantum bar system.[4] This finite edge band gap makes the pseudo-spin of the edge channels with the energy near the edge band gap region be different to the edge channels with the energy far away from the edge band gap. So the edge channel is scattered by the potential barrier if the energy is near the edge band gap. The Fig. 6.6 shows the reflection decreases when the W becomes larger. The finite edge band gap is due to the finite size effect so the edge band gap region is smaller if the W is larger. The edge channels are more robust if the edge band gap is smaller so this reflection decreasing supports our claim.

We have showed that the potential barrier can scatter the edge channels, but it doesn't mean that the edge channel can't totally transmit the potential barrier. The edge channel still totally transmits the potential if the energy is far away from the edge band gap.

6.2   Probing the fano-physics in the transport property

For the incident energy not near the edge band gap, the edge channel totally transmits the potential. In Fig. 6.3, we find there are some transmission dips far away from the edge band gap. Those dips aren't due to the reflection of the edge channels but due to the Fano resonance. In this section, we will proof the dips charaterized by Fano physics.

The Fig. 6.7 shows the probability density of the scattering state with incident energy $-0.2386meV$. The figure demonstrates that the scattering has a density peak localized

at the middle of the potential area. The density peak is contributed by the rasonance of the bulk channel. On the other hand, our data shows that all of this kind of dips is near the resonant energy of bulk channels and the dips are independent of the resonant energy of the edge channel. Therefore, the dips structure is caused by the the bulk resonance states.

We call the dip near the resonant energy of nth resonant k_x from mth higher valence bulk subband as Dip. m_n. The dips in Fig. 6.3 from right to left are Dip. 1_1, Dip. 2_1, Dip. 3_1 and Dip. 1_2. At those dips, there are an edge channel and at least two bulk channels are propagating modes. The transmission coefficient T^{MS} containing the process only dependent of those channels is similar to the FN (See Fig. 6.8.). The dips are determined by the propagating channels. However it is hardly to simplify the T^{MS} by dropping the less important procedure. To show the reason of this and proof the Fano physics, we analytically derive the transmission coefficient of a simple case.

For Markus König's band parameters[7] listed at Table 3.1, the transmission structure of H_W with $W = 200nm$ and $L = 100nm$ is showed in Fig. 6.9. (The transmission structure of this parameter has been calculated in ref[5].) The edge band gap is near $7meV$. At the energy range near highest dip, Dip. 1_1, there are one edge channel and one bulk channel are propagating mode. The transmission of FN and MS contributed by propagating mode only is showed in Fig. 6.10. The difference of the resonant energy is because we drop the decay channels. The transmission of two method is similar so we can use the T^{MS} to characterize the dip structure. In the set of channel vector, $\left(\psi_{+e}^{E-U_0}, \psi_{+b}^{E-U_0} \right)$, the T^{MS} is of the form.

$$T^{MS} \approx t' \frac{1}{1 - \gamma_{MS}} t. \tag{6.14}$$

$$1 - \gamma_{MS} = \begin{pmatrix} 1 - r_{ee} r'_{ee} - r_{eb} r'_{be} & -r_{ee} r'_{eb} - r_{eb} r'_{bb} \\ -r_{be} r'_{ee} - r_{bb} r'_{be} & 1 - r_{bb} r'_{bb} - r_{be} r'_{eb} \end{pmatrix}.$$

Where e indicates the edge channel and b indicates the resonant bulk channel.

The multiple scattering process is described by $1 - \gamma_{MS}$. We first drop the less important terms of it. The edge channel rarely reflected because the pseudo-spin of the edge channel is independent of the incident energy. We drop r'_{ee} and r_{ee} dependent terms. Be-
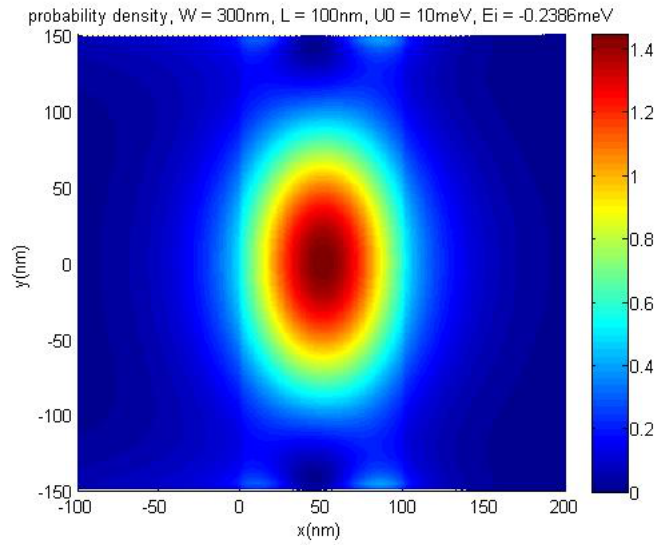
Figure 6.7: It is the probability density from FN of the scattering state with $E = -0.2386meV$, $W = 300nm$, $L = 100$ and $U_0 = 10meV$.
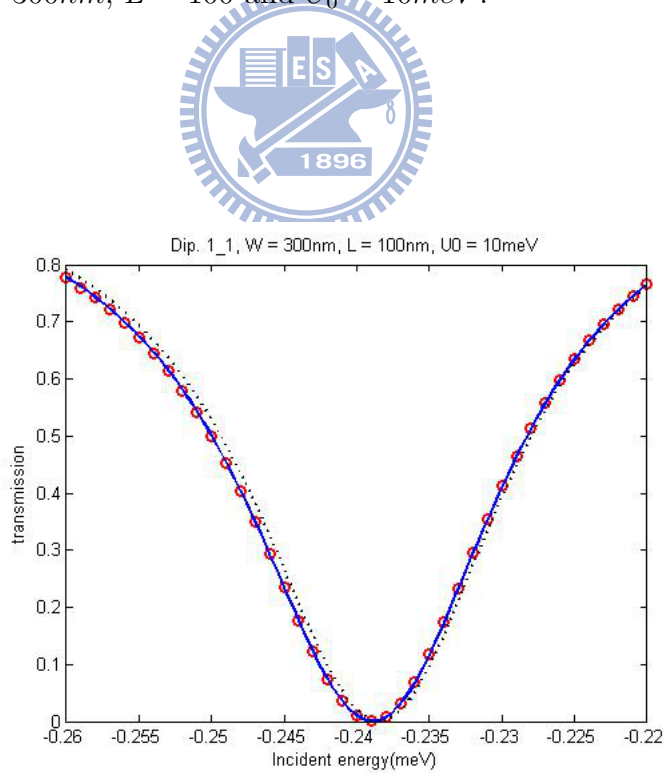
Figure 6.8: It is the transmission of Dip. 1_1 with $W = 300nm$, $L = 100$ and $U_0 = 10meV$. The red circle is MS contributed by propagating mode only. The black dot line is FN. The blue soild line is the Fano profile form, equation (6.24).
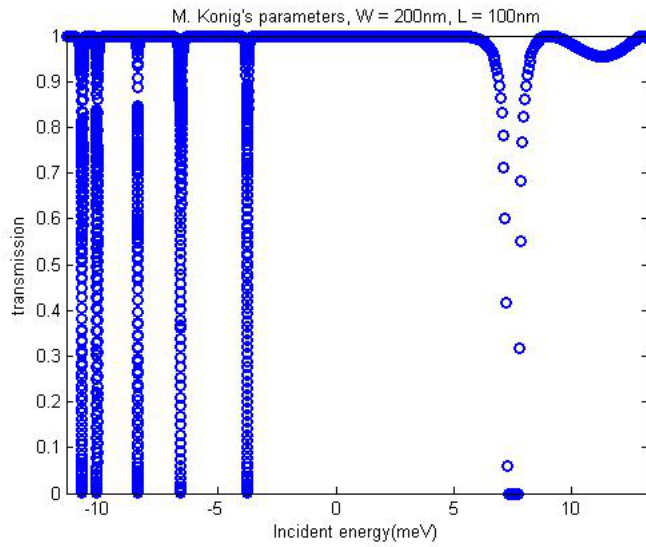
Figure 6.9: It is the transmission from FN versus the incident energy for H_W without DSOI. The band parameters of H_W is from Markus König's work.[7] The width W of the quantum channel is $200nm$. The length L of the potential $V(x)$ is $100nm$ and the value of U_0 is $10meV$.
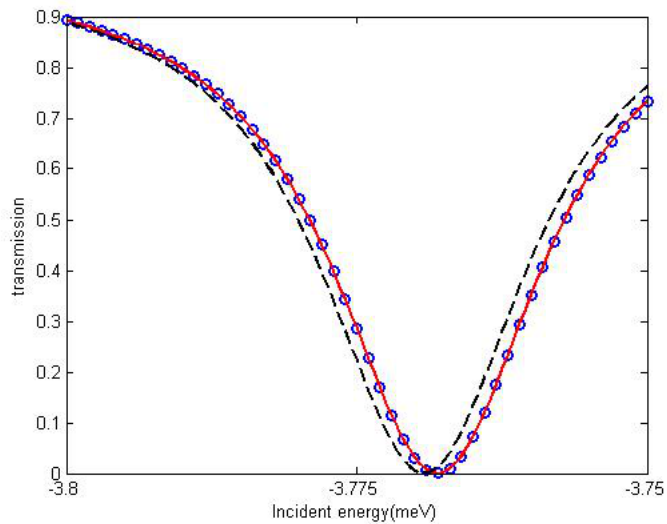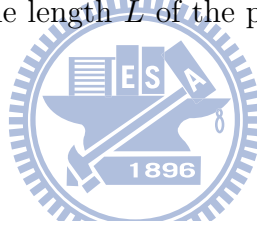
Figure 6.10: It is the transmission of Dip. 1_1 with $W = 200nm$, $L = 100$ and $U_0 = 10meV$ for Markus König's band parameters.[7] The black dash line is FN. The blue circle is MS contributed by propagating mode only. The red solid line is the Fano-profile form (equation (6.17)).
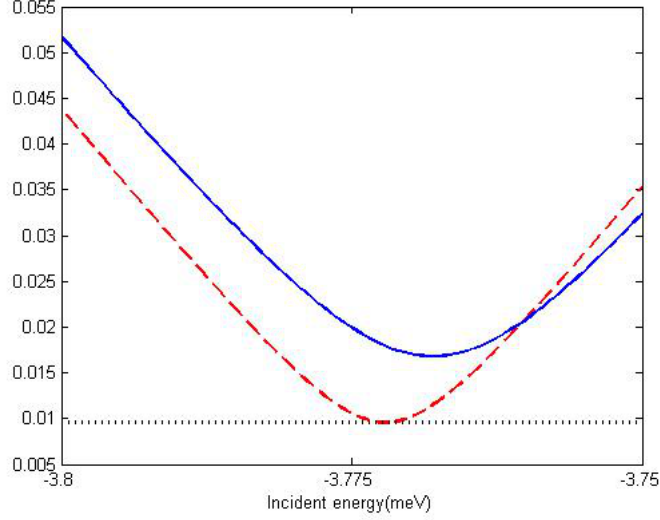
Figure 6.11: It is shows the values of $|1 - r_{bb}r'_{bb} - 2r_{eb}r'_{be}|$, $|1 - r_{bb}r'_{bb}|$ and $|2r_{eb}r'_{be}|$ near the resonant energy. The blue sold line is $|1 - r_{bb}r'_{bb} - 2r_{eb}r'_{be}|$. The red dash line is $|1 - r_{bb}r'_{bb}|$. The black dot sold line is $|2r_{eb}r'_{be}|$.

cause wave function of bulk and edge channels are mismatch, the bulk channel is almost scattered back to the bulk channel. We have $|r_{bb}r'_{bb}| \sim 1$ and $|r_{be}r'_{eb}| << 1$ so we drop $r_{eb}r'_{be}$ in $[1 - \gamma_{MS}]_{ee}$. The life time of the resonant state is very long so $|1 - r_{bb}r'_{bb}| \sim 0$ near the resonant energy. Therefore, the $r_{be}r'_{eb}$ in $[1 - \gamma_{MS}]_{bb}$ must be kept becuase it is the same order to $1 - r_{bb}r'_{bb}$ (See Fig.6.11.). The T^{MS} becomes this form.

$$1 - \gamma_{MS} \approx \begin{pmatrix} 1 & -r_{eb}r'_{bb} \\ -r_{bb}r'_{be} & 1 - r_{bb}r'_{bb} - r_{be}r'_{eb} \end{pmatrix}. \tag{6.15}$$

The system has inversion symmetry so we have $|r_{be}r'_{eb}| = |r_{eb}r'_{be}|$. The inversion matrix of $1 - \gamma_{MS}$ is of the form.

$$\frac{1}{1 - \gamma_{MS}} \approx \frac{1}{G} \begin{pmatrix} 1 - r_{bb}r'_{bb} - r_{be}r'_{eb} & r_{eb}r'_{bb} \\ r_{bb}r'_{be} & 1 \end{pmatrix}. \tag{6.16}$$

Where $G \approx 1 - r_{bb}r'_{bb} - 2r_{eb}r'_{be}$. We think that the dip structures originate from Fano resonance so we predict that G is of the form: $(\varepsilon + ia)^{-1}$. From the numerical fitting, the G is this form. Then, we obtain the value of a.

The T^{MS} becomes this form:

$$T^{MS} \approx t_0 \left(1 + \frac{iZa}{\varepsilon + ia} \right). \tag{6.17}$$

Where $t_0 = t'_e t_e$ and $\frac{iZa}{\varepsilon+ia} = \frac{1}{Gt_0} (t'_e r_{be} r'_{eb} t_e + t'_e r_{eb} r'_{bb} t_b + t'_b r_{bb} r'_{be} t_e + t'_b t_b)$. The life time of the resonant state is $\hbar/a$. The parameter Z is the corresponded Fano factor. The transmission from equation (6.17) is similar to the FN (See Fig. 6.10). The dip structure is described by the equation (6.17). The first term is contributed by a continuous channel and the second term is mainly contributed by a discretized quasi-bound state constructed by the resonant bulk channel. This transmission form is the Fano-profile form.

The transmission coefficient contributed by the quasi-bound state is of the form:

$$T_{qb} = \frac{t_0}{\varepsilon + ia}. \tag{6.18}$$

The quasi-bound state hasing long life time is strong so it is hard to kill this state. However, the state having longer life time is more sensitive to the perturbation near the resonant energy. It is because the value of a is too small to neglect some perturbation terms to a.

In our cases, there are two (more than two) bulk propagating channels and an edge channel in the potential area. One of the bulk channel is resonant at the dip energy. The other's resonant energy is far away from that energy range. The non-resonant bulk channel has significant effect on the dip structure so we need to derive a set of channel vectors which contains the resonant bulk state of the system to obtain the value of Z and a.

To simplify T^{MS}, we represent T^{MS} by the eigenstate $\psi'^{E-U_0}_{+m}$ of γ_{MS}.

$$\gamma_{MS}\psi'^{E-U_0}_{+m} = g^{E-U_0}_{+m}\psi'^{E-U_0}_{+m}. \tag{6.19}$$

Where $g^{E-U_0}_{+m}$ is the corresponded eigenvalue and it indicates which channel it is. The edge channel isn't back scattered by the potential so $g^{E-U_0}_{+e} \approx 0$. The resonant bulk channel forms the quasi-bound state so $angle\left(g^{E-U_0}_{+b}\right) \approx 0$. The others is contributed by the other bulk channels. (In some cases, some of them are contributed by decay channels.) We

define the set of channel vector $\left(\psi'^{E-U_0}_{+1}, \psi'^{E-U_0}_{+2}, ...\right) = \left(\psi'^{E-U_0}_{+b}, \psi'^{E-U_0}_{+e}, ...\right)$. The matrix γ_{MS} is non-hermitian so the set of the channel vector $\left(\psi'^{E-U_0}_{+m}\right)$ is not orthonormal. The proper set of channel must be orthonormal so we define another set of channel $\left(\tilde{\psi}^{E-U_0}_{+m}\right)$.

$$\left|\tilde{\psi}^{E-U_0}_{+1}\right\rangle = \left|\psi'^{E-U_0}_{+1}\right\rangle \qquad\qquad \text{for m = 1.} \qquad (6.20a)$$

$$\left|\tilde{\psi}^{E-U_0}_{+m}\right\rangle = N_m \left(\left|\psi'^{E-U_0}_{+m}\right\rangle - \sum_{n=1}^{m-1} \left|\tilde{\psi}^{E-U_0}_{+n}\right\rangle \left\langle \tilde{\psi}^{E-U_0}_{+n} \left| \psi'^{E-U_0}_{+m}\right.\right\rangle\right) \quad \text{for m > 1.} \qquad (6.20b)$$

In the set of channel vector $\left(\tilde{\psi}^{E-U_0}_{+m}\right)$ that contains the resonant bulk state, the T^{MS} is of the form.

$$T^{MS} \approx t' \frac{1}{1 - \gamma_{MS}} t = \tilde{t}' \frac{1}{1 - \tilde{\gamma}_{MS}} \tilde{t}. \qquad (6.21)$$

Where $[\tilde{\gamma}_{MS}]_{mn} = \left(\tilde{\psi}^{E-U_0}_{+m}\right)^\dagger \gamma_{MS} \tilde{\psi}^{E-U_0}_{+n}$, $\tilde{t}_m = \left(\tilde{\psi}^{E-U_0}_{+m}\right)^\dagger t$ and $\tilde{t}'_m = t' \tilde{\psi}^{E-U_0}_{+m}$. According to the definition of the channel $\tilde{\psi}^{E-U_0}_{+m}$, we can analytically derive the form of $\tilde{\gamma}_{MS}$ and $[\tilde{\gamma}_{MS}]_{mn} = 0$ for $m > n$. (The detial of proof is in the Appendix G.) For example Dip. 1_1, $\tilde{\gamma}_{MS}$ is of the form:

$$\tilde{\gamma}_{MS} = \begin{pmatrix} \tilde{\gamma}^{MS}_{11} & \tilde{\gamma}^{MS}_{12} & \tilde{\gamma}^{MS}_{13} \\ 0 & \tilde{\gamma}^{MS}_{22} & \tilde{\gamma}^{MS}_{23} \\ 0 & 0 & \tilde{\gamma}^{MS}_{33} \end{pmatrix}. \qquad (6.22)$$

(The transmision is mainly dependent on the propagating channels.)

In terms of $\tilde{\gamma}_{MS}$, we can obtain a more simple form of T^{MS}. To derive it, we seperate $\tilde{\gamma}_{MS}$ into $\tilde{\gamma}^{MS}_D$ and $\tilde{\gamma}^{MS}_U$. Where $\tilde{\gamma}^{MS}_D$ is all diagonal terms of $\tilde{\gamma}_{MS}$ and $\tilde{\gamma}^{MS}_U$ contains the other terms. Substituting $\tilde{\gamma}^{MS}_D$ and $\tilde{\gamma}^{MS}_U$ for $\tilde{\gamma}_{MS}$, T^{MS} becomes this form.

$$T^{MS} \approx \tilde{t}' \frac{1}{1 - \tilde{\gamma}_{MS}} \tilde{t} = \tilde{t}' \left[\tilde{\Gamma}^{MS} \sum_{m=0}^{\tilde{N}-1} \left(\tilde{\gamma}^{MS}_U \tilde{\Gamma}^{MS}\right)^m\right] \tilde{t}. \qquad (6.23)$$

Where $\tilde{N} = Rank\left(\tilde{\gamma}_{MS}\right)$ and $\tilde{\Gamma}^{MS} = \left(1 - \tilde{\gamma}^{MS}_D\right)^{-1}$. Becuase $(\tilde{\gamma}^{MS}_U \tilde{\Gamma}^{MS})^{\tilde{N}} = 0$, the higher order terms of $\tilde{\gamma}^{MS}_U \tilde{\Gamma}^{MS}$ are exactly zero. The T^{MS} becomes a finite summation of $\tilde{\Gamma}^{MS}$

and $\tilde{\gamma}_U^{MS}$. In this form, it is much easier to drop the small terms of T^{MS}.

For the Dip 1_1, Dip 2_1, Dip 3_1 and Dip 1_2, the $\tilde{t}'\tilde{\Gamma}^{MS}(\tilde{\gamma}_U^{MS}\tilde{\Gamma}^{MS})^2\tilde{t}$ term is small enough to be neglect. Therefore, we only keep the $\tilde{t}'\tilde{\Gamma}^{MS}\tilde{t}$ and $\tilde{t}'\tilde{\Gamma}^{MS}\tilde{\gamma}_U^{MS}\tilde{\Gamma}^{MS}\tilde{t}$ terms. The energy range we focus on is far away from the other resonant energies so we can only keep the directly tunneling term and the quasi-bound state dependent terms. The T^{MS} is Fano profile form.

$$T^{MS} \approx t_0 \left(1 + \frac{Zia}{\varepsilon + ia} \right). \tag{6.24}$$

Where $t_0 = \tilde{t}'_2\tilde{t}_2$ and $\frac{iZa}{\varepsilon+ia} = \frac{1}{\tilde{t}'_2\tilde{t}_2}\tilde{\Gamma}_{11}^{MS}\left(\tilde{t}'_1\tilde{t}_1 + \sum_{m=2}^{\tilde{N}} \tilde{t}'_1\left[\tilde{\gamma}_{MS}^U\right]_{1m}\tilde{\Gamma}_{mm}^{MS}\tilde{t}_m \right)$. The transmission of the Fano profile form is showed in Fig. 6.8. It is similar to the FN so the dips are characterized by Fano physics. The Fano factor Z is -1 for all this kind of the dips so the edge channel is totally back scattered at the resonant energy. This value of Z is independent of the value of the band parameter, L, W and U_0. It seems that the value of Z is protected by a symmetry which is unknowen. Because the edge channel is totally back scattering at the dip energy, we can use the dip structure to be a switch of edge current.

6.3 The transport property in the presence of DSOI

In this section, we calculate the transmission property of the quantum bar with DSOI. We include the DSOI terms in the effective 1D Hamiltonian that we have used in the section 7.1. The potential commutes with pseudo-parity operator π_p so we can use the effective Hamiltonian $\tilde{H}_W$ to describe system. The $\tilde{H}_W$ (equation (5.10)) reads

$$\tilde{H}_W = \begin{pmatrix} h'^W_+ (k_x) & 0 \\ 0 & h'^W_- (k_x) \end{pmatrix}, \tag{6.25}$$

where $h'^W_\mu = \tilde{E} + \mu\tilde{\delta} + \tilde{A}k_x + \tilde{B}k_x^2$ and the μ indicates the quantum number of pseudo-parity. The operator $\tilde{E}$, $\tilde{\delta}$, $\tilde{A}$ and $\tilde{B}$ are defined in equations (5.11)-(5.14). The $\mu = 1$ and $\mu = -1$ parts are decoupled. Besides, the $\mu = -1$ part is like the $\mu = 1$ part with minus

C. We can compute the scattering state only with the even part or the odd part only. According to equation (3.17), we can calculate the eigenstate of h'^W_μ for given energy E by diagonalizing this matrix h'_μ.

$$h'_\mu(E) = \begin{pmatrix} 1 & 0 \\ 0 & \tilde{B} \end{pmatrix}^{-1} \begin{pmatrix} 0 & 1 \\ -E + \tilde{E} + \mu\tilde{\delta} & \tilde{A} \end{pmatrix} \tag{6.26}$$

Then we obtain the eigenstate $\psi^E_{\mu pm}$ as this form.

$$\psi^E_{\mu pm}(x) = e^{ik^E_{\mu pm}x} f^E_{\mu pm}. \tag{6.27}$$

Where $f^E_{\mu pm}$ is the column vector of mth eigenstate with $k_x = k^E_{\mu pm}$ and the p is the propagation diection or decay diection of $\psi^E_{\mu pm}$. Doing the similar procedure in section 7.1 and 7.2, we can derive the scattering state $\Phi^E_{\mu p}$ and the transmission ceofficient $T^{MS}_{\mu p}$.

$$T^{MS}_{\mu p} = t'_{\mu p} \frac{1}{1 - \gamma^{MS}_{\mu p}} t_{\mu p} \tag{6.28}$$

$$\approx \tilde{t}'_{\mu p} \left[\tilde{\Gamma}^{MS}_{\mu p} \sum_{m=0}^{\tilde{N}-1} \left(\tilde{\gamma}^{MS}_{U,\mu p} \tilde{\Gamma}^{MS}_{\mu p} \right)^m \right] \tilde{t}_{\mu p}. \tag{6.29}$$

Where $\tilde{t}'_{\mu p}$, $\tilde{t}_{\mu p}$, $\tilde{\Gamma}^{MS}_{\mu p}$ and $\tilde{\gamma}^{MS}_{U,\mu p}$ in equation (6.29) are derived from the channel $\psi^E_{\mu pm}$ with the same equation of $\tilde{t}'$, $\tilde{t}$, $\tilde{\Gamma}^{MS}$ and $\tilde{\gamma}^{MS}_U$. The DSOI terms are independent of k_x so the current density of $\Phi^E_{\mu p}$ is the equal to equation (6.7). Then we can obtain the FN and MS result of the state $\Phi^E_{\mu p}$.

For given W, U_0, L and incident energy, the transmission is indepndet of the incident direction and the pseudo-parity of the scattering state. The reason of this result is unknow because the time reversal symmetry only makes the transmission of $\Phi^E_{\pm\pm}$ be equal to $\Phi^E_{\mp\mp}$. The symmetry between state Φ^E_{+p} and Φ^E_{-p} isn't due to the rotation symmetry because the rotation operator simultaneously changes the μ and p. In addition, the magnitude of the wave vector of the incident channel of $\Phi^E_{\mu+}$ (See Fig.6.18-6.19.) is different so there is no explanation for this result.

The Fig. 6.12 shows the transmission for fixed incident energy. The reflection of the cases with DSOI are smaller than the case of without DSOI. It is because the DSOI terms
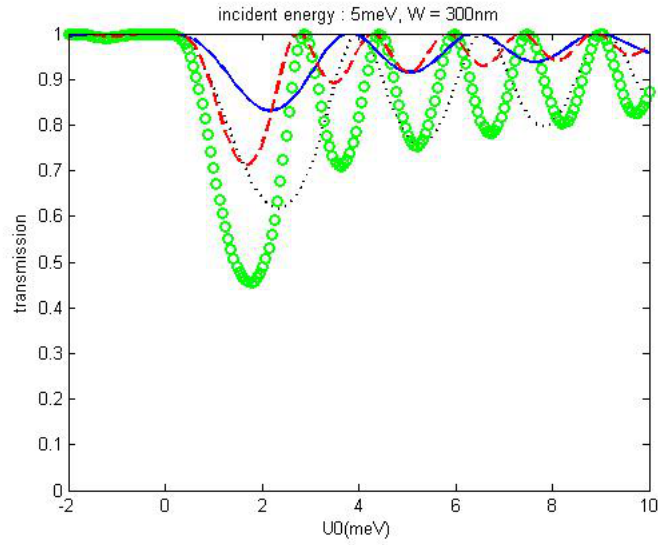
Figure 6.12: It is the transmission from FN versus U_0 for H_W and $\tilde{H}_W$. The width W of the quantum channel is $300nm$ and the incident energy is $5meV$. The blue solid line is for $L = 300nm$. The red dash line is for $L = 500nm$. The black dot solid line is for $L = 300nm$. The green circle is for $L = 500nm$. The soild line and dash line is for $\tilde{H}_W$ and The dot line and circle is for H_W.
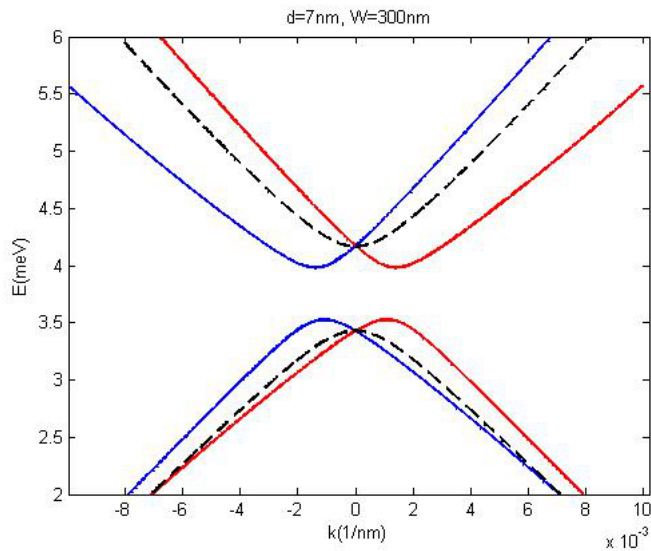
Figure 6.13: It shows edge band gap for H_W and $\tilde{H}_W$. The black dash line is for H_W. The solid lines are for $\tilde{H}_W$.

51

makes the edge band gap smaller (See Fig. 6.13.). The energy gap correction isn't due to the DSOI terms between the edge subbands but it is mainly due to the terms between the bulk and edge subbands. In the section 7.1, we have showed that the more smaller edge band gap is, the more robust edge channels are. It is more difficult to back scatter the edge channel with smaller edge band gap by the potential so the reflection become smaller.

The Fig. 6.14 shows the transmission structure for fixed U_0. The dip near $4meV$ is the edge band gap of the incident edge channel. The DSOI terms make the edge band gap smaller so the dip is more narrow than the no DSOI case. The dips below the edge band gap are also characterized by Fano physics. From the right to left, the dips are Dip. 1_1, Dip. 2_1, Dip. 3_1 and Dip. 1_2. Becuase the DSOI terms modulate the bulk channels, the minimum of the dips and the resonant energy are changed.

The dips are mainly depend on the propagating modes and their $T_{\mu p}^{MS}$ is also described by the equation (6.24). The a corresponds to the widthness of the dip and the t_0 corresponds to the maximum of the transmission. (Our result shows that the phase of t_0 is independent of μ and p.) The value of the t_0 and a is indenpendent of the μ and p because the transmission only depends on W, U_0, L and the incident energy (for given band parameter).

Becuase the DSOI terms modulate the bulk channels, the a and the Fano factor depend on the value of δ. The Fig 6.15-6.17 show the minimum, a and the Fano factor of the Dip. 1_1 are dependent on the value of δ. The minimum of the dips change with δ and we find that the value of δ for CdTe/HgTe/CdTe quantum well isn't small. The Dip. 1_1 is removed at $\delta = 0.4\delta$(ours) and appears again for larger δ. The δ is large enough to induce the dip again. The minimum of the dip is non-sensitive to the δ at the range of $\delta \approx \delta$(ours). It is hard to tune the Fano factor by changing δ. (In our case, the δ doesn't change with an electric field.)

The Fig. 6.18-6.19 show the maximum of the density of the scattering state is different for different pseudo-parity. It is becuase the Fano factor $Z_{\mu p}$ depends on the pseudo-parity (See Fig. 6.17). The Fano factor $Z_{\mu p}$ depends on the pseudo-parity and the incident direction.

The $Z_{\mu p}$ is always real for those kind of the dips. (We doesn't know the reason yet.)
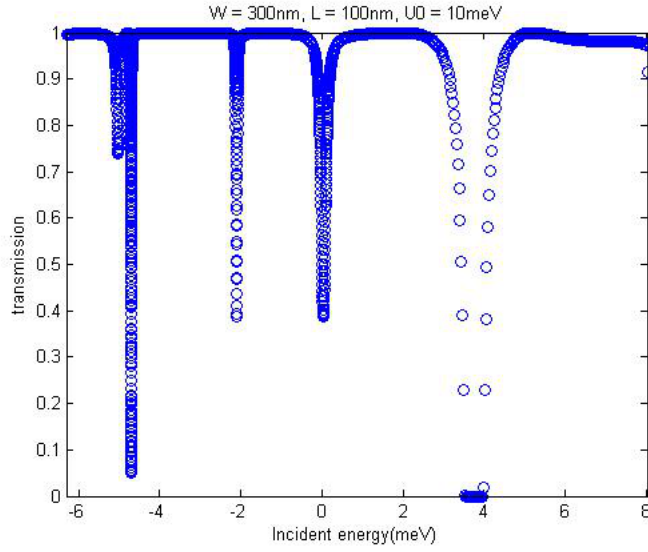
Figure 6.14: It is the transmission from FN versus the incident energy for $\tilde{H}_W$. The width W of the quantum channel is $300nm$. The length L of the potential $V(x)$ is $100nm$ and the value of U_0 is $10meV$.
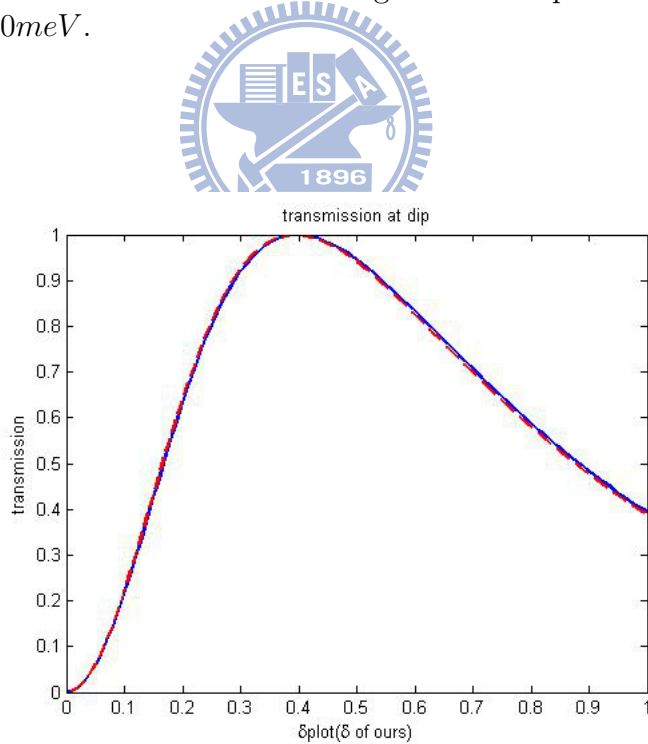
Figure 6.15: It shows the transmission at the Dip. 1_1 from FN and MS versus the value of δ of H_{eff}. The unit of the x-axis is our δ result at $d = 7nm$. The width W of the quantum channel is $300nm$. The length L of the potential $V(x)$ is $100nm$ and the value of U_0 is $10meV$. The dash line is the FN. The solid line is the MS with the propagating modes only.
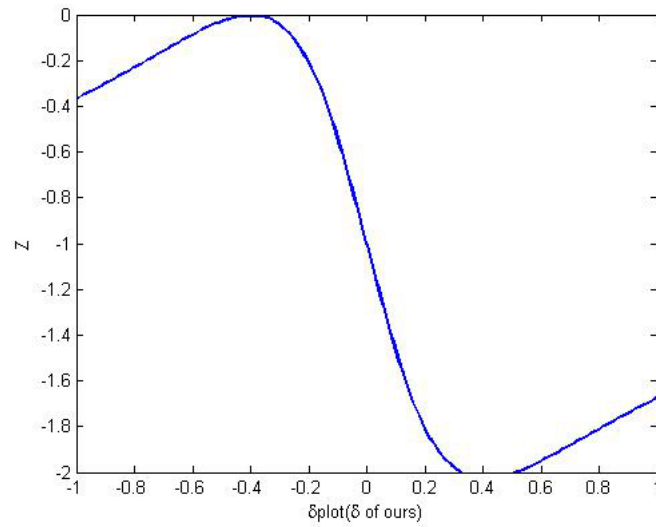
Figure 6.16: It shows the value of the Fano factor of the Dip. 1_1. The minus δ_{plot} range shows the result of h'^W_- because the h'^W is equal to the h'^W_+ with minus C value. The Fano factor derive from the equation (6.24). The other parameters are the same as Fig. 6.15.
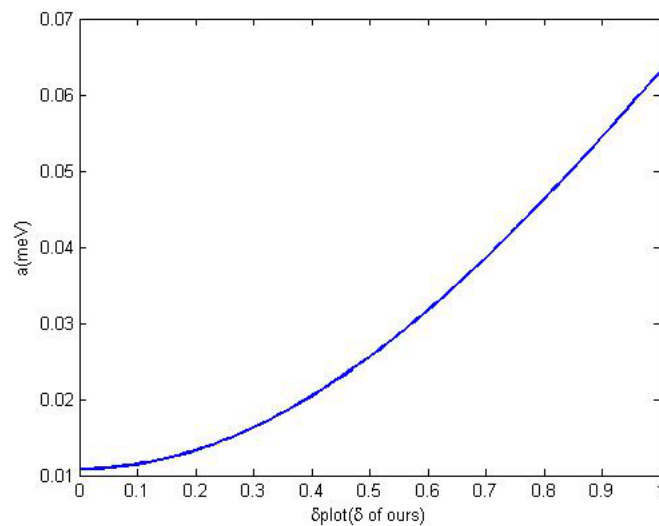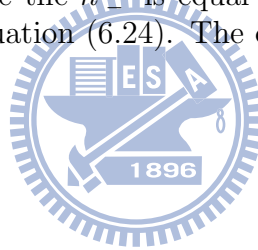
Figure 6.17: It shows the value of a of the Dip. 1_1. The other parameters are the same as Fig. 6.15.
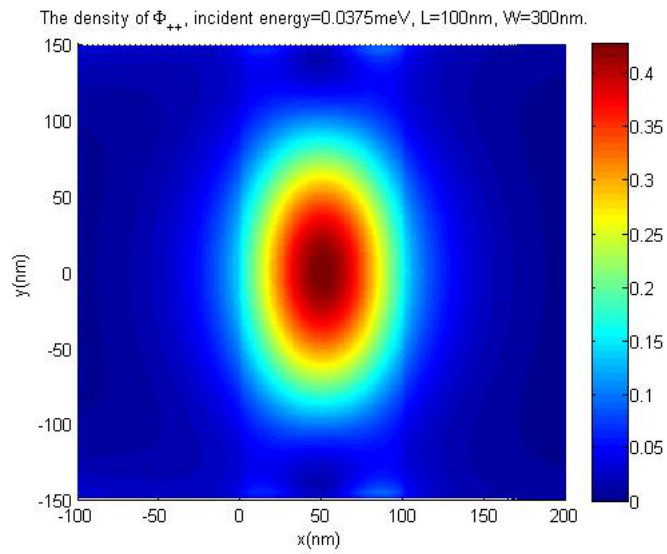
Figure 6.18: It shows the density of Φ_{++} from FN at the Dip. 1_1 (The incident energy is $0.0375 meV$.). The other parameters are the same as Fig. 6.15.
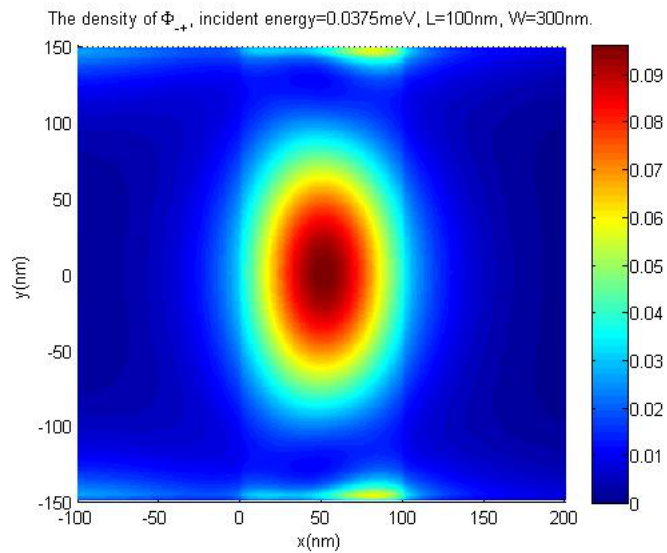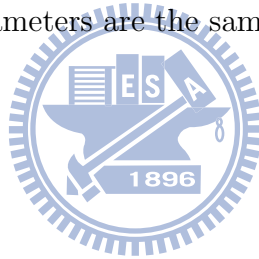
Figure 6.19: It shows the density of Φ_{-+} from FN at the Dip. 1_1 (The incident energy is $0.0375 meV$.). The other parameters are the same as Fig. 6.15.
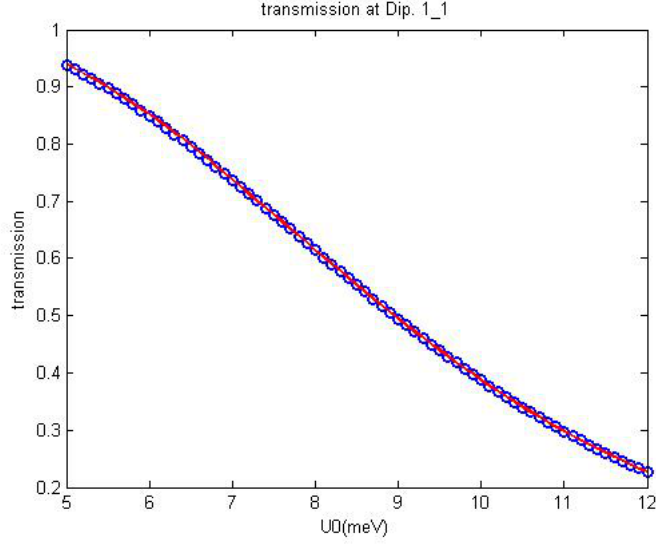
Figure 6.20: It shows the transmission at the Dip. 1_1 from FN and MS versus the value of U_0. The width W of the quantum channel is $300nm$ and the length L of the potential $V(x)$ is $100nm$. The circle is the FN. The solid line is the MS with the propagating modes and the longest decay mode only.
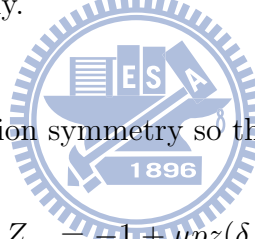
The system doesn't have inversion symmetry so the $Z_{\mu p}$ is dependent on μ.

$$Z_{\mu p} = -1 + \mu p z(\delta, U_0, L) \tag{6.30}$$

Where z is a function of δ and $z(\delta = 0) = 0$. In the presence of DSOI, the value of $Z_{\mu p}$ isn't -1 and it becomes dependent on the L and U_0. The Fig. 6.20 shows the minimum of the Dip. 1_1 versus U_0. We can tuning the minimum of the dip by changing U_0 so we can tuning the Fano factor by the U_0.

In Fig. 6.21-6.22, we show the values of the $Z_{\mu p}$ and a depend on U_0. In this case the longest decay channel contributes not small terms to $T_{\mu p}^{MS}$. We keep those terms to calculate the $Z_{\mu p}$ and a. In this case, the $\left(\tilde{\gamma}_{U,\mu p}^{MS} \tilde{\Gamma}_{\mu p}^{MS} \right)^3$ term is small enough to be negelected. The $T_{\mu p}^{MS}$ is of the form.

$$T_{\mu p}^{MS} \approx \tilde{t}_{\mu p}' \left[\tilde{\Gamma}_{\mu p}^{MS} \sum_{m=0}^{2} \left(\tilde{\gamma}_{U,\mu p}^{MS} \tilde{\Gamma}_{\mu p}^{MS} \right)^m \right] \tilde{t}_{\mu p} = t_0 \left(1 + \frac{Z_{\mu p} i a}{\varepsilon + ia} \right). \tag{6.31}$$

The $T_{\mu p}^{MS}$ is the Fano profile form so we seperate it into two part t_0 and $(it_0 Z_{\mu p} a)/(\varepsilon + ia)$.
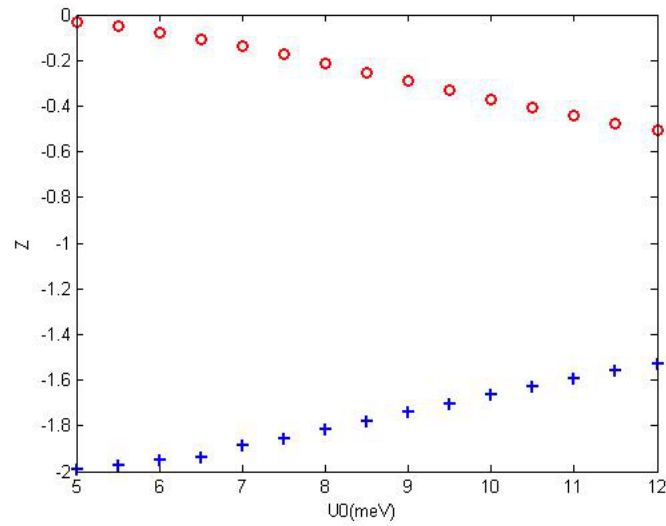
Figure 6.21: It shows the value of Fano factor of the Dip. 1_1. The $Z_{\mu p}$ is derived from equation (6.31). The circle is for $\mu = -1$. The plus sign is for $\mu = 1$. The other parameters are the same as Fig. 6.20.
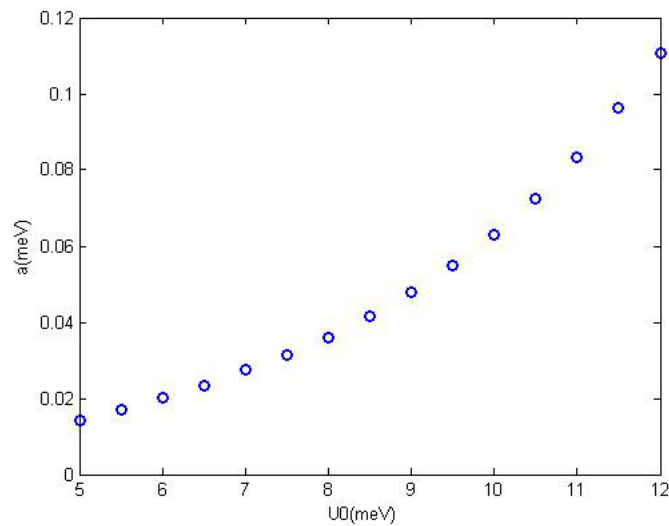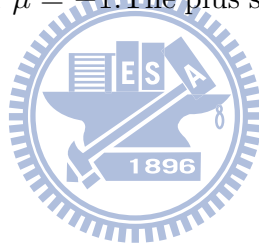
Figure 6.22: It shows the value of a of the Dip. 1_1. The other parameters are the same as Fig. 6.20. (At the potential range near $6.7meV$, we can't obtain a.)

Where the $\left[\tilde{\Gamma}_{\mu p}^{MS}\right]_{11}$ dependent term contributes $(t_0 Z_{\mu p} ia)/(\varepsilon + ia)$ and the t_0 contains the other terms.

From the result above, we find out that the Fano resonances can help us to swtich the location of the edge states. In section 6.2, we have showed the state $\Phi_{E,p}^{edge}$ that is the linear spuerposition of the $\psi_{E,+p}^{edge}$ and $\psi_{E,-p}^{edge}$ can be at one edge of the sample.

$$\Phi_{E,p}^{edge}(x,y) = \frac{1}{\sqrt{2}} e^{ik_{E,+p}^{edge}x} \left[f_{E,+p}^{edge}(y) + e^{i\Delta'(x)} f_{E,-p}^{edge}(y) \right]. \tag{6.32}$$

Where $f_{E,\mu p}^{edge}(y)$ is the column vector part of $\psi_{E,\mu p}^{edge}(x,y)$ and $\Delta'(x) = \Delta'_0 + \left(k_{E,-p}^{edge} - k_{E,+p}^{edge}\right)x$. If we can change $\Delta'(x)$ form $\Delta'(x_0)$ to $\Delta'(x_0) + \pi$, we can switch location of the $\Phi_{E,p}^{edge}$.

The transmission coefficient $T_{\mu p}^{MS}$ near the resonant energy of the Fano-type transmission dip is of the form.

$$T_{\mu p}^{MS} \approx t_0 \left(1 + \frac{Z_{\mu p} ia}{\varepsilon + ia}\right) = t_0 \frac{\varepsilon + \mu p z(\delta, U_0, L) ia}{\varepsilon + ia}. \tag{6.33}$$

If the incident state is $\Phi_{E,+}^{edge}$, the transmited state $T[\Phi_{E,+}^{edge}(x,y)]$ is

$$T[\Phi_{E,+}^{edge}(x,y)] = \frac{1}{\sqrt{2}} \left[f_{E,++}^{edge}(y) + e^{i\Delta'_p} f_{E,-+}^{edge}(y) \right]. \tag{6.34}$$

The relative phase Δ'_p at the resonant energy is of the form:

$$e^{i\Delta'_p} = \frac{+pz(\delta, U_0, L)ia}{-pz(\delta, U_0, L)ia} = -1. \tag{6.35}$$

If the incident state $\Phi_{E,p}^{edge}$ is at one edge of the sample, the transmited state $\tilde{\Phi}_{E,p}^{edge}$ is at the opposite edge. The location of the edge state can be switch by the square potential and the potential also changes the spin polarization of the edge state. (See section 6.2.) The Fig. 6.23-6.24 show that it works and the side of the edge state is really changed. The edge-switchung length L_c from the difference of k_x is about $30um$ in this case. Fano physics give a much shorter device to switch the spin and the location.

In Fig. 6.15, the edge state totally transmits the potential barrier but Fano resonance still exist at that energy. At that kind of case, the transmission property still obeys Fano physics. Therefore, there exist some structures that we can't distinguish by the

transmission. The structures can make the same thing that the dips can because they are all described by the Fano physics. For example, the Dip. 4_1 for $W = 300nm$, $L = 100nm$ and $U_0 = 15meV$ is removed from the transmission spectra in the pressnce of DSOI. The Fig. 6.25-6.26 show that pure spin edge state totally transmits the potential and the spin polarization is changed by the potential. (In this case the L_c is about $270um$.)
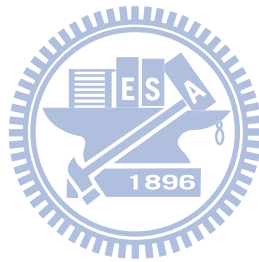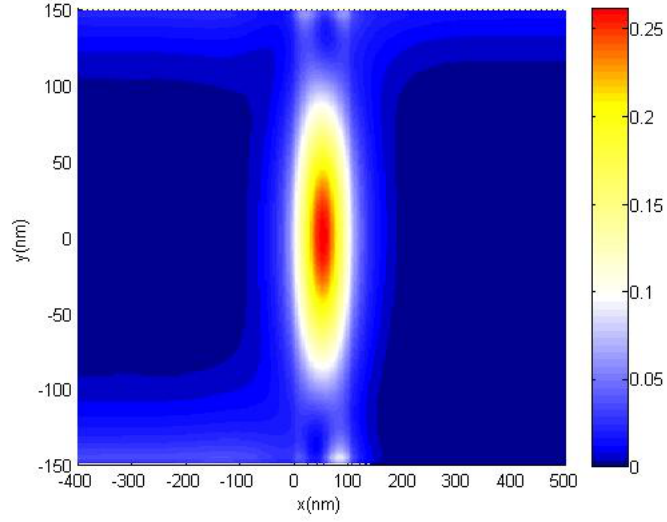
Figure 6.23: It shows the density of the $\Phi_{E,+}^{edge}(x,y)$. The potentila energy U_0 is $10meV$ and the incident energy is $0.0375meV$ (Dip. 1_1). The width W of the quantum channel is $300nm$ and the length L of the potential $V(x)$ is $100nm$. The incident state is localized at the edge $y = -150nm$. The reflection and transmission states are localized at the edge $y = 150nm$.
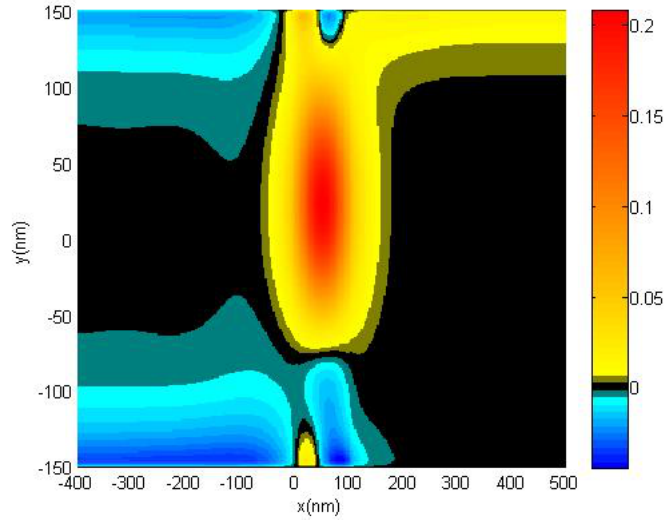
Figure 6.24: It shows the spin polarization density of the $\Phi_{E,+}^{edge}(x,y)$. The parameters of the system are as the same as Fig 6.23.
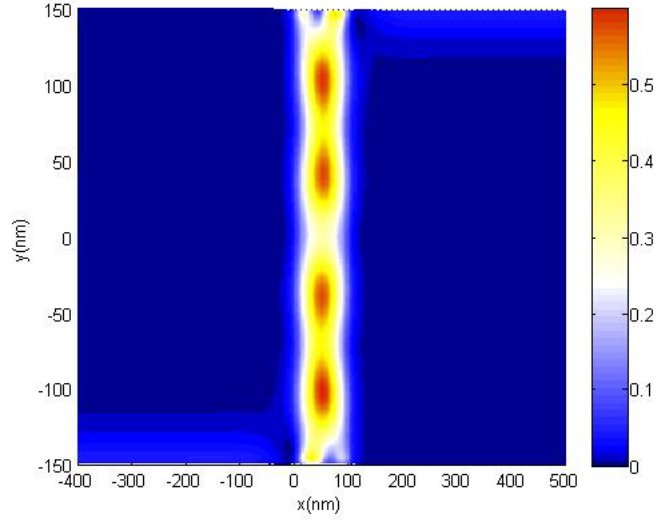
Figure 6.25: It shows the density of the $\Phi_{E,+}^{edge}(x,y)$. The potentila energy U_0 is $15meV$ and the incident energy is $-2.808meV$ (Dip. 4_1). The width W of the quantum channel is $300nm$ and the length L of the potential $V(x)$ is $100nm$. The incident state is localized at the edge $y = -150nm$. The reflection and transmission states are localized at the edge $y = 150nm$.
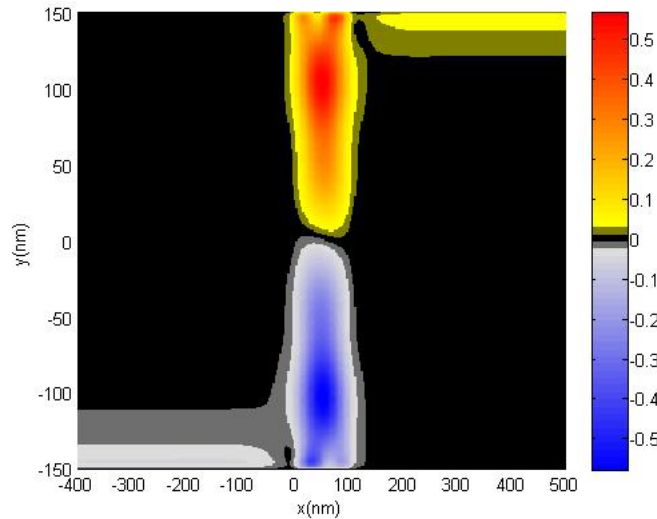
Figure 6.26: It shows the spin polarization density of the $\Phi_{E,+}^{edge}(x,y)$. The parameters of the system are as the same as Fig 6.25.

Chapter 7

Summary

7.1 Conclusion

In chapter 2, we have show our result of the effective 2D Hamiltonian which describe the energy range we are interesting in of the CdTe/HgTe/CdTe equantum well. DSOI couples the conduction and heavy hole bands. The coupling removes the energy crossing of the bands.

In chapter 3, we study the edge state solution in an semi-infinity boundary system. The gapless edge state exists for H_{eff} when $\Delta = MB - (B\delta/A)^2 > 0$ and $|B| > |D|$. The gapless property is due to time reversal symmetry and a pair of edge bands. DSOI doesn't induce any other edge bands so there are only two edge bands in the system. Beside, the time reversal symmetry protects a two level degeneracy at Γ point. Therefore the energy dispersion of the edge states must be crossing and the edge energy gap is still closed if we include DSOI. The edge bands are gapless and the system is still topologically non-trivial if $\Delta > 0$. On the other hand, the DSOImakes some systems that are topologically non-tirival without DSOI become topologically trivial. The DSOI does effect the topological property of the 2D electronic system.

In chapter 4, we try to obtain the topological number by chern number, winding number and spin chern number method. In chern number consideration, we can't tell the topological phase changing as the value of d changing. The chern number is zero with the eigenstate of the H_{eff} including δ. The zero property of the chern number is due

62

to the form of the eigenstates above. On the other hand, we can obtain the non-trivial chern number by another set of eigenstate for $\delta = 0$ case. The two kinds of eigenvectors describe the same system but the chern number of those two kinds of eigenfunction are different. Therefore the chern number is not invariant under guage transformation.

In winding number or spin chern number considerations, we can obtain the condition of the topological phase change. But winding number only works for 2×2 Hamiltonian and we must drop the region near the Γ point of the 2D k space to obtain this result. In addition, the topological phase diagram from spin chern number consideration is dependent on the generator (the detail of the derivation). Sometimes we can't know the topological number of a set of band parameter with only one generator. We need a proper way to obtain the generator.

In chapter 5, we derive the effective 1D Hamiltonian of a quantum bar. Then, we discuss the edge states and the edge channels in the quantum bar. The edge channels in the following are the eigenstates of the effective 1D Hamiltonian. The edge state in the following is the superposition of the edge channels with the same energy and propagation direction.

In section 5.1, we derive the effective 1D Hamiltonian of the width W quantum bar. The effective 1D Hamiltonian has a symmetry that we call pseudo-parity. The eigenstates have different pseudo-parity are only coupled by y-dependent potential (magnetic field). (The y-direction is the transverse direction.) Therefore, we use the pseudo-parity to simplify the calculations in chapter 6.

In section 5.2, we discuss the property of the edge states and the edge channels. Where the edge channels are the eigenstates of the 1D Hamiltonian with specific wave vector. The DSOI terms mix spin so the edge channels isn't a pure spin state. The edge channels are localized at the two edges so the magnetic impurity near any edges of the sample will effect all of edge channels.

On the other hand, by the edge injection, we can generate an edge state that is a pure spin state and localized at an edge of the sample Where the edge state is linear superposition of the edge channels that have the same energy and propagation direction. The location of the edge state is determined by the relative phase between the edge channels. The finite size effect[4] and DSOI make relative phase vary in x, the longitudinal

direction. The location of the edge state will change when it is propagating. The spin polarization of the edge state changes with the location so the spin polarization will automatically precess.

In chapter 6, we discuss the transmission property of edge states in a quantum bar. First we discuss the transmission structure through a square potential in no DSOI system. The edge band gap is not zero in a quantum bar system because of finite size effect. We show that the edge channels are back scattered by a potential at the energy range near the energy gap. The pseudo-spin of the edge channel at that energy range becomes energy dependent so the reflection is not zero. Though the non-zero edge band gap makes the edge channels scattered by the potential, the edge channel still totally transmits at the energy range not near the energy gap.

On the other hand, we show the transmission dips at the energy range not near the edge band gap is due to the Fano resonance. The edge channel forms the continuum spectrum and the resonance bulk channel froms the discrete state (quasi-bound state). Because the life time of the resonance bulk state are very long, we need to change the representation channel to calculate the Fano factor and life time of quasi-bound state. For the system without DSOI, the Fano factors are always -1 and the edge channels are totally back scattered at the dip energy.

Finally, we discuss the transmission structure through a square potential in the presence of DSOI. The edge channels are more robust against a potential because the edge energy gap is smaller to the no DSOI case. The edge energy gap reduction is mainly due to the coupling between edge and bulk subbands. On the other hand, the transmission dips at the energy range not near the edge band gap are still characterized by the Fano resonance. The Fano factors now depend on the potential energy (or the length of the potential). The edge channels aren't totally back scattered at the dip energy. The additional phase from the Fano resonance is dependent on the pseudo-parity. We can use this to change the spin polarization and the location side of the edge state. The potential can be much shorter than the edge-switching length L_c so we can change the spin without a very long (large) device.

7.2 Future work

According to the result in this thesis, we have three new questions to study. The first is the transmission property through the potential that breaks the pseudo-parity. The transverse position operator breaks the pseudo-parity symmetry. So the transmission of quantum point contact or a side gate is different to the case we consider. The potential may can split the spin of the edge bands so we may have another way to modulate the spin and the side of the edge bands.

The second is what is the origin of the surface states at the boundary between normal and topological non-trivial materials. The topological physics predicts we can find surface states at the boundary between the topological trivial and topological non-trivial materials. According to our study in the chapter 3, we find out that the bulk energy gap closing can change decay direction of the wave vector, vertical to the surface. Besides, the gap-closing can also change the topological number.[19] Therefore, the decay wave vectors having the same pseudo-spin direction at different region have opposite decay direction. The pair of decay wave vectors form a surface state at the surface. Is it the origin of the surface states?

The final is what is the transport of the edge channels in a very dirty quantum bar. In a quantum channel, DSOI makes the edge channels that have different pseudo-parity can be coupled by normal impurity. The phase difference bewteen the edge channels determines the spin polarization of the edge states. The spin of the edge state may not depend on L_c. On the other hand, the finite size effect makes the edge channels can be back scattered. DSOI lets the all edge channels can be coupled by impurity only. This can occur without any bulk channel at the Fermi energy. The transport of the edge channels in a very dirty system may not be a trivial question.

Appendix A

Detail derivation: From basic band formulation to effective 2D Hamiltonian

In this appendix, we start our derivation from the 3D 8×8 Kane Hamiltonian with DSOI.[6] The energy range we focus upon is far away from the split-off bands. To simplify the problem, we reduce the Hamiltonian into the 3D 6×6 Kane Hamiltonian. Some of the perturb terms are smaller than the others so we justify and drop the smaller terms.

Then, we show how to derive an effective 2D Hamiltonian with C terms that are originated from DSOI. For checking the band structure, we derive two effective 2D Hamiltonians. One is with the basis independent of DSOI terms and the other is with the basis depending on the Ck_z terms in $H^{3D}_{6 \times 6}$. Then we discuss the isotropy and the gap closing of the band structure. At the final section, we derive the effective 2D 4×4 Hamiltonian that we use in this thesis for describing the band structure of conduction and heavy hole bands.

Our result shows the energy crossing of the conduction and heavy hole bands is at well thickness $d_c \approx 6.6nm$ and it is not equal to ref.[1] This difference doesn't comes from keeping the correction of effective mass but comes from the difference of band parameter of Kane Hamiltonian. (In the ref[1], they use HgCdTe instead of CdTe.) Only the energy band gap of the effective four band Hamiltonian is much different to the other groups'

result and it doesn't change the topological physics (See chapter 6.).

Ck_z terms perform like constant in the effective 2D Hamiltonian so it must be kept when we keep γ terms (effective Luttinger parameters) in $H_{6\times6}^{3D}$. C terms remove the band crossing at Γ point but it doesn't make the global band gap always opened. It make the Dirac point becomes the Dirac ring with critical k_c and the gap is still closed at $d \approx 6.6nm$.

Even C and γ terms both make the band structure be anisotropic. The energy difference of conduction and heavy hole bands versus the direction of k is still small. By dropping the neglectable terms in $H_{10\times10}^{3D}$, we obtain the effective 4×4 Hamiltonian H_{eff} that has been announced at ref[7].

A.1   3D 8×8 Hamiltonian

The lattice structures of HgTe and CdTe are zinc blende structure so they do not have center of inversion. It makes those materials be BIA. This symmetry broken makes a spin orbital interaction well known as DSOI. We introduce DSOI effect by adding C terms in Kane Hamiltonian[6]. Those terms appear at H_h and H_{hs} listed below.

We start our study from Kane Hamiltonian that contains $\Gamma6$(conduction band), $\Gamma8$(hole band) and $\Gamma7$(split-off band) subbands. In the order of basis vector $(|\Gamma6, 1/2\rangle, |\Gamma6, -1/2\rangle,$ $|\Gamma8, 3/2\rangle, |\Gamma8, 1/2\rangle, |\Gamma8, -1/2\rangle, |\Gamma8, -3/2\rangle, |\Gamma7, 1/2\rangle, |\Gamma7, -1/2\rangle)$, 3D 8×8 Kane Hamiltonian $H_{8\times8}^{3D}$ is of the form:

$$H_{8\times8}^{3D} = \begin{pmatrix} H_c & H_{ch} & H_{cs} \\ H_{ch}^\dagger & H_h & H_{hs}^\dagger \\ H_{cs}^\dagger & H_{hs} & H_s \end{pmatrix}. \tag{A.1}$$

$$H_c = E_c + Tk^2.$$

$$H_s = E_s - \gamma_1 k^2.$$

$$H_{cs} = \begin{pmatrix} -\frac{1}{\sqrt{3}}Pk_z & -\frac{1}{\sqrt{3}}Pk_- \\ -\frac{1}{\sqrt{3}}Pk_+ & \frac{1}{\sqrt{3}}Pk_z \end{pmatrix}.$$

APPENDIX A. DETAIL DERIVATION: FROM BASIC BAND FORMULATION TO EFFECTIVE 2D HAMILTONIAN

$$H_{ch} = \begin{pmatrix} -\frac{1}{\sqrt{2}}Pk_+ & \sqrt{\frac{2}{3}}Pk_z & \frac{1}{\sqrt{6}}Pk_- & 0 \\ 0 & -\frac{1}{\sqrt{6}}Pk_+ & \sqrt{\frac{2}{3}}Pk_z & \frac{1}{\sqrt{2}}Pk_- \end{pmatrix}.$$

$$H_{hs} = \begin{pmatrix} \frac{1}{\sqrt{2}}R_{++} & -Q & \sqrt{\frac{3}{2}}R_{-+} & \sqrt{2}S_{-+} \\ -\sqrt{2}S_{+-} & \sqrt{\frac{3}{2}}R_{+-} & Q & -\frac{1}{\sqrt{2}}R_{-+} \end{pmatrix}.$$

$$H_h = \begin{pmatrix} \begin{matrix} E_v - T_H k_z^2 \\ -T_{Hp}k_p^2 \end{matrix} & R_{--} & S_{-+} & -\frac{\sqrt{3}}{2}Ck_- \\ R_{+-} & \begin{matrix} E_v - T_L k_z^2 \\ -T_{Lp}k_p^2 \end{matrix} & \frac{\sqrt{3}}{2}Ck_+ & S_{--} \\ S_{++} & \frac{\sqrt{3}}{2}Ck_- & \begin{matrix} E_v - T_L k_z^2 \\ -T_{Lp}k_p^2 \end{matrix} & -R_{-+} \\ -\frac{\sqrt{3}}{2}Ck_+ & S_{+-} & -R_{++} & \begin{matrix} E_v - T_H k_z^2 \\ -T_{Hp}k_p^2 \end{matrix} \end{pmatrix}.$$

Where $S_{\mu\nu} = \left(\gamma_+ k_\mu^2 + \gamma_- k_{-\mu}^2\right) + \nu C k_z$, $R_{\mu\nu} = \gamma k_\mu k_z + \frac{\nu}{2}Ck_{-\mu}$, $Q = \sqrt{2}\gamma_2\left(k_p^2 - 2k_z^2\right)$, $k^2 = k_x^2 + k_y^2 + k_z^2$, $k_p^2 = k_x^2 + k_y^2$ and $k_\mu = k_x + \mu i k_y$. The parameters list above are $T = \frac{\hbar^2}{2m_0}(1 + 2F)$, $T_H = \frac{\hbar^2}{2m_0}(\gamma_1 - 2\gamma_2)$, $T_L = \frac{\hbar^2}{2m_0}(\gamma_1 + 2\gamma_2)$, $T_{Hp} = \frac{\hbar^2}{2m_0}(\gamma_1 + \gamma_2)$, $T_{Lp} = \frac{\hbar^2}{2m_0}(\gamma_1 - \gamma_2)$, $\gamma = 2\sqrt{3}\frac{\hbar^2}{2m_0}\gamma_3$, and $\gamma_\mu = \frac{\sqrt{3}}{2}\frac{\hbar^2}{2m_0}(\gamma_2 + \mu\gamma_3)$.

m_0 is the mass of free electron. The parameter E_c, E_v, E_s, P, F, γ_1, γ_2, γ_3 and C depend on the material and their values are listed at Table A.1.

Table A.1: The band structure parameter of HgTe and CdTe

	E_c	E_v	E_s	P	F
HgTe	$-0.303eV$	$0eV$	$-1.08eV$	$8.46eV\cdot\text{Å}$	0
CdTe	$1.036eV$	$-0.57eV$	$-1.48eV$	$8.46eV\cdot\text{Å}$	-0.09

	γ_1	γ_2	γ_3	C[13]
HgTe	4.1	0.5	1.3	$-74.6meV\cdot\text{Å}$
CdTe	1.47	-0.28	0.03	$-23.4meV\cdot\text{Å}$

[a] All parameters except C are listed at Ref.[12]
[b] We set $E_v^{Hg} = 0$ and $E_v^{Hg} - E_v^{Cd} = 0.57eV$[12]

A.2 3D 6×6 Hamiltonian

The split-off band is far away the energy range we want to analyze. Therefore we drop split-off band but keep 2nd order terms by Loẅdin perturbation theory. We call the new Hamiltonian as 3D 6 × 6 Hamiltonian $H_{6\times6}^{3D}$.

In the next chapter, we want to derive the 2D effective Hamiltonian by expanding $H_{6\times6}^{3D}$ with the eigenfunction of $H_{6\times6}^{3D}(0,0,-i\partial_z)$. The k_z term is like constant and the Kane Hamiltonian describes the band structure near Γ point. Therefore we can drop some terms in 2nd order perturb terms because they are smaller than the others for small k. We drop k^3 and k^4 terms but keep $k_x k_z^2$ and $k_y k_z^2$ terms. Furthermore, the P terms are much larger than the others so the effect of P^0 terms in 2nd order perturb term are small enough to be neglected.

The 3D 6 × 6 Hamiltonian is

$$H_{6\times6}^{3D} \equiv H^{(0)} + H^{(1)} + H^{(2)}. \tag{A.2}$$

Where $H^{(i)}$ is ith order term. Their forms are

$$(H^{(0)})_{mn} = H_{mn}^0, \tag{A.3a}$$

$$(H^{(1)})_{mn} = H'_{mn}, \tag{A.3b}$$

$$(H^{(2)})_{mn} = \frac{1}{2}\sum_l H'_{ml} H'_{ln} \left(\frac{1}{E_m - E_l} + \frac{1}{E_n - E_l} \right). \tag{A.3c}$$

H^0 is a Hamiltonian with eigenenergies E_i of $\Gamma6$, $\Gamma8$, and $\Gamma7$ subbands. H'_{mn} is $(H_{8\times8}^{3D})_{mn}$ except for E_i. The variables m and n indicate $\Gamma6$ and $\Gamma8$ subbands and the variable l indicates $\Gamma7$ subbands. $H_{6\times6}^{3D}$ contains the eigenenergy($H^{(0)}$) of $\Gamma6$ and $\Gamma8$ subbands and all interaction between those subbands ($H^{(1)}$).

$$H^{(0)} + H^{(1)} = \begin{pmatrix} H_c & H_{ch} \\ H_{ch}^\dagger & H_h \end{pmatrix}. \tag{A.4}$$

APPENDIX A. DETAIL DERIVATION: FROM BASIC BAND FORMULATION TO EFFECTIVE 2D HAMILTONIAN

To simplify $H^{(2)}$, we let R and Q as those forms:

$$Q^\dagger = \left(\begin{array}{cc} H_{cs}^\dagger & H_{hs} \end{array} \right), \tag{A.5a}$$

$$R^\dagger = \left(\begin{array}{cc} \frac{H_{cs}^\dagger}{E_c - E_s} & \frac{H_{hs}}{E_h - E_s} \end{array} \right). \tag{A.5b}$$

We can rewrite $H^{(2)}$ as this form:

$$H^{(2)} = \frac{1}{2} \left(R^\dagger Q + Q^\dagger R \right) = \left(\begin{array}{cc} \frac{H_{cs}^\dagger H_{cs}}{E_c - E_s} & H_{cs}^\dagger H_{hs} \Delta_{chs} \\ H_{hs}^\dagger H_{cs} \Delta_{chs} & \frac{H_{hs}^\dagger H_{hs}}{E_v - E_s} \end{array} \right). \tag{A.6}$$

Where $\Delta_{chs} = \frac{1}{2} \left(\frac{1}{E_c - E_s} + \frac{1}{E_v - E_s} \right)$. $H_{hs}^\dagger H_{hs}$ contributes P^0 terms so we drop it. Therefore the 3D 6×6 Hamiltonian is

$$H_{6\times6}^{3D} = \left(\begin{array}{cc} H_c + H_c^{(2)} & H_{ch} + H_{ch}^{(2)} \\ H_{ch}^\dagger + H_{ch}^{(2)\dagger} & H_h \end{array} \right). \tag{A.7}$$

The $H_c^{(2)}$ and $H_{ch}^{(2)}$ come from 2nd order perturbation term. The $H_c^{(2)}$ term is the effective mass correction term of the conduction band and is of the form:

$$H_c^{(2)} = \frac{P^2}{3 \left(E_c - E_s \right)} k^2. \tag{A.8}$$

We define $T_c = T + \frac{P^2}{3(E_c - E_s)}$ so $H_c + H_c^{(2)}$ becomes this form:

$$H_c + H_c^{(2)} = E_c + T_c k^2. \tag{A.9}$$

After dropping the terms we neglected, $H_{ch}^{(2)}$ is of the following form:

$$H_{ch}^{(2)\dagger} = \begin{pmatrix} -\frac{1}{\sqrt{2}}\begin{bmatrix} P_c k_+ k_z \\ -P_3 k_- k_z^2 \end{bmatrix} & -\frac{1}{3\sqrt{2}}\begin{bmatrix} P_c\left(k_p^2 - 2k_z^2\right) \\ +3P_- K k_z \end{bmatrix} \\[2em] \frac{1}{\sqrt{6}}\begin{bmatrix} P_c k_+^2 \\ -\left(2P_3 - P_-\right)k_p^2 k_z \end{bmatrix} & -\frac{1}{\sqrt{6}}\begin{bmatrix} P_c k_+ k_z \\ +\left(2P_- - P_3\right)k_- k_z^2 \end{bmatrix} \\[2em] \frac{1}{\sqrt{6}}\begin{bmatrix} -P_c k_- k_z \\ +\left(2P_- - P_3\right)k_+ k_z^2 \end{bmatrix} & \frac{1}{\sqrt{6}}\begin{bmatrix} -P_c k_-^2 \\ -\left(2P_3 - P_-\right)k_p^2 k_z \end{bmatrix} \\[2em] \frac{1}{3\sqrt{2}}\begin{bmatrix} P_c\left(k_p^2 - 2k_z^2\right) \\ -3P_- K k_z \end{bmatrix} & \frac{1}{\sqrt{2}}\begin{bmatrix} -P_c k_- k_z \\ -P_3 k_+ k_z^2 \end{bmatrix} \end{pmatrix}. \quad (A.10)$$

Where $K = \frac{1}{2}\left(k_+^2 + k_-^2\right)$, $k^2 = k_x^2 + k_y^2 + k_z^2$, $k_p^2 = k_x^2 + k_y^2$, $k_\mu = k_x + \mu i k_y$,
$P_c = \frac{\sqrt{3}(2E_c - E_v - E_s)}{4(E_v - E_s)(E_c - E_s)} PC$, $P_3 = \frac{2(2E_c - E_v - E_s)}{\sqrt{3}(E_c - E_v)(E_c - E_s)} P\gamma$ and $P_- = \frac{4(2E_c - E_v - E_s)}{\sqrt{3}(E_c - E_v)(E_c - E_s)} P\gamma_-$.

A.3   2D Hamiltonian

We consider a CdTe/HgTe/CdTe quantum well structure showed in Fig. A.1. In z-direction, there is a HgTe layer thickness of d nm between two CdTe layers. We set $z = 0$ at the middle of HgTe layer. For deriving the 2D effective Hamiltonian, we separate the 3D 6×6 Hamiltonian $H_{6\times6}^{3D}$ into two parts, H_0 and H'. Here we treat all k_x and k_y dependent terms in $H_{6\times6}^{3D}$ as perturbation(H'). In the set of basis vector ($|\Gamma6, 1/2\rangle$, $|\Gamma6, -1/2\rangle$, $|\Gamma8, 3/2\rangle$, $|\Gamma8, 1/2\rangle$, $|\Gamma8, -1/2\rangle$, $|\Gamma8, -3/2\rangle$), H_0 is of the form:

$$H_0 = \begin{bmatrix} E_c + T_c k_z^2 & 0 & 0 & \sqrt{\frac{2}{3}}Pk_z & 0 & 0 \\ 0 & E_c + T_c k_z^2 & 0 & 0 & \sqrt{\frac{2}{3}}Pk_z & 0 \\ 0 & 0 & E_v + T_v k_z^2 & 0 & 0 & 0 \\ \sqrt{\frac{2}{3}}Pk_z & 0 & 0 & E_v + T_L k_z^2 & 0 & 0 \\ 0 & \sqrt{\frac{2}{3}}Pk_z & 0 & 0 & E_v + T_L k_z^2 & 0 \\ 0 & 0 & 0 & 0 & 0 & E_v + T_v k_z^2 \end{bmatrix}. \quad (A.11)$$

71

APPENDIX A. DETAIL DERIVATION: FROM BASIC BAND FORMULATION TO EFFECTIVE 2D HAMILTONIAN
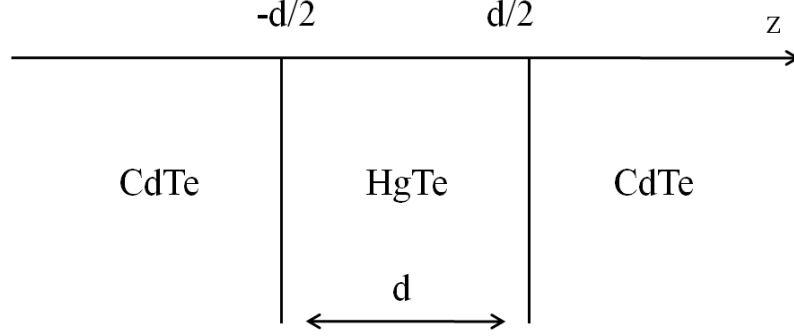
Figure A.1: It shows the CdTe/HgTe/CdTe quantum well structure. We set $z = 0$ at the middle of HgTe region in the following calculation.

E_c, E_v, T_c, T_H and T_L are function of z and all they are in this form

$$\chi(z) = \chi^{Hg} \left[\theta \left(z + \frac{d}{2} \right) - \theta \left(z - \frac{d}{2} \right) \right] + \chi^{Cd} \left[\theta \left(-z + \frac{d}{2} \right) + \theta \left(z - \frac{d}{2} \right) \right]. \quad (A.12)$$

Where $\theta(z)$ is step function. χ^{Hg} is band parameter of HgTe and χ^{Cd} is band parameters of CdTe.

The $|\Gamma 8, \pm 3/2\rangle$ subbands are decoupled to the other subbands and form the heavy hole subbands $|Hi, \pm\rangle$. Because P terms are much larger than T_c and T_L terms, we must keep them for calculating the eigenenergy. The $|\Gamma 6, \pm 1/2\rangle$ and $|\Gamma 8, \pm 1/2\rangle$ subbands are coupled by $\sqrt{\frac{2}{3}} P k_z$ terms and form the conduction subband $|E1, \pm\rangle$ and light hole subband $|L1, \pm\rangle$. k_z is an odd parity operator. The symmetry of $|\Gamma 6, \pm 1/2\rangle$ and $|\Gamma 8, \pm 1/2\rangle$ subbands is different in z-direction. The $|\Gamma 6, \pm 1/2\rangle$ part of $E1$ subband is even. The $|\Gamma 6, \pm 1/2\rangle$ part of $L1$ subband is odd. The detial of the basis is in appendix B.

The eigenenergy of $H1$, $H2$, $H3$, $E1$ and $L1$ is showed in Fig. A.2. The energys of conduction and light hole subband are different from ref[1]. The energy crossing of the conduction and heavy hole bands is shifted to $d_c \approx 6.58 nm$. It is not because we have keep the effective mass corretion terms but because the band parameter of Kane Hamiltonian they use are different.

The effective mass corretion not only effects the eigenenergy but determines the sign of the M_1^E in $H_{10 \times 10}^{2D}$ we will define later. If we are to drop this terms, the M_1^E will always be negative. According to it, we can see that effective mass corretion is already kept
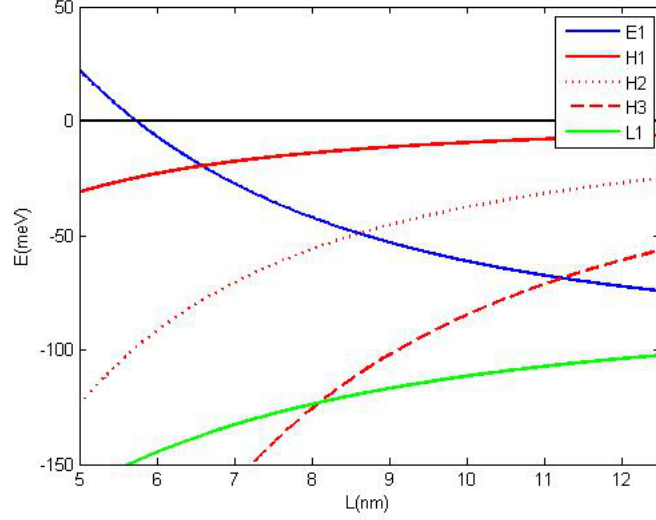
Figure A.2: This picture shows the eigenenergies of the subbands versus the well thickness d. The blue line is E1. The red line is H1. The red dash line is H2. The red dot line is H3. The green line is L1.

in ref[1]. In their system, they doesn't use CdTe to be the barrier material. They use $Hg_0.3/Cd_0.7Te$ to be the barrier material so the band parameter of Kane Hamiltonian is different. It mainly effects the eigenenergy of conduction and light hole subbands.

We define the set of basis vectors $(|E1,+\rangle, |H1,+\rangle, |E1,-\rangle, |H1,+\rangle, |H3,+\rangle, |H3,-\rangle, |H2,+\rangle, |H2,-\rangle, |L1,+\rangle, |L1,-\rangle)$. The effective 2D 10×10 Hamiltonain $H_{10\times10}^{2D}$ is defined as

$$\left[H_{10\times10}^{2D}(k_x, k_y)\right]_{ij} = \langle i| H_{6\times6}^{3D}(k_x, k_y, k_z) |j\rangle. \tag{A.13}$$

Where $|i\rangle$ is ith element of basis set. In our calculation we have treat the k_z dependent terms as

$$\chi k_z = \frac{1}{2}\{\chi, k_z\}. \tag{A.14}$$

$$\chi k_z^2 = k_z \chi k_z. \tag{A.15}$$

Where χ is some band structure parameters like γ. In general, the band structure parameters are not the same in two materials so k_z operating on χ will precdures a δ-function on the boundary. This δ-function contributes a term propertional to $\chi^{Hg} - \chi^{Cd}$. For

APPENDIX A. DETAIL DERIVATION: FROM BASIC BAND FORMULATION TO EFFECTIVE 2D HAMILTONIAN

example, the matrix element $[H^{2D}_{10\times 10}]_{12}$ is of the form:

$$\langle 1 | H^{3D}_{6\times 6}(k_x, k_y, k_z) | 2 \rangle = k_+ \int \begin{bmatrix} \frac{1}{\sqrt{2}} P E_1(z) H_1(z) \\ -iE_2(z)\gamma [\partial_z H_1(z)] \\ -i\frac{1}{2} E_2(z) H_1(z) [\partial_z \gamma] \\ -\frac{1}{\sqrt{2}} P_3 [\partial_z E_1(z)][\partial_z H_1(z)] \end{bmatrix} dz. \tag{A.16}$$

Because γ depends on materials and is in the form of equation(A.12), third term of equation (B.5) doesn't vanish.

According to the symmetry of basis, the effective 2D 10×10 Hamiltonain $H^{2D}_{10\times 10}$ is of the form:

$$H^{2D}_{10\times 10} = \begin{pmatrix} H^{2D}_{eff} & H^{2D}_1 \\ (H^{2D}_1)^\dagger & H^{2D}_2 \end{pmatrix}. \tag{A.17}$$

$$H^{2D}_{eff} = \begin{pmatrix} E_1^E + M_1^E k^2 & A_1 k_+ & 0 & 0 \\ A_1 k_- & E_1^H + M_1^H k^2 & 0 & 0 \\ 0 & 0 & E_1^E + M_1^E k^2 & A_1 k_- \\ 0 & 0 & A_1 k_+ & E_1^H + M_1^H k^2 \end{pmatrix}.$$

$$(H^{2D}_1)^\dagger = \begin{pmatrix} A_3 k_- & M_4^H k^2 & 0 & 0 \\ 0 & 0 & A_3 k_+ & M_4^H k^2 \\ 0 & 0 & iI_2 k_+^2 + iJ_2 k_-^2 & 0 \\ -iI_2 k_-^2 - iJ_2 k_+^2 & 0 & 0 & 0 \\ 0 & 0 & iDk_- & iI_1 k_+^2 + iJ_1 k_-^2 \\ -iDk_+ & -iI_1 k_-^2 - iJ_1 k_+^2 & 0 & 0 \end{pmatrix}.$$

$$
H_2^{2D} =
\begin{pmatrix}
E_3^H + M_3^H k^2 & 0 & 0 & 0 & 0 & iI_3 k_+^2 + iJ_3 k_-^2 \\
0 & E_3^H + M_3^H k^2 & 0 & 0 & -iI_3 k_-^2 - iJ_3 k_+^2 & 0 \\
0 & 0 & E_2^H + M_2^H k^2 & 0 & A_2 k_- & 0 \\
0 & 0 & 0 & E_2^H + M_2^H k^2 & 0 & A_2 k_+ \\
0 & iI_3 k_+^2 + iJ_3 k_-^2 & A_2 k_+ & 0 & E_1^L + M_1^L k^2 & 0 \\
-iI_3 k_-^2 - iJ_3 k_+^2 & 0 & 0 & A_2 k_- & 0 & E_1^L + M_1^L k^2
\end{pmatrix}.
$$

A.4 2D Hamiltonian with Dresselhaus spin-orbital interaction (DSOI)

Considering the 3D 6×6 Hamiltonian $H_{6\times6}^{3D}$ including DSOI, the Hamiltonian at Γ point is of the form:

$$
H_{6\times6}^{3D}(0,0,k_z) =
\begin{bmatrix}
E_c + T_c k_z^2 & 0 & 0 & \sqrt{\tfrac{2}{3}} P k_z & 0 & -\tfrac{\sqrt{2}}{3} P_c k_z^2 \\
0 & E_c + T_c k_z^2 & \tfrac{\sqrt{2}}{3} P_c k_z^2 & 0 & \sqrt{\tfrac{2}{3}} P k_z & 0 \\
0 & \tfrac{\sqrt{2}}{3} P_c k_z^2 & E_v - T_H k_z^2 & 0 & C k_z & 0 \\
\sqrt{\tfrac{2}{3}} P k_z & 0 & 0 & E_v - T_L k_z^2 & 0 & -C k_z \\
0 & \sqrt{\tfrac{2}{3}} P k_z & C k_z & 0 & E_v - T_L k_z^2 & 0 \\
-\tfrac{\sqrt{2}}{3} P_c k_z^2 & 0 & 0 & -C k_z & 0 & E_v - T_H k_z^2
\end{bmatrix}.
$$

$$(A.18)$$

The C and P_c terms are much smaller than the others showed in equation (A.18) so we can treat them as perturbation or keep them in calculating the basis vector of effective 2D Hamiltonian. If we treat them as perturbation, the basis vector is as the same as what we derived in the last section. Because the symmetry of DSOI term is different to the others in $H_{6\times6}^{3D}$, C and P_c contribute nothing to the terms already existing in $H_{10\times10}^{2D}$ (equation (A.17)). With the terms induced by DSOI, the effective 2D 10×10 Hamiltonian $H_{10\times10}^{2D}$

is of the form:

$$H_{10\times10}^{2D} = \begin{pmatrix} H_{eff}^{2D} & H_1^{2D} \\ (H_1^{2D})^\dagger & H_2^{2D} \end{pmatrix}. \tag{A.19}$$

$$H_{eff}^{2D} = \begin{pmatrix} E_1^E + M_1^E k^2 & A_1 k_+ & a_E k_+ & \delta_1 + M_1^C k^2 \\ A_1 k_- & E_1^H + M_1^H k^2 & \delta_1 + M_1^C k^2 & a_1 k_- \\ a_E k_- & \delta_1 + M_1^C k^2 & E_1^E + M_1^E k^2 & A_1 k_- \\ \delta_1 + M_1^C k^2 & a_1 k_+ & A_1 k_+ & E_1^H + M_1^H k^2 \end{pmatrix}.$$

$$(H_1^{2D})^\dagger = \begin{pmatrix} A_3 k_- & M_4^H k^2 & \delta_3 + M_3^C k^2 & a_4 k_- \\ \delta_3 + M_3^C k^2 & a_4 k_+ & A_3 k_+ & M_4^H k^2 \\ i D_2^C k_+ & 0 & i I_2 k_+^2 + i J_2 k_-^2 & 0 \\ -i I_2 k_-^2 - i J_2 k_+^2 & 0 & -i D_2^C k_- & 0 \\ -i I^C k_+^2 - i J^C k_-^2 & -i D_1^C k_- & i D k_- & i I_1 k_+^2 + i J_1 k_-^2 \\ -i D k_+ & -i I_1 k_-^2 - i J_1 k_+^2 & i I^C k_-^2 + i J^C k_+^2 & i D_1^C k_+ \end{pmatrix}.$$
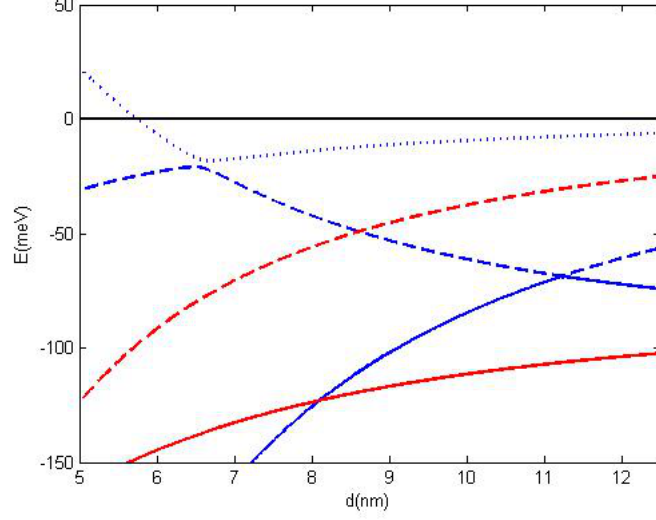
Figure A.3: This figure shows the eigenenergy of $H_{10\times10}^{3D}$ at Γ point with DSOI. $E1$, $H1$ and $H3$ are coupled by Ck_z and blue lines show the energy at Γ point for them. $L1$ and $H2$ are coupled by Ck_z and denote red lines.

$$H_2^{2D} = \begin{pmatrix}
E_3^H + M_3^H k^2 & a_3 k_- & 0 & iD_3^C k_+ & iI_3 k_+^2 + iJ_3 k_-^2 \\
a_3 k_+ & E_3^H + M_3^H k^2 & 0 & 0 & -iI_3 k_-^2 - iJ_3 k_+^2 & -iD_3^C k_- \\
0 & 0 & E_2^H + M_2^H k^2 & a_2 k_- & A_2 k_- & \delta_2 + M_2^C k^2 \\
0 & 0 & a_2 k_+ & E_2^H + M_2^H k^2 & \delta_2 + M_2^C k^2 & A_2 k_+ \\
-iD_3^C k_- & iI_3 k_+^2 + iJ_3 k_-^2 & A_2 k_+ & \delta_2 + M_2^C k^2 & E_1^L + M_1^L k^2 & a_L k_+ \\
-iI_3 k_-^2 - iJ_3 k_+^2 & iD_3^C k_+ & \delta_2 + M_2^C k^2 & A_2 k_- & a_L k_- & E_1^L + M_1^L k^2
\end{pmatrix}.$$

Where δ_i, a_i, a_E, a_L, D_i^C, M_i^C, I_i^C and J_i^C term are contributed by C and P_c terms. Becuase δ_i terms are constants and they couple $E1$ and $H1$ subbands, the energy crossing at Γ point will be anti-crossing (See Fig. A.3).

On the other hand, we can keep C and P_c terms in computing the basis vector. In

77

this new set of basis, we can derive a new effective 2D 10×10 Hamiltonain $\tilde{H}_{10\times10}^{2D}$. For deriving the new basis vector, we define the new H_0 as equation (A.19) with $P_c = 0$. The P_c terms are smaller than C terms so we treat them as perturbation to simplify the equation.

Pk_z couples $|\Gamma6, \pm1/2\rangle$ and $|\Gamma8, \pm1/2\rangle$ subbands. Ck_z couples $|\Gamma8, \pm1/2\rangle$ and $|\Gamma8, \mp3/2\rangle$ subbands. So $|\Gamma6, \pm1/2\rangle$ and $|\Gamma8, \mp3/2\rangle$ component have the same symmetry and are real. $|\Gamma8, \pm1/2\rangle$ component have the opposite symmetry of the others and is pure imaginary. $|\Gamma6, \pm1/2\rangle$, $|\Gamma8, \pm1/2\rangle$ and $|\Gamma8, \mp3/2\rangle$ are coupled together to form $\left|\tilde{S}i, \pm\right\rangle$ and $\left|\tilde{A}i, \pm\right\rangle$ subbands. Where $\left|\tilde{S}i, \pm\right\rangle$ subbands' $|\Gamma6, \pm1/2\rangle$ component is even function and $\left|\tilde{A}i, \pm\right\rangle$ subbands' $|\Gamma6, \pm1/2\rangle$ component is odd function. The detial of the basis is in appendix C.

The eigenenergy of $\tilde{S}$ and $\tilde{A}$ subbands are showed at Fig. A.4. The Pk_z and Ck_z terms make the curve of S subband not cross to each other. The energy at Γ point of two methods are similar(See Fig. A.5). It shows we can treat C and P_c terms as perturbation and the band structure of two method are comparable.

When d is larger than d_c. $\left|\tilde{S}2, \pm\right\rangle$ is similiar to $|E1, \pm\rangle$ and $\left|\tilde{S}1, \mp\right\rangle$ is similiar to $|H1, \pm\rangle$. For comparing the result, we define the set of basis vector($\left|\tilde{S}2, +\right\rangle$, $\left|\tilde{S}1, -\right\rangle$, $\left|\tilde{S}2, -\right\rangle$, $\left|\tilde{S}1, +\right\rangle$, $\left|\tilde{S}3, +\right\rangle$, $\left|\tilde{S}3, -\right\rangle$, $\left|\tilde{A}1, +\right\rangle$, $\left|\tilde{A}1, -\right\rangle$, $\left|\tilde{A}2, +\right\rangle$, $\left|\tilde{A}2, -\right\rangle$). The effective 2D 10×10 Hamiltonian $\tilde{H}_{10\times10}^{2D}$ is defined as

$$\left[\tilde{H}_{10\times10}^{2D}(k_x, k_y)\right]_{ij} = \left\langle\tilde{i}\right| H_{6\times6}^{3D}(k_x, k_y, k_z) \left|\tilde{j}\right\rangle. \tag{A.20}$$

Where $\left|\tilde{i}\right\rangle$ is ith element of basis set. According to the symmetry property of $\tilde{S}$ and $\tilde{A}$ subbands, $\tilde{H}_{10\times10}^{2D}$ is of the form:

$$\tilde{H}_{10\times10}^{2D} = \begin{pmatrix} \tilde{H}_{eff}^{2D} & \tilde{H}_1^{2D} \\ (\tilde{H}_1^{2D})^\dagger & \tilde{H}_2^{2D} \end{pmatrix}. \tag{A.21}$$
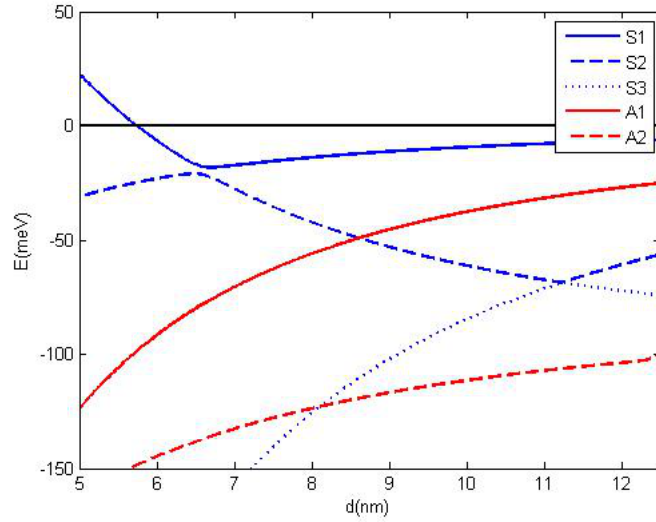
Figure A.4: It shows the eigenenergy of $\tilde{S}$ and $\tilde{A}$ subbands. The blue line is the eigenenergy of $\tilde{S}$ subband versus d. The red line is the eigenenergy of $\tilde{A}$ subband versus d.
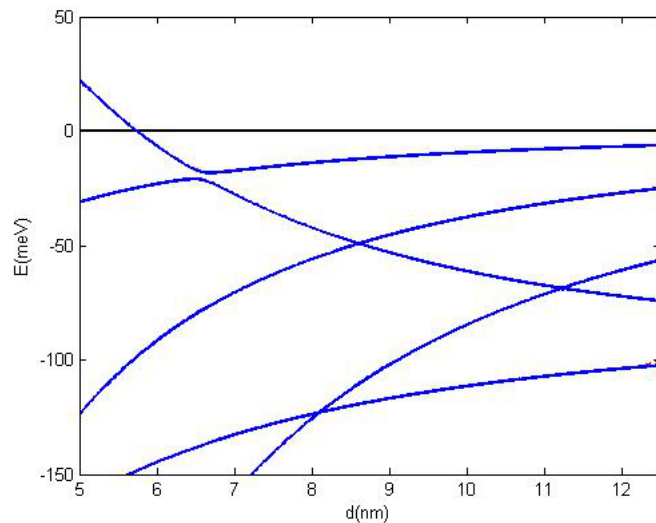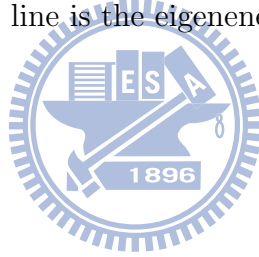
Figure A.5: The blue solid line is the eigenenergy of $H_{10\times10}^{3D}$ at Γ point versus d. The red dash line is the eigenenergy of $\tilde{H}_{10\times10}^{3D}$ at Γ point versus d.

$$\tilde{H}_{eff}^{2D} = \begin{pmatrix} \tilde{E}_2^S + \tilde{\delta}_2 \\ +\tilde{M}_2 k^2 & \tilde{A}_2 k_+ & \tilde{A}_3 k_+ & \tilde{\delta}_6 + \tilde{M}_6 k^2 \\ \\ \tilde{A}_2 k_- & \begin{matrix} \tilde{E}_1^S + \tilde{\delta}_1 \\ +\tilde{M}_1 k^2 \end{matrix} & \tilde{\delta}_6 + \tilde{M}_6 k^2 & \tilde{A}_1 k_- \\ \\ \tilde{A}_3 k_- & \tilde{\delta}_6 + \tilde{M}_6 k^2 & \begin{matrix} \tilde{E}_2^S + \tilde{\delta}_2 \\ +\tilde{M}_2 k^2 \end{matrix} & \tilde{A}_2 k_- \\ \\ \tilde{\delta}_6 + \tilde{M}_6 k^2 & \tilde{A}_1 k_+ & \tilde{A}_2 k_+ & \begin{matrix} \tilde{E}_1^S + \tilde{\delta}_1 \\ +\tilde{M}_1 k^2 \end{matrix} \end{pmatrix}.$$

$$(\tilde{H}_1^{2D})^\dagger = \begin{pmatrix} \tilde{\delta}_8 \\ +\tilde{M}_8 k^2 & \tilde{A}_4 k_+ & \tilde{A}_5 k_+ & \begin{matrix} \tilde{\delta}_7 \\ +\tilde{M}_7 k^2 \end{matrix} \\ \\ \tilde{A}_5 k_- & \begin{matrix} \tilde{\delta}_7 \\ +\tilde{M}_7 k^2 \end{matrix} & \begin{matrix} \tilde{\delta}_8 \\ +\tilde{M}_8 k^2 \end{matrix} & \tilde{A}_4 k_- \\ \\ \begin{matrix} -i\tilde{J}_3 k_-^2 \\ -i\tilde{L}_3 k_+^2 \end{matrix} & i\tilde{I}_1 k_- & i\tilde{I}_3 k_- & \begin{matrix} -i\tilde{J}_1 k_-^2 \\ -i\tilde{L}_1 k_+^2 \end{matrix} \\ \\ -i\tilde{I}_3 k_+ & \begin{matrix} i\tilde{J}_1 k_+^2 \\ +i\tilde{L}_1 k_-^2 \end{matrix} & \begin{matrix} i\tilde{J}_3 k_+^2 \\ +i\tilde{L}_3 k_-^2 \end{matrix} & -i\tilde{I}_1 k_+ \\ \\ \begin{matrix} -i\tilde{J}_4 k_-^2 \\ -i\tilde{L}_4 k_+^2 \end{matrix} & i\tilde{I}_2 k_- & i\tilde{I}_4 k_- & \begin{matrix} -i\tilde{J}_2 k_-^2 \\ -i\tilde{L}_2 k_+^2 \end{matrix} \\ \\ -i\tilde{I}_4 k_+ & \begin{matrix} i\tilde{J}_2 k_+^2 \\ +i\tilde{L}_2 k_-^2 \end{matrix} & \begin{matrix} i\tilde{J}_4 k_+^2 \\ +i\tilde{L}_4 k_-^2 \end{matrix} & -i\tilde{I}_2 k_+ \end{pmatrix}.$$

80

$$\tilde{H}_2^{2D} = \begin{pmatrix} \tilde{E}_3^S + \tilde{\delta}_3 \\ +\tilde{M}_3 k^2 & \tilde{A}_6 k_+ & i\tilde{J}_5 k_+^2 \\ +i\tilde{L}_5 k_-^2 & i\tilde{I}_5 k_- & i\tilde{J}_6 k_+^2 \\ +i\tilde{L}_6 k_-^2 & i\tilde{I}_6 k_- \\ \\ \tilde{A}_6 k_- & \tilde{E}_3^S + \tilde{\delta}_3 \\ +\tilde{M}_3 k^2 & -i\tilde{I}_5 k_+ & -i\tilde{J}_5 k_-^2 \\ -i\tilde{L}_5 k_+^2 & -i\tilde{I}_6 k_+ & -i\tilde{J}_6 k_-^2 \\ -i\tilde{L}_6 k_+^2 \\ \\ -i\tilde{J}_5 k_-^2 \\ -i\tilde{L}_5 k_+^2 & i\tilde{I}_5 k_- & \tilde{E}_4^S + \tilde{\delta}_4 \\ \tilde{M}_4 k^2 & \tilde{A}_7 k_+ & \tilde{\delta}_9 \\ +\tilde{M}_9 k^2 & \tilde{A}_8 k_+ \\ \\ -i\tilde{I}_5 k_+ & i\tilde{J}_5 k_+^2 \\ +i\tilde{L}_5 k_-^2 & \tilde{A}_7 k_- & \tilde{E}_4^S + \tilde{\delta}_4 \\ \tilde{M}_4 k^2 & \tilde{A}_8 k_- & \tilde{\delta}_9 \\ +\tilde{M}_9 k^2 \\ \\ -i\tilde{J}_6 k_-^2 \\ -i\tilde{L}_6 k_+^2 & i\tilde{I}_6 k_- & \tilde{\delta}_9 \\ +\tilde{M}_9 k^2 & \tilde{A}_8 k_+ & \tilde{E}_5^S + \tilde{\delta}_5 \\ \tilde{M}_5 k^2 & \tilde{A}_9 k_+ \\ \\ -i\tilde{I}_6 k_+ & i\tilde{J}_6 k_+^2 \\ +i\tilde{L}_6 k_-^2 & \tilde{A}_8 k_- & \tilde{\delta}_9 \\ +\tilde{M}_9 k^2 & \tilde{A}_9 k_- & \tilde{E}_5^S + \tilde{\delta}_5 \\ \tilde{M}_5 k^2 \end{pmatrix}.$$

A.5   2D band structure: Isotropy and gap-closing

In the section 3.2, we have showed that the DSOI terms make the $E1$ and $H1$ subbands anti-crossing. But It doesn't mean that the global energy band gap between conduction ($E1$) and heavy hole ($H1$) bands is always opened. To study whether the gap is cloesd or not, we start our study from the effective Hamiltonian with $E1$ and $H1$ subbands only. For the basis without case, the effective Hamiltonian with $E1$ and $H1$ subbands only is of the form:

$$H_{eff}^{2D}(k_x, k_y; d) = \begin{pmatrix} E_1^E + M_1^E k^2 & A_1 k_+ & a_E k_+ & \delta_1 + M_1^C k^2 \\ A_1 k_- & E_1^H + M_1^H k^2 & \delta_1 + M_1^C k^2 & a_1 k_- \\ a_E k_- & \delta_1 + M_1^C k^2 & E_1^E + M_1^E k^2 & A_1 k_- \\ \delta_1 + M_1^C k^2 & a_1 k_+ & A_1 k_+ & E_1^H + M_1^H k^2 \end{pmatrix}. \quad \text{(A.22)}$$

APPENDIX A. DETAIL DERIVATION: FROM BASIC BAND FORMULATION TO EFFECTIVE 2D HAMILTONIAN

The eigenenergy $E_{\rho\mu}$ is of the form (See Appendix E):

$$E_{\rho\mu} = E_0 + Dk^2 + \mu\frac{(a_E + a_1)}{2}k$$
$$+\rho\sqrt{\left(A_1 k + \mu\left[\delta_1 + M_1^C k^2\right]\right)^2 + \left(M - Bk^2 - \mu\frac{[a_E - a_1]}{2}k\right)^2}. \qquad (A.23)$$

Where $D = \frac{1}{2}\left(M_1^E + M_1^H\right)$, $B = \frac{1}{2}\left(M_1^E - M_1^H\right)$, $M = \frac{1}{2}\left(E_{H1} - E_{E1}\right)$ and $E_0 = \frac{1}{2}\left(E_{H1} + E_{E1}\right)$. The energy dispersion is isotropy becuase the anisotropy is mainly induced by k_+^2 and k_-^2 at H_1^{2D}. Only when we including the effect from $H2$ and $L1$ subbands, the bands structure will be anitropy.

The value of a_E and a_1 are much smaller than A_1. The zero-gap exists when the two bands with the same μ touch at the same k_c. The value of energy gap is similar to $min\left(2\sqrt{\left(A_1 k + \mu\left[\delta_1 + M_1^C k^2\right]\right)^2 + \left(M - Bk^2 - \mu\frac{[a_E - a_1]}{2}k\right)^2}\right)$. From numerical calculation, we find out that the energy gap is closed at $d = d_c \approx 6.58nm$. $A_1\delta_1$ is positive so k_c is the root of $A_1 k - \delta_1 - M_1^C k^2 = 0$. We have $A_1 >> \delta_1$ and M_1^C so $k_c \approx \delta/A|_{d=d_c} = 4.36 \times 10^{-3}nm^{-1}$.(See Fig. A.6.) Therfore the DSOI terms don't remove the gap-closing. It makes the Dirac point become the Dirac ring and the global band gap is still closed at a special well width d_c.

Then we do the similar procedure to discuss the gap-closing picture in the effective Hamiltonian with the basis incuding C. For $d < 8nm$, the $E1$ and $H1$ couple together to form the $\tilde{S}1$ and $\tilde{S}2$ subbands so we study the effective Hamiltonian with $S1$ and $S2$ subbands only.

$$\tilde{H}_{eff}^{2D}(k_x, k_y; d) = \begin{pmatrix} \tilde{E}_2^S + \tilde{\delta}_2 + \tilde{M}_2 k^2 & \tilde{A}_2 k_+ & \tilde{A}_3 k_+ & \tilde{\delta}_6 + \tilde{M}_6 k^2 \\ \tilde{A}_2 k_- & \tilde{E}_1^S + \tilde{\delta}_1 + \tilde{M}_1 k^2 & \tilde{\delta}_6 + \tilde{M}_6 k^2 & \tilde{A}_1 k_- \\ \tilde{A}_3 k_- & \tilde{\delta}_6 + \tilde{M}_6 k^2 & \tilde{E}_2^S + \tilde{\delta}_2 + \tilde{M}_2 k^2 & \tilde{A}_2 k_- \\ \tilde{\delta}_6 + \tilde{M}_6 k^2 & \tilde{A}_1 k_+ & \tilde{A}_2 k_+ & \tilde{E}_1^S + \tilde{\delta}_1 + \tilde{M}_1 k^2 \end{pmatrix}. \qquad (A.24)$$

APPENDIX A. DETAIL DERIVATION: FROM BASIC BAND FORMULATION TO EFFECTIVE 2D HAMILTONIAN

The eigenenergy $\tilde{E}_{\rho\mu}$ is of the form (See Appendix D):

$$\tilde{E}_{\rho\mu} = \tilde{E}_0 + \tilde{D}k^2 + \mu\frac{1}{2}\left(\tilde{A}_1 + \tilde{A}_3\right)k$$
$$+ \rho\sqrt{\left(\tilde{A}_2 k + \mu\left[\tilde{\delta}_6 + \tilde{M}_6 k^2\right]\right)^2 + \left(\tilde{M} - \tilde{B}k^2 - \mu\frac{1}{2}\left[\tilde{A}_1 - \tilde{A}_3\right]k\right)^2}. \quad \text{(A.25)}$$

Where $\tilde{D} = \left(\tilde{M}_1 + \tilde{M}_2\right)/2$, $\tilde{B} = \left(\tilde{M}_1 - \tilde{M}_2\right)/2$, $\tilde{M} = \left(\tilde{E}_{S1} + \tilde{\delta}_1 - \tilde{E}_{S2} - \tilde{\delta}_2\right)/2$ and $\tilde{E}_0 = \left(\tilde{E}_{S1} + \tilde{\delta}_1 + \tilde{E}_{S2} + \tilde{\delta}_2\right)/2$. The band structure is still isotropy when we drop the effect from $\tilde{A}1$ and $\tilde{A}2$ subbands.

Because $\left|\tilde{A}_1 - \tilde{A}_3\right| >> \left|\tilde{A}_1 + \tilde{A}_3\right|$, the zero-gap exists when the two bands with the same μ touch at the same $\tilde{k}_c$. The value of energy gap is similar to $min\left(2\sqrt{\left(\tilde{A}_2 k + \mu\left[\tilde{\delta}_6 + \tilde{M}_6 k^2\right]\right)^2 + \left(\tilde{M} - \tilde{B}k^2 - \mu\frac{1}{2}\left[\tilde{A}_1 - \tilde{A}_3\right]k\right)^2}\right)$. From numerical calculation, we find out that the energy gap is closed at $d = d_c \approx 6.56nm$. The difference between this case and the case with the basis without DSOI may come from the high oder terms of Ck_z. The high oder terms of Ck_z kept in $\tilde{H}^{3D}_{10\times10}$ is dropped in $H^{3D}_{10\times10}$. It changes the gap closing point. $\tilde{k}_c$ is the root of $\tilde{M} - \tilde{B}k^2 - \mu\frac{1}{2}\left[\tilde{A}_1 - \tilde{A}_3\right]k = 0$. We have $\tilde{A}^2 >> \left|\tilde{M}\tilde{B}\right|$, so $\tilde{k}_c \approx \left|2\tilde{M}/\left(\tilde{A}_1 - \tilde{A}_3\right)\right|\Big|_{d=d_c} \approx 4.75 \times 10^{-3}nm^{-1}$.(See Fig.A.7.)

Now we study the gap-closing in the effective 10×10 Hamiltonian. We shows the $min(\tilde{E}2 - \tilde{E}3)$ at the 2D k-space versus d in the Fig. A.9. Where $\tilde{E}2$ and $\tilde{E}3$ are the energies of middle two bands of conduction and heavy hole bands.(See Fig. A.8.) The energy gap is closed at $d \approx 6.583nm$ for basis without C and closed at $d \approx 6.558nm$ for basis with C. We also obtain $k_c \approx 4.358 \times 10^{-3}nm^{-1}$ and $\tilde{k}_c \approx 4.781 \times 10^{-3}nm^{-1}$. The band structure is anisotropy so the value of d_c depends on the direction of k. For basis without C the difference of d_c is about $10^{-7}nm$ and the difference of k_c is about $10^{-8}nm^{-1}$. The difference for basis with C is in the same order. The differences of d_c and k_c are so small that the d_c and k_c are isotropy.

We has showed that the d_c and k_c are isotropy. Is the band structure is isotropy? In Fig.A.10-A.13, we show the energy difference versus ϕ, the angle of k vector, with fixed amplitude of k vector. We find out the energy difference is about $10^{-4}meV$ for $k = 0.01nm^{-1}$. The energy difference between $k = 0$ and $k = 0.01nm^{-1}$ is 2meV. The energy difference in the ϕ is much smaller than in the amplitude of k vector so the band

structure is nearly isotropy. The isotropy property is because of the anisotropy depending
on k^2. The band structure is mainly determined by the k linear term so the band structure
is isotropy for small k.
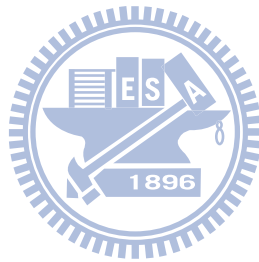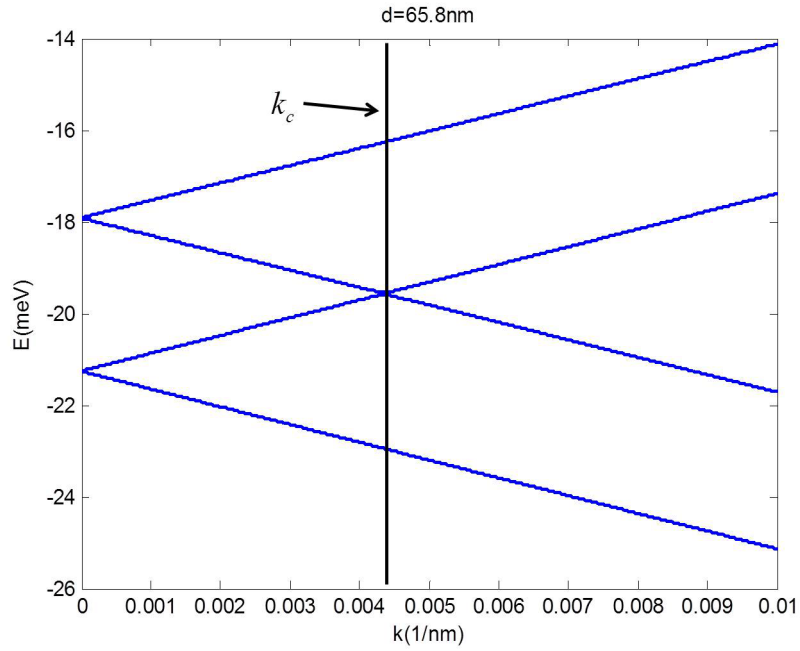
Figure A.6: This figure shows the energy dispersion of H_{eff}^{2D} with $d = 6.58nm$. The black vertical indicates the k_c.
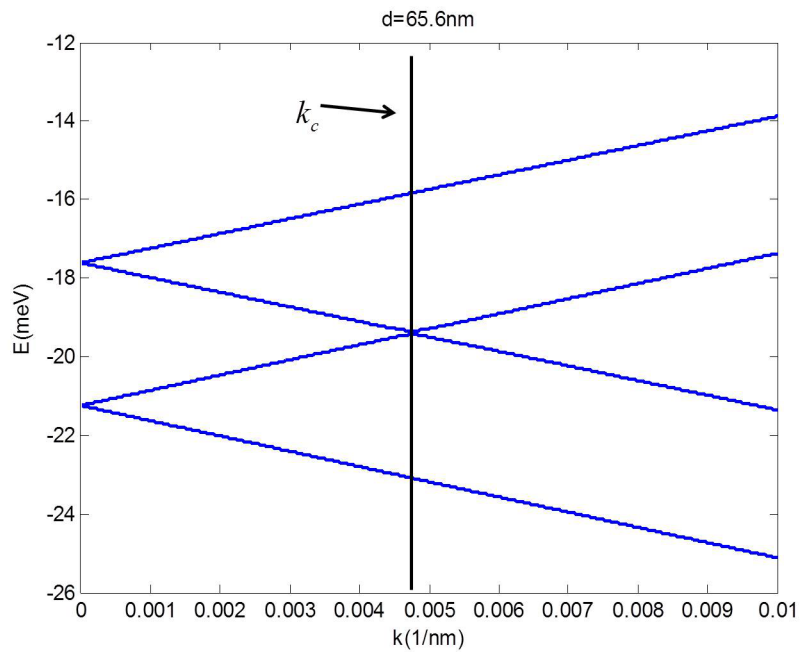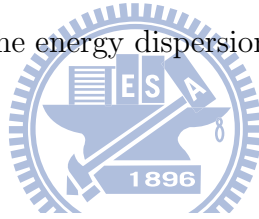
Figure A.7: This figure shows the energy dispersion of $\tilde{H}_{eff}^{2D}$ with $d = 6.56nm$. The black vertical indicates the k_c.
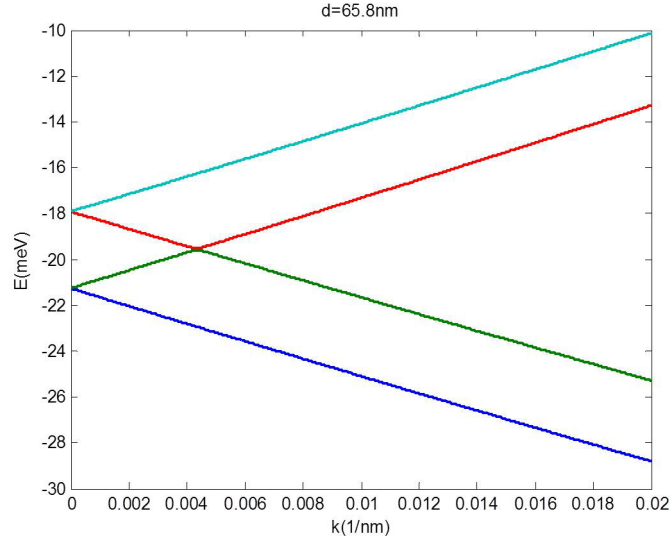
Figure A.8: This figure shows energy structure of conduction and heavy hole ($\tilde{S}1$ and $\tilde{S}2$) bands. The $\tilde{E}1$ is the energy of the 1st highest band. The $\tilde{E}2$ is the energy of the 2nd highest band. The $\tilde{E}3$ is the energy of the 3rd highest band. The $\tilde{E}4$ is the energy of the 4th highest band.
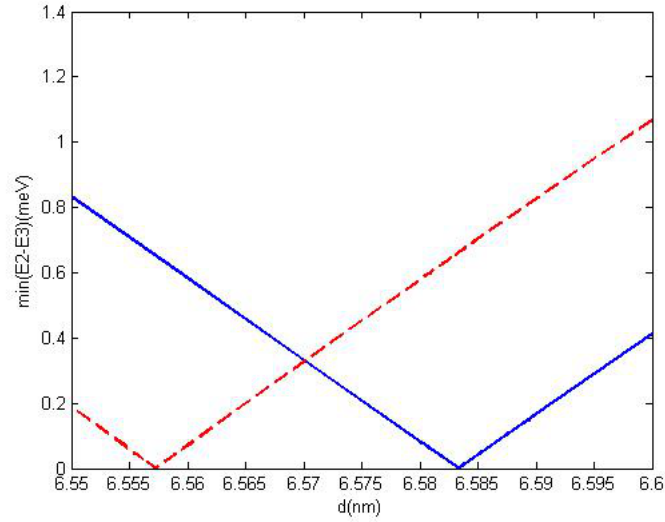
Figure A.9: This figure shows $min(\tilde{E}2 - \tilde{E}3)$. The blue solid line is for the H_{eff}^{2D}. The red dash line is for the $\tilde{H}_{eff}^{2D}$.
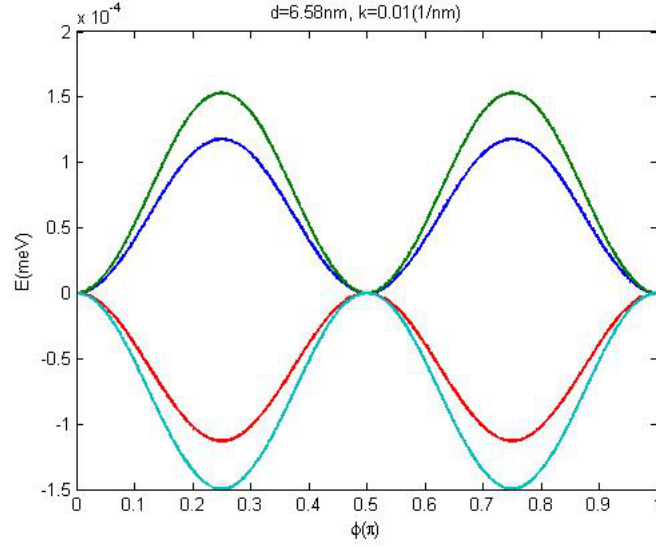
Figure A.10: This figure shows the energy difference of $H_{10 \times 10}^{2D}$ versus ϕ(angle of k) at $d = 6.58nm$. Here we show the value of $\tilde{E}i(\phi) - \tilde{E}i(\phi = 0)$ at $k = 0.01nm^{-1}$.
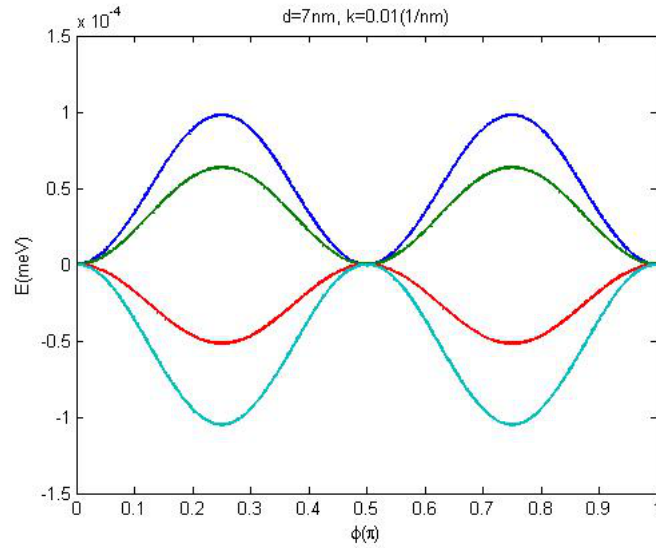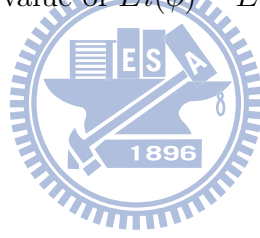
Figure A.11: This figure shows the energy difference of $H_{10 \times 10}^{2D}$ versus ϕ(angle of k) at $d = 7nm$. Here we show the value of $\tilde{E}i(\phi) - \tilde{E}i(\phi = 0)$ at $k = 0.01nm^{-1}$.
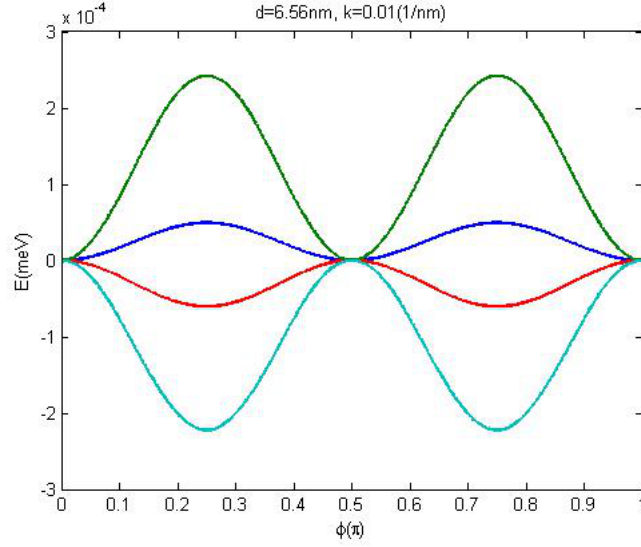
Figure A.12: This figure shows the energy difference of $\tilde{H}_{10\times10}^{2D}$ versus ϕ(angle of k) at $d = 6.56nm$. Here we show the value of $\tilde{E}i(\phi) - \tilde{E}i(\phi = 0)$ at $k = 0.01nm^{-1}$.
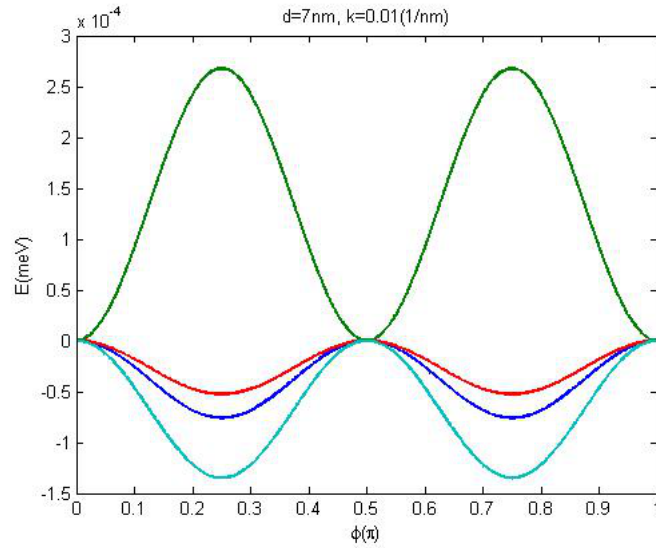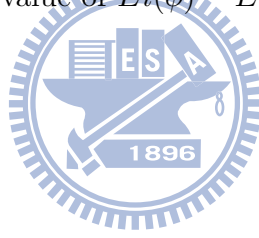
Figure A.13: This figure shows the energy difference of $\tilde{H}_{10\times10}^{2D}$ versus ϕ(angle of k) at $d = 7nm$. Here we show the value of $\tilde{E}i(\phi) - \tilde{E}i(\phi = 0)$ at $k = 0.01nm^{-1}$.

A.6 effective 4×4 **Hamiltonian**

The band structure of two route of effective 10×10 Hamiltonian is similar to the other
when d is not near d_c. We can use any one effective Hamiltonian to describe the system
at $d = 7nm$(See Fig. A.14). In the following analysis, we use the effective Hamiltonian
$H_{10 \times 10}^{2D}$ to study the topological nature of the system.
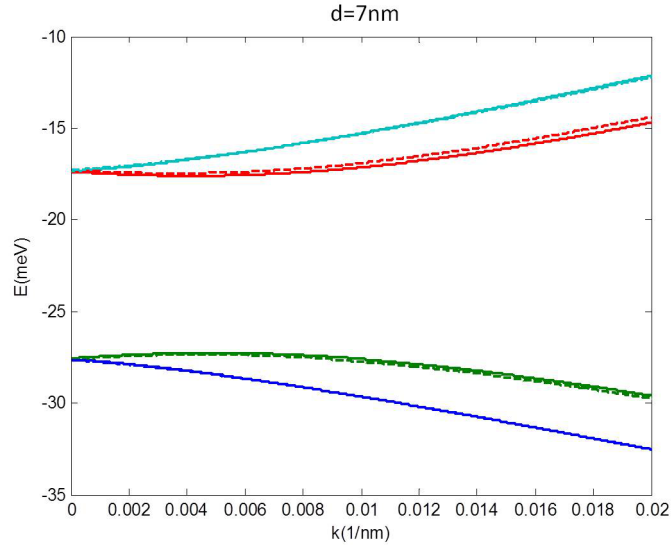
Figure A.14: It shows the eigenenergy of $\tilde{H}_{10 \times 10}^{2D}$ and $H_{10 \times 10}^{2D}$ with the well thickness 7nm.
The solid line is the eigenenergy of $H_{10 \times 10}^{2D}$. The dash line is the eigenenergy of $\tilde{H}_{10 \times 10}^{2D}$.

In the current work[4], the edge state is discovered in the energy gap between the
conduction ($E1$) and heavy hole ($H1$) bands, so we focus upon the energy range near
$E1$ and $H1$ subbands. We reduce the effective Hamiltonian $H_{10 \times 10}^{2D}$ to an effective 4×4
Hamiltonian H_{eff} with Loẅdin perturbation theory up to 2nd order. In the set of basis
$(|E1, +\rangle, |H1, +\rangle, |E1, -\rangle, |H1, -\rangle)$, H_{eff} is of the form:

$$H_{eff} = H^{(0)} + H^{(1)} + H^{(2)}. \tag{A.26}$$

$H^{(0)}$ is the eigenenergy of $E1$ and $H1$ subbands. $H^{(1)}$ is of the form:

$$H^{(1)} = \begin{pmatrix} \left(M_1^E + M'^E_1\right)k^2 & (A+A')\,k_+ & (a+a')\,k_+ & \begin{matrix}\delta+\delta' \\ +M^C k^2\end{matrix} \\ (A+A')\,k_- & M_1^H k^2 & \begin{matrix}\delta+\delta' \\ +M^C k^2\end{matrix} & (a_1+a'_1)\,k_- \\ (a+a')\,k_- & \begin{matrix}\delta+\delta' \\ +M^C k^2\end{matrix} & \left(M_1^E + M'^E_1\right)k^2 & (A+A')\,k_- \\ \begin{matrix}\delta+\delta' \\ +M^C k^2\end{matrix} & (a_1+a'_1)\,k_+ & (A+A')\,k_+ & M_1^H k^2 \end{pmatrix}. \quad \text{(A.27)}$$

The M'^E_1, A', a', δ', M^C and a'_1 are donated by P_c, P_- and P_3. The contribution form those terms is much smaller than the other terms like C and γ so we drop those terms. Furthermore the M^C terms just correct the value of M_1^E and M_1^H and we can make those terms zero by an unitary transformation. Dropping those terms doesn't affect the physical picture of H_{eff}. The a and a_1 are also dropped because C is much smaller than P and we also can make a or a_1 zero in the similar way of M^C. Here we only keep the P^2 terms in $H^{(2)}$ because P is much larger than the others terms.

We redefine the parameters kept in H_{eff}.

$$H_{eff} = Dk^2 + \begin{pmatrix} -M + Bk^2 & Ak_+ & 0 & \delta \\ Ak_- & M - Bk^2 & \delta & 0 \\ 0 & \delta & -M + Bk^2 & Ak_- \\ \delta & 0 & Ak_+ & M - Bk^2 \end{pmatrix}. \quad \text{(A.28)}$$

Where $M = \frac{E_1^H - E_1^E}{2}$, $B = \frac{M_1^E - M_1^H}{2}$, $D = \frac{M_1^E + M_1^H}{2}$ and $A = A_1$. The definition of M_1^E, M_1^H, A_j and δ are

$$M_1^E = \int \left[T_c|E_1(z)|^2 - T_{Lp}|E_2(z)|^2\right]dz + \left(\frac{A_3}{E_1^E - E_3^H}\right)^2 + \left(\frac{D}{E_1^E - E_1^L}\right)^2;$$

$$M_1^H = -\int T_{Hp}H_1(z)H_1(z)\,dz;$$

$$\delta = \frac{1}{2}\int E_2(z)\{C, k_z\}H_1(z)\,dz;$$

$$D = -i\int \frac{P}{\sqrt{6}}\left[E_1(z)L_2(z) + E_2(z)L_1(z)\right]dz;$$

$$A_j = \int \left[\frac{P}{\sqrt{2}}E_1(z)H_j(z) + \frac{1}{2}E_2(z)\{\gamma, k_z\}H_j(z)\right]dz.$$

APPENDIX A. DETAIL DERIVATION: FROM BASIC BAND FORMULATION TO EFFECTIVE 2D HAMILTONIAN

Table A.2: The band structure parameter of H_{eff}

	$M(meV)$	$B(meV/nm^2)$	$D(meV/nm^2)$	$A(meV/nm)$	$\delta(meV)$
ours	4.83	753	578	376	1.68
S.C. Zhang[1]	6.86	169	5.14	346	
Markus König[7]	10	686	512	364	1.6

[a] This band parameter is for $d = 7nm$.
[b] In ref[1], they didn't include DSOI.

Where the definition of $E_1(z)$, $E_2(z)$, $L_1(z)$, $L_2(z)$ and $H_j(z)$ are in Appendix B. The value of parameters is showed at Table A.2. Our parameter A, B, D and δ are similar to other's result. Only the value of M is much different to the other group. The physics of two set of band parameters is the same (See chapter 6.).

We show the band structure from H_{eff} and $H_{10\times10}^{2D}$ at Fig. A.15. Those two Hamiltonian gives the similar energy dispersion so we can use H_{eff} to study the topological physics of CdTe/HgTe/CdTe quantum well system.
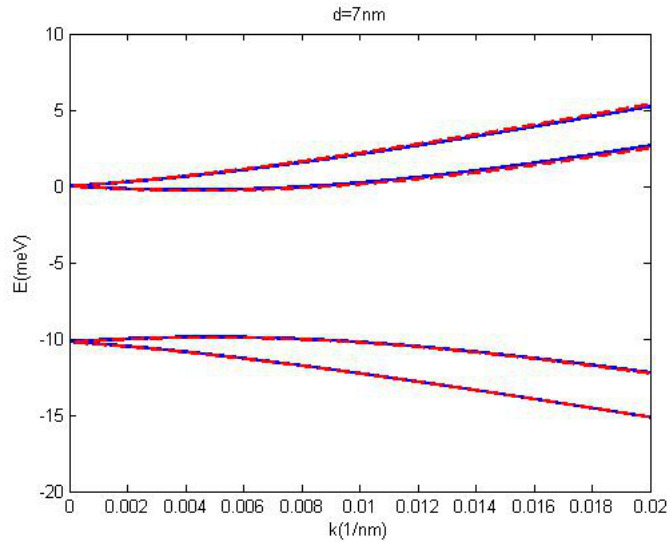
Figure A.15: It shows the eigenenergy of conduction and heavy hole bands from two effective Hamiltonian. The blue solid line is from $H_{10\times10}^{2D}$. The red dash line is from H_{eff}.

Appendix B

Basis definition of $H_{10 \times 10}^{2D}$

Both $|Hi, +\rangle$ and $|Hi, -\rangle$ subbands are the solution of the same differential equation. We define $\mp H_i(z)$ as the space part of $|Hi, \pm\rangle$.

$$\langle Hi, +| z\rangle = \begin{pmatrix} 0 & 0 & -H_i(z) & 0 & 0 & 0 \end{pmatrix}.$$

$$\langle Hi, -| z\rangle = \begin{pmatrix} 0 & 0 & 0 & 0 & 0 & H_i(z) \end{pmatrix}.$$

Where $H_i(z)$ is the eigenfunction with eigenenergy E_i^H of Schrödinger equation:

$$[E_v(z) + \partial_z T_H(z) \partial_z] H_i(z) = E_i^H H_i(z). \tag{B.1}$$

The wave function has specific symmetry at z-direction. We define $H_i(z)$ with odd i as even function and $H_i(z)$ with even i as odd function. For the even function, $H_i(z)$'s form is

$$H_i(z) = \begin{cases} b_i^H e^{\beta_i^H z} & z < -d/2 \\ a_i^H \cos(\alpha_i^H z) & \text{for } -d/2 < z < d/2 \\ b_i^H e^{-\beta_i^H z} & d/2 < z \end{cases}.$$

For the odd function, $H_i(z)$'s form is

$$H_i(z) = \begin{cases} b_i^H e^{\beta_i^H z} & z < -d/2 \\ a_i^H \sin(\alpha_i^H z) & \text{for } -d/2 < z < d/2 \\ -b_i^H e^{-\beta_i^H z} & d/2 < z \end{cases}.$$

Where $\alpha_i^H = \sqrt{\frac{E_\nu^{Hg} - E_i^H}{T_H^{Hg}}}$ and $\beta_i^H = \sqrt{\frac{E_i^H - E_\nu^{Cd}}{T_H^{Cd}}}$. We get the eigenenergy E_i^H through the boundary condition that is from continuity of wave function and Schrödinger equation. For the even function, the boundary condition at $z = -d/2$ is

$$-T_H^{Cd}\beta_i^H \cos\left(\frac{\alpha_i^H d}{2}\right) + T_H^{Hg}\alpha_i^H \sin\left(\frac{\alpha_i^H d}{2}\right) = 0. \tag{B.2}$$

For the odd function, the boundary condition at $z = -d/2$ is

$$T_H^{Cd}\beta_i^H \sin\left(\frac{\alpha_i^H d}{2}\right) + T_H^{Hg}\alpha_i^H \cos\left(\frac{\alpha_i^H d}{2}\right) = 0. \tag{B.3}$$

For $|E1, \pm\rangle$ and $|L1, \pm\rangle$ subbands, Pk_z terms make the symmetry of the $|\Gamma6, \pm1/2\rangle$ component opposite to the $|\Gamma8, \pm1/2\rangle$ component. We set the $|\Gamma6, \pm1/2\rangle$ component is pure real so Pk_z terms also make the $|\Gamma8, \pm1/2\rangle$ component pure imaginary.

We defined $E^1(z)$ as the space part of $|\Gamma6, \pm1/2\rangle$ subbands and $E^2(z)$ as the space part of $|\Gamma8, \pm1/2\rangle$ subbands.

$$\langle E1, +| \, z\rangle = \left(\begin{array}{cccccc} E_1(z) & 0 & 0 & -E_2(z) & 0 & 0 \end{array} \right).$$
$$\langle E1, -| \, z\rangle = \left(\begin{array}{cccccc} 0 & E_1(z) & 0 & 0 & -E_2(z) & 0 \end{array} \right).$$

Where $E_2(z)$ is pure imaginary and $E_1(z)$ is real. They satisfy the set of Schrödinger equations.

$$[E_c(z) - \partial_z T_c(z)\partial_z] E_1(z) - \sqrt{\frac{2}{3}}P\partial_z E_2(z) = E_1^E E_1(z). \tag{B.4a}$$

$$[E_v(z) + \partial_z T_L(z)\partial_z] E_2(z) - \sqrt{\frac{2}{3}}P\partial_z E_1(z) = E_1^E E_2(z). \tag{B.4b}$$

Where E_1^E is eigenenergy of $E1$ subband. We let $e^{\delta^E z}$ as the solution of HgTe region and $e^{\gamma^E z}$ as the solution of CdTe region. δ^E and γ^E are functions of E_1^E and determined by

Schrödinger equation(B.4).

$$\left(E_c^{Cd} - E_1^E - T_c{}^{Cd}(\gamma^E)^2\right)\left(E_v^{Cd} - E_1^E + T_L{}^{Cd}(\gamma^E)^2\right) + \frac{2}{3}\left[P\gamma^E\right]^2 = 0. \qquad \text{(B.5)}$$

$$\left(E_c^{Hg} - E_1^E - T_c{}^{Hg}(\delta^E)^2\right)\left(E_v^{Hg} - E_1^E + T_L{}^{Hg}(\delta^E)^2\right) + \frac{2}{3}\left[P\delta^E\right]^2 = 0. \qquad \text{(B.6)}$$

All γ^E are pure real (See Fig. B.2) but the part of δ^E may be imaginary. The functional form of conduction band will dependent on E_1^E. When $E_1^E > E_v^{Hg}$, two of δ^E will be imaginary (See Fig. B.1). $E_1(z)$ is even function[1] so $E_1(z)$ and $E_2(z)$ are of the forms:

$$E_1(z) = \begin{cases} C_1 \mathrm{e}^{\gamma_1^E z} + C_2 \mathrm{e}^{\gamma_2^E z} & z < -d/2 \\ A_1 \cosh(\delta_1^E z) + A_2 \cos(\delta_2^E z) & \text{for } -d/2 \leq z \leq d/2 \\ C_1 \mathrm{e}^{-\gamma_1^E z} + C_2 \mathrm{e}^{-\gamma_2^E z} & z > d/2 \end{cases}.$$

$$E_2(z) = \begin{cases} C_1 D_1 \mathrm{e}^{\gamma_1^E z} + C_2 D_2 \mathrm{e}^{\gamma_2^E z} & z < -d/2 \\ A_1 B_1 \sinh(\delta_1^E z) + A_2 B_2 \sin(\delta_2^E z) & \text{for } -d/2 \leq z \leq d/2 \\ -C_1 D_1 \mathrm{e}^{-\gamma_1^E z} - C_2 D_2 \mathrm{e}^{-\gamma_2^E z} & z > d/2 \end{cases}.$$

From equation(B.4a), we have $D_i = -i\sqrt{\frac{3}{2}}\frac{E_c^{Cd} - E_1^E - T_c^{Cd}(\gamma_i^E)^2}{P\gamma_i^E}$, $B_1 = -i\sqrt{\frac{3}{2}}\frac{E_c^{Hg} - E_1^E - T_c^{Hg}(\delta_1^E)^2}{P\delta_1^E}$ and $B_2 = -i\sqrt{\frac{3}{2}}\frac{E_c^{Hg} - E_1^E + T_c^{Hg}(\delta_2^E)^2}{P\delta_2^E}$. γ_i^E and δ_1^E are positive real and we let $\delta_2^E = \mathrm{Im}[\delta_2^E]$. From the continuity of wave function and Schrödinger equation at boundary $z = -d/2$, we derive the set of equations determining eigenenergy :

$$A_1 \cosh\left[\frac{\delta_1^E d}{2}\right] + A_2 \cos\left[\frac{\delta_2^E d}{2}\right] - \sum_{i=1}^{2} C_i \exp\left[-\frac{\gamma_i^E d}{2}\right] = 0, \qquad \text{(B.7a)}$$

$$A_1 B_1 \sinh\left[\frac{\delta_1^E d}{2}\right] + A_2 B_2 \sin\left[\frac{\delta_2^E d}{2}\right] + \sum_{i=1}^{2} C_i D_i \exp\left[-\frac{\gamma_i^E d}{2}\right] = 0, \qquad \text{(B.7b)}$$

$$T_c^{Hg}\left(\delta_1^E A_1 \sinh\left[\frac{\delta_1^E d}{2}\right] - \delta_2^E A_2 \sin\left[\frac{\delta_2^E d}{2}\right]\right) + \sum_{i=1}^{2} T_c^{Cd}\gamma_i^E C_i \exp\left[-\frac{\gamma_i^E d}{2}\right] = 0; \qquad \text{(B.7c)}$$

$$T_L^{Hg}\left(\delta_1^E A_1 B_1 \cosh\left[\frac{\delta_1^E d}{2}\right] + \delta_2^E A_2 B_2 \cos\left[\frac{\delta_2^E d}{2}\right]\right) - \sum_{i=1}^{2} T_L^{Cd}\gamma_i^E C_i D_i \exp\left[-\frac{\gamma_i^E d}{2}\right] = 0.$$

$$\text{(B.7d)}$$

When $E_c^{Hg} < E_1^E < E_v^{Hg}$, all δ^E are real(See Fig. B.1). The functional forms of $E_1(z)$

APPENDIX B. BASIS DEFINITION OF $H^{2D}_{10\times10}$
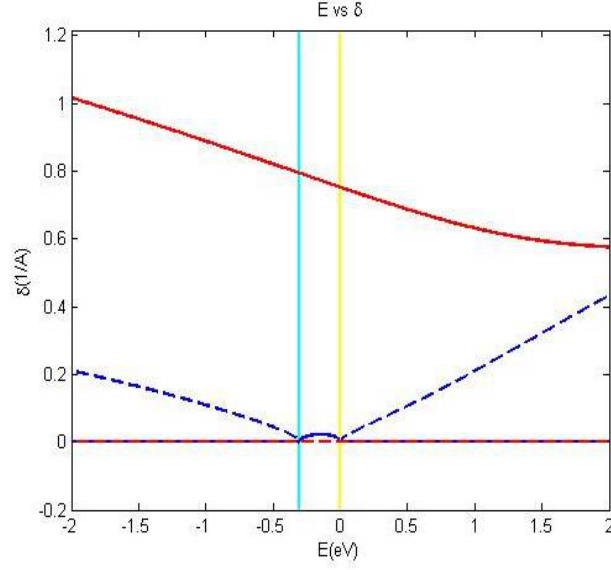
Figure B.1: This picture show the solution of δ^E. The solid line is the real part. The dash line is the imaginary part. The right vertical line is $E_v^{Hg}(=0eV)$. The left vertical line is $E_c^{Hg}(=-0.303eV)$. When E_1^E is between E_v^{Hg} and E_c^{Hg}, all δ^E are real. Otherwise two of δ^E will be pure imaginary. Here we only show two of roots. The other root are minus times of the roots showed here.
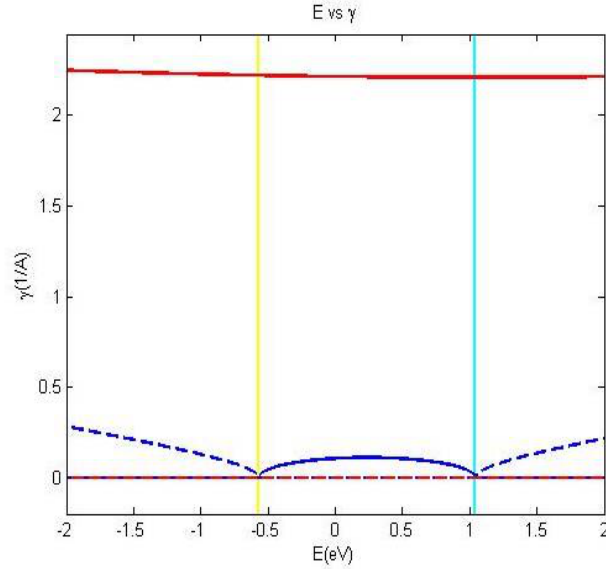
Figure B.2: This picture show the solution of γ^E. The solid line is the real part. The dash line is the imaginary part. The left vertical line is $E_v^{Cd}(=-0.57eV)$. The right vertical line is $E_c^{Cd}(=1.036eV)$. In the energy range $E_v^{Cd} < E_1^E < E_c^{Cd}$, all γ^E are real. Here we only show two of roots. The other root are minus times of the roots showed here.

and $E_2(z)$ are

$$
E_1\left(z\right) = \begin{cases}
C_1\mathrm{e}^{\gamma_1^E z} + C_2\mathrm{e}^{\gamma_2^E z} & z < -d/2 \\
A_1\cosh(\delta_1^E z) + A_2\cosh(\delta_2^E z) & \text{for } -d/2 \le z \le d/2 \\
C_1\mathrm{e}^{-\gamma_1^E z} + C_2\mathrm{e}^{-\gamma_2^E z} & z > d/2
\end{cases} ;
$$

$$
E_2\left(z\right) = \begin{cases}
C_1 D_1\mathrm{e}^{\gamma_1^E z} + C_2 D_2\mathrm{e}^{\gamma_2^E z} & z < -d/2 \\
A_1 B_1\sinh(\delta_1^E z) + A_2 B_2\sinh(\delta_2^E z) & \text{for } -d/2 \le z \le d/2 \\
-C_2 D_1\mathrm{e}^{-\gamma_1^E z} - C_2 D_2\mathrm{e}^{-\gamma_2^E z} & z > d/2
\end{cases} .
$$

Where $D_i = -i\sqrt{\dfrac{3}{2}\dfrac{E_c^{Cd}-E_1^E-T_c^{Cd}(\gamma_i^E)^2}{P\gamma_i^E}}$ and $B_i = -i\sqrt{\dfrac{3}{2}\dfrac{E_c^{Hg}-E_1^E-T_c^{Hg}(\delta_i^E)^2}{P\delta_i^E}}$. From the same condition of equation(B.7), the eigenenergy is determined by the set of equations:

$$
\sum_{i=1}^{2}\left(A_i\cosh\left[\frac{\delta_i^E d}{2}\right] - C_i\exp\left[-\frac{\gamma_i^E d}{2}\right]\right) = 0, \tag{B.8a}
$$

$$
\sum_{i=1}^{2}\left(A_i B_i\sinh\left[\frac{\delta_i^E d}{2}\right] + C_i D_i\exp\left[-\frac{\gamma_i^E d}{2}\right]\right) = 0, \tag{B.8b}
$$

$$
\sum_{i=1}^{2}\left(T_c^{Hg}\delta_i^E A_i\sinh\left[\frac{\delta_i^E d}{2}\right] + T_c^{Cd}\gamma_i^E C_i\exp\left[-\frac{\gamma_i^E d}{2}\right]\right) = 0; \tag{B.8c}
$$

$$
\sum_{i=1}^{2}\left(T_L^{Hg}\delta_i^E A_i B_i\cosh\left[\frac{\delta_i^E d}{2}\right] + T_L^{Cd}\gamma_i^E C_i D_i\exp\left[-\frac{\gamma_i^E d}{2}\right]\right) = 0. \tag{B.8d}
$$

We can follow the similar procedure to get the eigenenergy of $L1$ subbands. The form of light hole subband is

$$
\langle L1,+|\,z\rangle = \left(\begin{array}{cccccc} L_1\left(z\right) & 0 & 0 & -L_2\left(z\right) & 0 & 0 \end{array}\right).
$$
$$
\langle L1,-|\,z\rangle = \left(\begin{array}{cccccc} 0 & L_1\left(z\right) & 0 & 0 & -L_2\left(z\right) & 0 \end{array}\right).
$$

Where $L_2(z)$ is pure imaginary and $L_1(z)$ is real. The Schrödinger equation describes $L1$

subband is the set of the equations:

$$[E_c(z) - \partial_z T_c(z)\partial_z]L_1(z) - \sqrt{\frac{2}{3}}P\partial_z L_2(z) = E_1^L L_1(z). \tag{B.9}$$

$$[E_v(z) + \partial_z T_L(z)\partial_z]L_2(z) - \sqrt{\frac{2}{3}}P\partial_z L_1(z) = E_1^L L_2(z). \tag{B.10}$$

Where E_1^L is the eigenenergy of $L1$ subband. $L_1(z)$ is odd function[1] so $L_1(z)$ and $L_2(z)$ are of the forms:

$$L_1(z) = \begin{cases} C_1 e^{\gamma_1^L z} + C_2 e^{\gamma_2^L z} & z < -d/2 \\ A_1 \sinh(\delta_1^L z) + A_2 \sinh(\delta_2^L z) & \text{for } -d/2 \le z \le d/2 \\ -C_1 e^{-\gamma_1^L z} - C_2 e^{-\gamma_2^L z} & z > d/2 \end{cases}.$$

$$L_2(z) = \begin{cases} C_1 D_1 e^{\gamma_1^L z} + C_2 D_2 e^{\gamma_2^L z} & z < -d/2 \\ A_1 B_1 \cosh(\delta_1^L z) + A_2 B_2 \cosh(\delta_2^L z) & \text{for } -d/2 \le z \le d/2 \\ C_2 D_1 e^{-\gamma_1^L z} + C_2 D_2 e^{-\gamma_2^L z} & z > d/2 \end{cases}.$$

Where $D_i = -i\sqrt{\frac{3}{2}}\frac{E_c^{Cd} - E_1^L - T_c^{Cd}(\gamma_i^L)^2}{P\gamma_i^L}$ and $B_i = -i\sqrt{\frac{3}{2}}\frac{E_c^{Hg} - E_1^L - T_c^{Hg}(\delta_i^L)^2}{P\delta_i^L}$. All γ_i^L and δ_i^L are real. Those γ_i^L and δ_i^L are the root of eqs(B.5) and eqs(B.6) by substituting E_1^L for E_1^E. The eigenenergy is determined by the set of equation:

$$\sum_{i=1}^{2}\left(A_i \sinh\left[\frac{\delta_i^L d}{2}\right] - C_i \exp\left[-\frac{\gamma_i^L d}{2}\right]\right) = 0. \tag{B.11a}$$

$$\sum_{i=1}^{2}\left(A_i B_i \cosh\left[\frac{\delta_i^L d}{2}\right] + C_i D_i \exp\left[-\frac{\gamma_i^L d}{2}\right]\right) = 0. \tag{B.11b}$$

$$\sum_{i=1}^{2}\left(T_c^{Hg}\delta_i^L A_i \cosh\left[\frac{\delta_i^L d}{2}\right] + T_c^{Cd}\gamma_i^L C_i \exp\left[-\frac{\gamma_i^L d}{2}\right]\right) = 0. \tag{B.11c}$$

$$\sum_{i=1}^{2}\left(T_L^{Hg}\delta_i^L A_i B_i \sinh\left[\frac{\delta_i^L d}{2}\right] + T_L^{Cd}\gamma_i^L C_i D_i \exp\left[-\frac{\gamma_i^L d}{2}\right]\right) = 0. \tag{B.11d}$$

Appendix C

Basis definition of $\tilde{H}^{2D}_{10 \times 10}$

For $\tilde{S}i$ subbands, we define $\left| \tilde{S}i, \pm \right\rangle$ as the form:

$$\left\langle \tilde{S}i, + \right| z \rangle = \left(\begin{array}{cccccc} \tilde{S}^i_1(z) & 0 & 0 & -\tilde{S}^i_2(z) & 0 & \tilde{S}^i_3(z) \end{array} \right).$$

$$\left\langle \tilde{S}i, - \right| z \rangle = \left(\begin{array}{cccccc} 0 & \tilde{S}^i_1(z) & -\tilde{S}^i_3(z) & 0 & -\tilde{S}^i_2(z) & 0 \end{array} \right).$$

Where $\tilde{S}^i_2(z)$ is pure imaginary and $\tilde{S}^i_1(z)$ and $\tilde{S}^i_3(z)$ are real. The Schrödinger equation of $\tilde{S}i$ subband is the set of equation listed below.

$$\left(E_c(z) + T_c(z)k_z^2 \right) \tilde{S}^i_1(z) + \sqrt{\frac{2}{3}} P k_z \tilde{S}^i_2(z) = \tilde{E}^S_i \tilde{S}^i_1(z). \tag{C.1a}$$

$$\left(E_v(z) - T_L(z)k_z^2 \right) \tilde{S}^i_2(z) + \sqrt{\frac{2}{3}} P k_z \tilde{S}^i_1(z) - C(z)k_z \tilde{S}^i_3(z) = \tilde{E}^S_i \tilde{S}^i_2(z). \tag{C.1b}$$

$$\left(E_v(z) - T_H(z)k_z^2 \right) \tilde{S}^i_3(z) - C(z)k_z \tilde{S}^i_2(z) = \tilde{E}^S_i \tilde{S}^i_3(z). \tag{C.1c}$$

Where $\tilde{E}^S_i$ is the eigenenergy of $\tilde{S}i$ subbands. We let $e^{\tilde{\delta}^S z}$ as the solution of HgTe region and $e^{\tilde{\gamma}^S z}$ as the solution of CdTe region. The following equations determine $\tilde{\delta}^S$ and $\tilde{\gamma}^S$:

$$\left(\varepsilon_i^{Hg,c} - T_c^{Hg}(\tilde{\delta}^S)^2 \right) \left(\varepsilon_i^{Hg,v} + T_L^{Hg}(\tilde{\delta}^S)^2 \right) \left(\varepsilon_i^{Hg,v} + T_H^{Hg}(\tilde{\delta}^S)^2 \right)$$
$$+ \frac{2}{3} P^2 (\tilde{\delta}^S)^2 \left(\varepsilon_i^{Hg,v} + T_H^{Hg}(\tilde{\delta}^S)^2 \right) + (C^{Hg})^2 (\tilde{\delta}^S)^2 \left(\varepsilon_i^{Hg,v} - T_c^{Hg}(\tilde{\delta}^S)^2 \right) = 0. \tag{C.2}$$

$$\left(\varepsilon_i^{Cd,c} - T_c^{Cd}(\tilde{\gamma}^S)^2 \right) \left(\varepsilon_i^{Cd,v} + T_L^{Cd}(\tilde{\gamma}^S)^2 \right) \left(\varepsilon_i^{Cd,v} + T_H^{Cd}(\tilde{\gamma}^S)^2 \right)$$
$$+ \frac{2}{3} P^2 (\tilde{\gamma}^S)^2 \left(\varepsilon_i^{Cd,v} + T_H^{Cd}(\tilde{\gamma}^S)^2 \right) + (C^{Cd})^2 (\tilde{\gamma}^S)^2 \left(\varepsilon_i^{Cd,c} - T_c^{Cd}(\tilde{\gamma}^S)^2 \right) = 0. \tag{C.3}$$

Where $\varepsilon_i^{Hg,c} = E_c^{Hg} - \tilde{E}_i^S$, $\varepsilon_i^{Hg,v} = E_v^{Hg} - \tilde{E}_i^S$, $\varepsilon_i^{Cd,c} = E_c^{Cd} - \tilde{E}_i^S$ and $\varepsilon_i^{Cd,v} = E_v^{Cd} - \tilde{E}_i^S$. For all $\tilde{S}i$ subbands, $\tilde{\gamma}^S$s are all real(See Fig. (C.2)). The two pair of $\tilde{\delta}^S$ are real the others are pure imaginary(See Fig. (C.1)). $\tilde{S}_1^i(z)$, $\tilde{S}_2^i(z)$ and $\tilde{S}_3^i(z)$ are of the forms:

$$
\tilde{S}_1^i(z) = \begin{cases}
\displaystyle\sum_{j=1}^{3} \tilde{p}_j^S e^{\tilde{\gamma}_j^S z} & z < -\frac{d}{2} \\[2ex]
\displaystyle\sum_{j=1}^{2} \tilde{a}_j^S \cosh\left(\delta_j^S z\right) + \tilde{a}_3^S \cos\left(\tilde{\delta}_3^S z\right) & \text{for } -\frac{d}{2} < z < \frac{d}{2} \\[2ex]
\displaystyle\sum_{j=1}^{3} \tilde{p}_i^S e^{-\tilde{\gamma}_j^S z} & \frac{d}{2} < z
\end{cases}
$$

$$
\tilde{S}_2^i(z) = \begin{cases}
\displaystyle\sum_{j=1}^{3} \tilde{p}_j^S \tilde{q}_j^S e^{\tilde{\gamma}_j^S z} & z < -\frac{d}{2} \\[2ex]
\displaystyle\sum_{j=1}^{2} \tilde{a}_j^S \tilde{b}_j^S \sinh\left(\delta_j^S z\right) + \tilde{a}_3^S \tilde{b}_3^S \sin\left(\tilde{\delta}_3^S z\right) & \text{for } -\frac{d}{2} < z < \frac{d}{2} \\[2ex]
\displaystyle\sum_{j=1}^{3} -\tilde{p}_j^S \tilde{q}_j^S e^{-\tilde{\gamma}_j^S z} & \frac{d}{2} < z
\end{cases}
$$

$$
\tilde{S}_3^i(z) = \begin{cases}
\displaystyle\sum_{j=1}^{3} \tilde{p}_j^S \tilde{r}_j^S e^{\tilde{\gamma}_i^S z} & z < -\frac{d}{2} \\[2ex]
\displaystyle\sum_{j=1}^{2} \tilde{a}_j^S \tilde{c}_j^S \cosh\left(\delta_i^S z\right) + \tilde{a}_3^S \tilde{c}_3^S \cos\left(\tilde{\delta}_3^S z\right) & \text{for } -\frac{d}{2} < z < \frac{d}{2} \\[2ex]
\displaystyle\sum_{j=1}^{3} \tilde{p}_j^S \tilde{r}_j^S e^{-\tilde{\gamma}_i^S z} & \frac{d}{2} < z
\end{cases}
$$

From equations (C.1a) and (C.1b), we obtain $\tilde{b}_j^S = -i\sqrt{\frac{3}{2}}\frac{\varepsilon_i^{Hg,c} - T_c^{Hg}\left(\tilde{\delta}_j^S\right)^2}{iP\tilde{\delta}_j^S}$,

$\tilde{c}_j^S = \sqrt{\frac{3}{2}}\frac{\varepsilon_i^{Hg,v}\varepsilon_i^{Hg,c} + \left(\varepsilon_i^{Hg,c}T_L^{Hg} - \varepsilon_i^{Hg,v}T_c^{Hg} + \frac{2}{3}P^2\right)\left(\tilde{\delta}_j^S\right)^2 - T_c^{Hg}T_L^{Hg}\left(\tilde{\delta}_j^S\right)^4}{PC^{Hg}\left(\tilde{\delta}_j^S\right)^2}$,

$\tilde{b}_3^S = -i\sqrt{\frac{3}{2}}\frac{\varepsilon_i^{Hg,c} + T_c^{Hg}\left(\tilde{\delta}_3^S\right)^2}{P\tilde{\delta}_3^S}$, $\tilde{c}_3^S = -\sqrt{\frac{3}{2}}\frac{\varepsilon_i^{Hg,v}\varepsilon_i^{Hg,c} - \left(\varepsilon_i^{Hg,c}T_L^{Hg} - \varepsilon_i^{Hg,v}T_c^{Hg} + \frac{2}{3}P^2\right)\left(\tilde{\delta}_3^S\right)^2 - T_c^{Hg}T_L^{Hg}\left(\tilde{\delta}_3^S\right)^4}{PC^{Hg}\left(\tilde{\delta}_3^S\right)^2}$,

$\tilde{q}_j^S = -i\sqrt{\frac{3}{2}}\frac{\varepsilon_i^{Cd,c} - T_c^{Cd}\left(\tilde{\gamma}_j^S\right)^2}{P\tilde{\gamma}_j^S}$ and $\tilde{r}_j^S = \sqrt{\frac{3}{2}}\frac{\varepsilon_i^{Cd,v}\varepsilon_i^{Cd,c} + \left(\varepsilon_i^{Cd,c}T_L^{Cd} - \varepsilon_i^{Cd,v}T_c^{Cd} + \frac{2}{3}P^2\right)\left(\tilde{\gamma}_j^S\right)^2 - T_c^{Cd}T_L^{Cd}\left(\tilde{\gamma}_j^S\right)^4}{PC^{Cd}\left(\tilde{\gamma}_j^S\right)^2}$.

$\tilde{\gamma}_j^S$, $\tilde{\delta}_1^S$ and $\tilde{\delta}_2^S$ are positive real and we let $\tilde{\delta}_3^S = Im[\tilde{\delta}_3^S]$. From the continuity of wave

function at boundary $z = -d/2$, we derive the set of equations:

$$\sum_{j=1}^{2} \tilde{a}^S_j \cosh\left(\frac{\tilde{\delta}^S_j d}{2}\right) + \tilde{a}^S_3 \cos\left(\frac{\tilde{\delta}^S_3 d}{2}\right) - \sum_{j=1}^{3} \tilde{p}^S_j \exp\left(-\frac{\tilde{\gamma}^S_j d}{2}\right) = 0. \tag{C.4a}$$

$$\sum_{j=1}^{2} \tilde{a}^S_j \tilde{b}^S_j \sinh\left(\frac{\tilde{\delta}^S_j d}{2}\right) + \tilde{a}^S_3 \tilde{b}^S_3 \sin\left(\frac{\tilde{\delta}^S_3 d}{2}\right) + \sum_{j=1}^{3} \tilde{p}^S_j \tilde{q}^S_j \exp\left(-\frac{\tilde{\gamma}^S_j d}{2}\right) = 0. \tag{C.4b}$$

$$\sum_{j=1}^{2} \tilde{a}^S_j \tilde{c}^S_j \cosh\left(\frac{\tilde{\delta}^S_j d}{2}\right) + \tilde{a}^S_3 \tilde{c}^S_3 \cos\left(\frac{\tilde{\delta}^S_3 d}{2}\right) - \sum_{j=1}^{3} \tilde{p}^S_j \tilde{r}^S_j \exp\left(-\frac{\tilde{\gamma}^S_j d}{2}\right) = 0. \tag{C.4c}$$

The Schrödinger equation is continuous at boundary $z = -d/2$. We have

$$\lim_{\varepsilon\to0} \int_{-d/2-\varepsilon}^{-d/2+\varepsilon} [\left(E_c(z) + T_c(z)k_z^2\right)\tilde{S}^i_1(z) + \sqrt{\frac{2}{3}}Pk_z\tilde{S}^i_2(z)]dz = 0. \tag{C.5a}$$

$$\lim_{\varepsilon\to0} \int_{-d/2-\varepsilon}^{-d/2+\varepsilon} [\left(E_v(z) - T_L(z)k_z^2\right)\tilde{S}^i_2(z) + \sqrt{\frac{2}{3}}Pk_z\tilde{S}^i_1(z) - C(z)k_z\tilde{S}^i_3(z)]dz = 0. \tag{C.5b}$$

$$\lim_{\varepsilon\to0} \int_{-d/2-\varepsilon}^{-d/2+\varepsilon} [\left(E_v(z) - T_H(z)k_z^2\right)\tilde{S}^i_3(z) - C(z)k_z\tilde{S}^i_2(z)]dz = 0. \tag{C.5c}$$

C depends on the materials so it is a function of z. By treating Ck_z terms in the equation(C.5b) and (C.5b) as $\frac{1}{2}\{C, k_z\}$, we obtain

$$\frac{1}{2}\lim_{\varepsilon\to0} \int_{-d/2-\varepsilon}^{-d/2+\varepsilon} \{C, k_z\} f(z)\,dz = -\frac{i}{2}f(-\frac{d}{2})(C^{Hg} - C^{Cd}). \tag{C.6}$$

The $(k_z C)$ term contribute a δ-function at the boundary. This δ-function givens an addition in the boundary condition. From equation(C.5) and (C.6), we derive the set of

equations:

$$T_c^{Hg}\left[\sum_{j=1}^{2}\tilde{\delta}_j^S\tilde{a}_j^S\sinh\left(\frac{\tilde{\delta}_j^S d}{2}\right)+\tilde{\delta}_3^S\tilde{a}_3^S\sin\left(\frac{\tilde{\delta}_3^S d}{2}\right)\right]+\sum_{j=1}^{3}T_c^{Cd}\tilde{\gamma}_j^S\tilde{p}_j^S\exp\left(-\frac{\tilde{\gamma}_j^S d}{2}\right)=0.$$

(C.7a)

$$T_L^{Hg}\left[\sum_{j=1}^{2}\tilde{\delta}_j^S\tilde{a}_j^S\tilde{b}_j^S\cosh\left(\frac{\tilde{\delta}_j^S d}{2}\right)+\tilde{\delta}_3^S\tilde{a}_3^S\tilde{b}_3^S\cos\left(\frac{\tilde{\delta}_3^S d}{2}\right)\right]+\sum_{j=1}^{3}T_L^{Cd}\tilde{\gamma}_j^S\tilde{p}_j^S\tilde{q}_j^S\exp\left(-\frac{\tilde{\gamma}_j^S d}{2}\right)$$
$$=-\frac{i}{2}\left[C^{Hg}\left[\sum_{j=1}^{2}\tilde{a}_j^S\tilde{c}_j^S\cosh\left(\frac{\tilde{\delta}_j^S d}{2}\right)+\tilde{a}_3^S\tilde{c}_3^S\cos\left(\frac{\tilde{\delta}_3^S d}{2}\right)\right]-\sum_{j=1}^{3}C^{Cd}\tilde{p}_j^S\tilde{r}_j^S\exp\left(-\frac{\tilde{\gamma}_j^S d}{2}\right)\right].$$

(C.7b)

$$T_H^{Hg}\left[\sum_{j=1}^{2}\tilde{\delta}_j^S\tilde{a}_j^S\tilde{c}_j^S\sinh\left(\frac{\tilde{\delta}_j^S d}{2}\right)-\tilde{\delta}_3^S\tilde{a}_3^S\tilde{c}_3^S\sin\left(\frac{\tilde{\delta}_3^S d}{2}\right)\right]+\sum_{j=1}^{3}T_H^{Cd}\tilde{\gamma}_j^S\tilde{p}_j^S\tilde{r}_j^S\exp\left(-\frac{\tilde{\gamma}_j^S d}{2}\right)$$
$$-\frac{i}{2}\left[C^{Hg}\left[\sum_{j=1}^{2}\tilde{a}_j^S\tilde{b}_j^S\sinh\left(\frac{\tilde{\delta}_j^S d}{2}\right)+\tilde{a}_3^S\tilde{b}_3^S\sin\left(\frac{\tilde{\delta}_3^S d}{2}\right)\right]+\sum_{j=1}^{3}C^{Cd}\tilde{p}_j^S\tilde{q}_j^S\exp\left(-\frac{\tilde{\gamma}_j^S d}{2}\right)\right].$$

(C.7c)

Those two sets of equation above determine the eigenenergy.

We can do the similiar produre to find $\tilde{A}i$ subbands. We define $\left|\tilde{A}i,\pm\right\rangle$ as the fors:

$$\left\langle\tilde{A}i,+\right|z\rangle=\left(\begin{array}{cccccc}\tilde{A}_1^i(z) & 0 & 0 & -\tilde{A}_2^i(z) & 0 & \tilde{A}_3^i(z)\end{array}\right).$$
$$\left\langle\tilde{A}i,-\right|z\rangle=\left(\begin{array}{cccccc}0 & \tilde{A}_1^i(z) & -\tilde{A}_3^i(z) & 0 & -\tilde{A}_2^i(z) & 0\end{array}\right).$$

Where $\tilde{A}_2^i(z)$ is pure imaginary and $\tilde{A}_1^i(z)$ and $\tilde{A}_3^i(z)$ are real. The Schrödinger equation of $\tilde{A}i$ subband is the set of equation listed below.

$$\left(E_c(z)+T_c(z)k_z^2\right)\tilde{A}_1^i(z)+\sqrt{\frac{2}{3}}Pk_z\tilde{A}_2^i(z)=\tilde{E}_i^A\tilde{A}_1^i(z).\qquad\text{(C.8a)}$$

$$\left(E_v(z)-T_L(z)k_z^2\right)\tilde{A}_2^i(z)+\sqrt{\frac{2}{3}}Pk_z\tilde{A}_1^i(z)-C(z)k_z\tilde{A}_3^i(z)=\tilde{E}_i^A\tilde{A}_2^i(z).\qquad\text{(C.8b)}$$

$$\left(E_v(z)-T_H(z)k_z^2\right)\tilde{A}_3^i(z)-C(z)k_z\tilde{A}_2^i(z)=\tilde{E}_i^A\tilde{A}_3^i(z).\qquad\text{(C.8c)}$$

Where $\tilde{E}_i^A$ is the eigenenergy of $\tilde{A}i$ subbands. The functional form of $\tilde{A}_1^i(z)$, $\tilde{A}_2^i(z)$ and

Figure C.1: This picture show the solution of $\tilde{\delta}^S$. The solid line is the real part. The dash line is the imaginary part. The right vertical line is $E_v^{Hg}(= 0eV)$. The left vertical line is $E_c^{Hg}(= -0.303eV)$. When $\tilde{E}^S$ is between E_v^{Hg} and $E_c^{Cd}(= 1.036eV)$, two of $\tilde{\delta}^E$ are pure imaginary. The other $\tilde{\delta}^S$s are real. Here we only show three of roots. The other root are minus times of the the roots showed here.

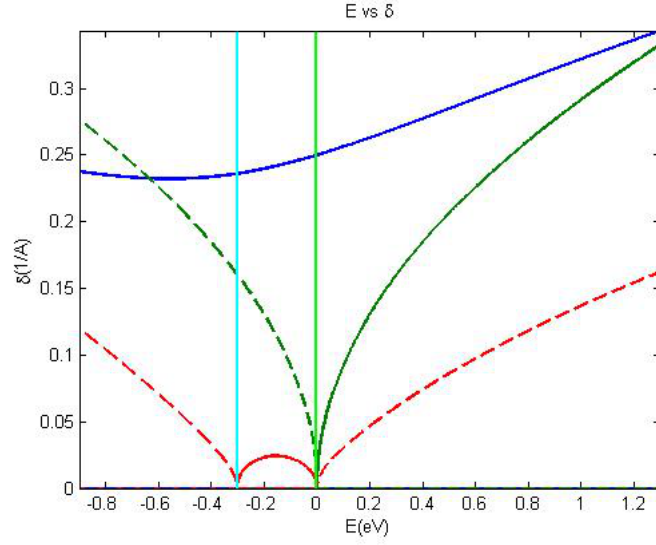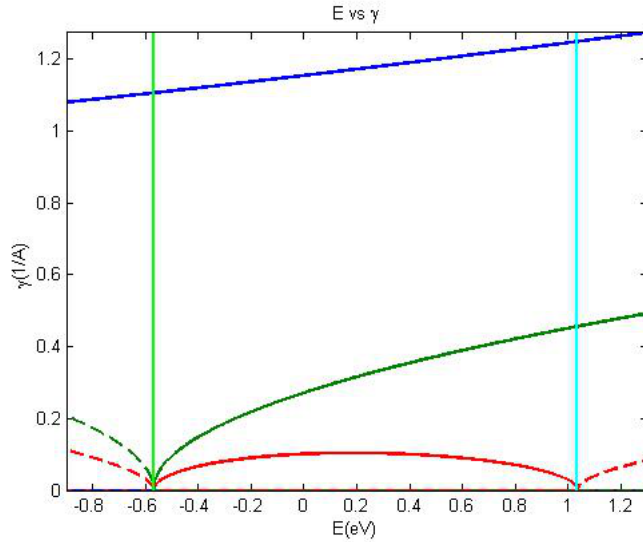Figure C.2: This picture show the solution of $\tilde{\gamma}^S$. The solid line is the real part. The dash line is the imaginary part. The left vertical line is $E_v^{Cd}(= -0.57eV)$. The right vertical line is $E_c^{Cd}(= 1.036eV)$. In the energy range $E_v^{Cd} < E_1^E < E_c^{Cd}$, all $\tilde{\gamma}^S$ are real. Here we only show three of roots. The other root are minus times of the roots showed here.

$\tilde{A}^i_3(z)$ are

$$\tilde{A}^i_1(z) = \begin{cases} \sum_{j=1}^{3} \tilde{p}^A_j e^{\tilde{\gamma}^A_j z} & z < -\frac{d}{2} \\ \sum_{j=1}^{2} \tilde{a}^A_j \sinh\left(\delta^A_j z\right) + \tilde{a}^A_3 \sin\left(\tilde{\delta}^A_3 z\right) & \text{for } -\frac{d}{2} < z < \frac{d}{2} \\ \sum_{j=1}^{3} -\tilde{p}^A_j e^{-\tilde{\gamma}^A_j z} & \frac{d}{2} < z \end{cases}.$$

$$\tilde{A}^i_2(z) = \begin{cases} \sum_{j=1}^{3} \tilde{p}^A_j \tilde{q}^A_j e^{\tilde{\gamma}^A_j z} & z < -\frac{d}{2} \\ \sum_{j=1}^{2} \tilde{a}^A_j \tilde{b}^A_j \cosh\left(\delta^A_j z\right) + \tilde{a}^A_3 \tilde{b}^A_3 \cos\left(\tilde{\delta}^A_3 z\right) & \text{for } -\frac{d}{2} < z < \frac{d}{2} \\ \sum_{j=1}^{3} \tilde{p}^A_j \tilde{q}^A_j e^{-\tilde{\gamma}^A_j z} & \frac{d}{2} < z \end{cases}.$$

$$\tilde{A}^i_3(z) = \begin{cases} \sum_{j=1}^{3} \tilde{p}^A_j \tilde{r}^A_j e^{\tilde{\gamma}^A_j z} & z < -\frac{d}{2} \\ \sum_{j=1}^{2} \tilde{a}^A_j \tilde{c}^A_j \sinh\left(\delta^A_j z\right) + \tilde{a}^A_3 \tilde{c}^A_3 \sin\left(\tilde{\delta}^A_3 z\right) & \text{for } -\frac{d}{2} < z < \frac{d}{2} \\ \sum_{j=1}^{3} -\tilde{p}^A_j \tilde{r}^A_j e^{-\tilde{\gamma}^A_j z} & \frac{d}{2} < z \end{cases}.$$

Where $\tilde{b}^A_j = -i\sqrt{\frac{3}{2}}\frac{\varepsilon^{Hg,c}_i - T^{Hg}_c\left(\tilde{\delta}^A_j\right)^2}{iP\tilde{\delta}^A_j}$, $\tilde{c}^A_j = \sqrt{\frac{3}{2}}\frac{\varepsilon^{Hg,v}_i \varepsilon^{Hg,c}_i + \left(\varepsilon^{Hg,c}_i T^{Hg}_L - \varepsilon^{Hg,v}_i T^{Hg}_c + \frac{2}{3}P^2\right)\left(\tilde{\delta}^A_j\right)^2 - T^{Hg}_c T^{Hg}_L\left(\tilde{\delta}^A_j\right)^4}{PC^{Hg}\left(\tilde{\delta}^A_j\right)^2}$,

$\tilde{b}^A_3 = i\sqrt{\frac{3}{2}}\frac{\varepsilon^{Hg,c}_i + T^{Hg}_c\left(\tilde{\delta}^A_3\right)^2}{P\tilde{\delta}^A_3}$, $\tilde{c}^A_3 = -\sqrt{\frac{3}{2}}\frac{\varepsilon^{Hg,v}_i \varepsilon^{Hg,c}_i - \left(\varepsilon^{Hg,c}_i T^{Hg}_L - \varepsilon^{Hg,v}_i T^{Hg}_c + \frac{2}{3}P^2\right)\left(\tilde{\delta}^A_3\right)^2 - T^{Hg}_c T^{Hg}_L\left(\tilde{\delta}^A_3\right)^4}{PC^{Hg}\left(\tilde{\delta}^A_3\right)^2}$,

$\tilde{q}^A_j = -i\sqrt{\frac{3}{2}}\frac{\varepsilon^{Cd,c}_i - T^{Cd}_c\left(\tilde{\gamma}^A_j\right)^2}{P\tilde{\gamma}^A_j}$ and $\tilde{r}^A_j = \sqrt{\frac{3}{2}}\frac{\varepsilon^{Cd,v}_i \varepsilon^{Cd,c}_i + \left(\varepsilon^{Cd,c}_i T^{Cd}_L - \varepsilon^{Cd,v}_i T^{Cd}_c + \frac{2}{3}P^2\right)\left(\tilde{\gamma}^A_j\right)^2 - T^{Cd}_c T^{Cd}_L\left(\tilde{\gamma}^A_j\right)^4}{PC^{Cd}\left(\tilde{\gamma}^A_j\right)^2}$.

$\tilde{\gamma}^A_j$, $\tilde{\delta}^A_1$ and $\tilde{\delta}^A_2$ are positive real and we let $\tilde{\delta}^A_3 = Im[\tilde{\delta}^A_3]$. From the continuity of wave function at boundary $z = -d/2$, we derive the set of equations:

$$\sum_{j=1}^{2} \tilde{a}^A_j \sinh\left(\frac{\tilde{\delta}^A_j d}{2}\right) + \tilde{a}^A_3 \sin\left(\frac{\tilde{\delta}^A_3 d}{2}\right) + \sum_{j=1}^{3} \tilde{p}^A_j \exp\left(-\frac{\tilde{\gamma}^A_j d}{2}\right) = 0. \tag{C.9a}$$

$$\sum_{j=1}^{2} \tilde{a}^A_j \tilde{b}^A_j \cosh\left(\frac{\tilde{\delta}^A_j d}{2}\right) + \tilde{a}^A_3 \tilde{b}^A_3 \cos\left(\frac{\tilde{\delta}^A_3 d}{2}\right) - \sum_{j=1}^{3} \tilde{p}^A_j \tilde{q}^A_j \exp\left(-\frac{\tilde{\gamma}^A_j d}{2}\right) = 0. \tag{C.9b}$$

$$\sum_{j=1}^{2} \tilde{a}^A_j \tilde{c}^A_j \sinh\left(\frac{\tilde{\delta}^A_j d}{2}\right) + \tilde{a}^A_3 \tilde{c}^A_3 \sin\left(\frac{\tilde{\delta}^A_3 d}{2}\right) + \sum_{j=1}^{3} \tilde{p}^A_j \tilde{r}^A_j \exp\left(-\frac{\tilde{\gamma}^A_j d}{2}\right) = 0. \tag{C.9c}$$

APPENDIX C. BASIS DEFINITION OF $\tilde{H}^{2D}_{10\times10}$

From Schrödinger equation at boundary $z = -d/2$, we derive the set of equations:

$$T_c^{Hg}\left[\sum_{j=1}^{2}\tilde{\delta}_j^A\tilde{a}_j^A\cosh\left(\frac{\tilde{\delta}_j^A d}{2}\right) + \tilde{\delta}_3^A\tilde{a}_3^A\cos\left(\frac{\tilde{\delta}_3^A d}{2}\right)\right] - \sum_{j=1}^{3}T_c^{Cd}\tilde{\gamma}_j^A\tilde{p}_j^A\exp\left(-\frac{\tilde{\gamma}_j^A d}{2}\right) = 0.$$

$$\text{(C.10a)}$$

$$T_L^{Hg}\left[\sum_{j=1}^{2}\tilde{\delta}_j^A\tilde{a}_j^A\tilde{b}_j^A\sinh\left(\frac{\tilde{\delta}_j^A d}{2}\right) - \tilde{\delta}_3^A\tilde{a}_3^A\tilde{b}_j^A\sin\left(\frac{\tilde{\delta}_3^A d}{2}\right)\right] + \sum_{j=1}^{3}T_L^{Cd}\tilde{\gamma}_j^A\tilde{p}_j^A\tilde{q}_j^A\exp\left(-\frac{\tilde{\gamma}_j^A d}{2}\right)$$

$$= -\frac{i}{2}\left[C^{Hg}\left[\sum_{j=1}^{2}\tilde{a}_j^A\tilde{c}_j^A\sinh\left(\frac{\tilde{\delta}_j^A d}{2}\right) + \tilde{a}_3^A\tilde{c}_3^A\sin\left(\frac{\tilde{\delta}_3^A d}{2}\right)\right] + \sum_{j=1}^{3}C^{Cd}\tilde{p}_j^A\tilde{r}_j^A\exp\left(-\frac{\tilde{\gamma}_j^A d}{2}\right)\right].$$

$$\text{(C.10b)}$$

$$T_H^{Hg}\left[\sum_{j=1}^{2}\tilde{\delta}_j^A\tilde{a}_j^A\tilde{c}_j^A\cosh\left(\frac{\tilde{\delta}_j^A d}{2}\right) + \tilde{\delta}_3^A\tilde{a}_3^A\tilde{c}_3^A\cos\left(\frac{\tilde{\delta}_3^A d}{2}\right)\right] - \sum_{j=1}^{3}T_{Hg}^{Cd}\tilde{\gamma}_j^A\tilde{p}_j^A\tilde{r}_j^A\exp\left(-\frac{\tilde{\gamma}_j^A d}{2}\right)$$

$$= -\frac{i}{2}\left[C^{Hg}\left[\sum_{j=1}^{2}\tilde{a}_j^A\tilde{b}_j^A\cosh\left(\frac{\tilde{\delta}_j^A d}{2}\right) + \tilde{a}_3^A\tilde{b}_j^A\cos\left(\frac{\tilde{\delta}_3^A d}{2}\right)\right] - \sum_{j=1}^{3}C^{Cd}\tilde{p}_j^A\tilde{q}_j^A\exp\left(-\frac{\tilde{\gamma}_j^A d}{2}\right)\right].$$

$$\text{(C.10c)}$$

Those two sets of equation above determine the eigenenergy.

Appendix D

The time reversal operator for H_{eff}

The time reversal operator Θ is of the form:

$$\Theta = U_\Theta K. \tag{D.1}$$

K is the conjagate operator and U_Θ is the unitary transformation. The definition of U_Θ is

$$[U_\Theta]_{ij} = \langle i | \Theta | j \rangle . \tag{D.2}$$

Where $|i\rangle$ is the ith basis vector. The time reversal relation of the angular momentum state $|j, m\rangle$ is

$$\Theta |j, m\rangle = e^{i\pi[j-m]} |j, -m\rangle . \tag{D.3}$$

From the definition of basis vectors, we have

$$|H1, \pm\rangle = \mp H_1 (z) |\Gamma 8, \pm 3/2\rangle . \tag{D.4}$$

$$|E1, \pm\rangle = E_1 (z) |\Gamma 6, \pm 1/2\rangle + E_2 (z) |\Gamma 8, \pm 1/2\rangle . \tag{D.5}$$

The quantum number j of $\Gamma 6$ subbands is $1/2$, and the quantum number j of $\Gamma 8$ subbands is $3/2$. $E_2(z)$ is pure imaginary and $H_1(z)$ and $E_1(z)$ are real. According to the property

of the basis vector, the time reversal relation of $E1$ and $H1$ subbands is

$$\Theta\left|H1,\pm\right\rangle = \mp\left|H1,\mp\right\rangle. \tag{D.6}$$

$$\Theta\left|E,\pm\right\rangle = \pm\left|E,\mp\right\rangle. \tag{D.7}$$

In the set of basis vector $(\left|E1,+\right\rangle, \left|H1,+\right\rangle, \left|E1,-\right\rangle, \left|H1,-\right\rangle)$, the time reversal operator Θ is of the form:
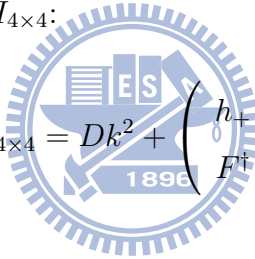
$$\Theta = \begin{pmatrix} 0 & -\sigma_z \\ \sigma_z & 0 \end{pmatrix} K. \tag{D.8}$$

Appendix E

The eigenvalue and eigenvector of the special 4×4 Hamiltonian

Consider a 4×4 Hamiltonian $H_{4 \times 4}$:

$$H_{4 \times 4} = Dk^2 + \begin{pmatrix} h_+ & F \\ F^\dagger & h_- \end{pmatrix}.$$ (E.1)

Where h_τ and F are

$$h_\tau = \begin{pmatrix} -M + Bk^2 & Ak_\tau \\ Ak_{-\tau} & M - Bk^2 \end{pmatrix}.$$

$$F = \begin{pmatrix} ak_+ & \delta + bk^2 \\ \delta + bk^2 & a'k_- \end{pmatrix}.$$

The relation between h_+ and h_- is

$$h_- = V_\mu h_+ V_\mu^\dagger.$$ (E.2)

Where $V_\mu = \mu e^{-i\sigma_z \phi}$, the k is the amplitude of the k vector and the ϕ is the polar angle of the k vector. Let the eigenvector φ of this form:

$$\varphi^\dagger = \begin{pmatrix} \tilde{\varphi}^\dagger & \tilde{\varphi}^\dagger V_\mu^\dagger \end{pmatrix}.$$ (E.3)

APPENDIX E. THE EIGENVALUE AND EIGENVECTOR OF THE SPECIAL 4×4 HAMILTONIAN

The Schödinger equation becomes a set of equations:

$$\left(Dk^2 + h_+\right)\tilde{\varphi} + FV_\mu\tilde{\varphi} = E\tilde{\varphi}. \tag{E.4a}$$

$$\left(Dk^2 + V_\mu h_+ V_\mu^\dagger\right)V_\mu\tilde{\varphi} + F^\dagger\tilde{\varphi} = EV_\mu\tilde{\varphi}. \tag{E.4b}$$

Because FV_μ is hermitian, the equations (E.4a) and (E.4b) are the same.

$$FV_\mu = \mu \begin{pmatrix} ak & (\delta + bk^2)e^{i\phi} \\ (\delta + B'k^2)e^{-i\phi} & a'k \end{pmatrix}. \tag{E.5}$$

Therefore, we can derive the eigenenergy of $H_{4\times4}$ by the 2×2 Hamiltonian $H_{2\times2}^\mu$.

$$H_{2\times2}^\mu = Dk^2 + \begin{pmatrix} -M + Bk^2 + \mu ak & \left(Ak + \mu\left[\delta + bk^2\right]\right)e^{i\phi} \\ \left(Ak + \mu\left[\delta + bk^2\right]\right)e^{-i\phi} & M - Bk^2 + \mu a'k \end{pmatrix}. \tag{E.6}$$

The eigenenergy is

$$E_{\rho\mu} = Dk^2 + \mu a_+ k + \rho\sqrt{\left(M - Bk^2 + \mu a_- k\right)^2 + \left(Ak + \mu\left[\delta + bk^2\right]\right)^2}. \tag{E.7}$$

Where $a_\nu = (a + \nu a')/2$. We have the form of $\tilde{\varphi}$ so we also have the form of φ.

$$\varphi_{\rho\mu} = \frac{N_{\rho\mu}}{\sqrt{2}} \begin{pmatrix} \left[Ak + \mu\left(\delta + bk^2\right)\right]e^{i\phi} \\ \left[E_{\rho\mu} - Dk^2 + M - Bk^2 - \mu a'k\right] \\ \mu\left[Ak + \mu\left(\delta + bk^2\right)\right] \\ \mu\left[E_{\rho\mu} - Dk^2 + M - Bk^2 - \mu a'k\right]e^{i\phi} \end{pmatrix}. \tag{E.8}$$

Appendix F

Basis definition of H_W.

Substituting $-i\partial_y$ for k_y, H_0 is of the form:

$$H_0(W) = \begin{pmatrix} h_+(0, -\partial_y; W) & 0 \\ 0 & h_-(0, -\partial_y; W) \end{pmatrix}. \tag{F.1}$$

Where

$$h_\tau(0, -i\partial_y; W) = \begin{pmatrix} -M - [B+D]\,{\partial_y}^2 & \tau A\partial_y \\ -\tau A\partial_y & M + [B-D]\,{\partial_y}^2 \end{pmatrix}. \tag{F.2}$$

We have $h_- = \sigma_z h_+ \sigma_z$ so we can obtain the form of the eigenstates.

$$\langle S;\ i, +|\ y\rangle = \begin{pmatrix} S_1^i(y) & S_2^i(y) & 0 & 0 \end{pmatrix}.$$

$$\langle A;\ i, +|\ y\rangle = \begin{pmatrix} A_1^i(y) & A_2^i(y) & 0 & 0 \end{pmatrix}.$$

$$\langle S;\ i, -|\ y\rangle = \begin{pmatrix} 0 & 0 & S_1^i(y) & -S_2^i(y) \end{pmatrix}.$$

$$\langle A;\ i, +|\ y\rangle = \begin{pmatrix} 0 & 0 & A_1^i(y) & -A_2^i(y) \end{pmatrix}.$$

Where $S_1^i(y)$ and $S_2^i(y)$ are the elements of $|Si, +\rangle$. $A_1^i(y)$ and $A_2^i(y)$ are the elements of $|Ai, +\rangle$. H_0 is real so $S_1^i(y)$, $S_2^i(y)$, $A_1^i(y)$ and $A_2^i(y)$ are all real.

The Schrödinger equation of S subbands is the set of equation:

$$-\left(M + [B+D]\,\partial_y^2\right) S_1^i(y) + A\partial_y S_2^i(y) = E_i^S S_1^i(y). \tag{F.3a}$$

$$\left(M + [B-D]\,\partial_y^2\right) S_2^i(y) - A\partial_y S_1^i(y) = E_i^S S_2^i(y). \tag{F.3b}$$

APPENDIX F. BASIS DEFINITION OF H_W.

Where E_i^S is the eigenenergy. We let $e^{\lambda y}$ be the solution of $S_1^i(y)$ and $S_2^i(y)$. From equation (F.3), we derive the form of λ:

$$\lambda_\nu^2 = \frac{\alpha + \nu\beta}{B^2 - D^2}. \tag{F.4}$$

Where $\alpha = -MB + E_i^S D + \frac{A^2}{2}$ and $\beta = \sqrt{\alpha^2 + ([E_i^S]^2 - M^2)(B^2 - D^2)}$. The value of A^2 is larger than $2M(B - D)$ and MB is positive in our parameter and ref[1]. Therefore when $|E_i^S| < M$, we can find that all λs are real and the eigenstate in this energy range is edge like state. In the other hand, when $|E_i^S| > M$, we can find that two λs are pure imaginary and the eigenstate in this energy range is bulk like state.

$S_1^i(y)$ is even and $S_2^i(y)$ is odd. For edge like state, $S_1^i(y)$ and $S_2^i(y)$ are of the forms:

$$S_1^i(y) = P_+ \frac{\cosh[\lambda_+ y]}{\cosh[\lambda_+ w]} + P_- \frac{\cosh[\lambda_- y]}{\cosh[\lambda_- w]}. \tag{F.5a}$$

$$S_2^i(y) = P_+ Q_+ \frac{\sinh[\lambda_+ y]}{\sinh[\lambda_+ w]} + P_- Q_- \frac{\sinh[\lambda_- y]}{\sinh[\lambda_- w]}. \tag{F.5b}$$

Where $w = W/2$. Taking this form into equation(F.3b), we obtain $Q_+ = \frac{1}{A\lambda_+}\left(M + E_i^S - \frac{\alpha - \beta}{B - D}\right)\tanh[\lambda_+ w]$ and $Q_- = \frac{1}{A\lambda_-}\left(M + E_i^S - \frac{\alpha + \beta}{B - D}\right)\tanh[\lambda_- w]$. Because the value of A is very large, the value of λ is too large to numerically calculate the eigenenergy with the normal form of wave function. We set the wave function in this way[4] to avoid the numerally overflow near the edges. The wave function is zero at the edge. Therefore the equation that determines the eigenenergy is of the form:

$$Q_- = Q_+. \tag{F.6}$$

For bulk like state, $S_1^i(y)$ and $S_2^i(y)$ are of the forms:

$$S_1^i(y) = P_+ \frac{\cosh[\lambda_+ y]}{\cosh[\lambda_+ w]} + P_- \cos[\lambda_- y]. \tag{F.7a}$$

$$S_2^i(y) = P_+ Q_+ \frac{\sinh[\lambda_+ y]}{\sinh[\lambda_+ w]} + P_- Q_- \sin[\lambda_- y]. \tag{F.7b}$$

Where $\lambda_- = Im[\lambda_-]$, $Q_+ = \frac{1}{A\lambda_+}\left(M + E_i^S - \frac{\alpha - \beta}{B - D}\right)\tanh[\lambda_+ w]$ and $Q_- = \frac{1}{A\lambda_-}\left(M + E_i^S - \frac{\alpha + \beta}{B - D}\right)$. For the similar reason of edge like state, the wave function

of λ_+ part must be this form. The wave function is zero at the edge. Therefore the equation that determines the eigenenergy is of the form:

$$Q_- \sin\left[\lambda_- w\right] = Q_+ \cos\left[\lambda_- w\right]. \tag{F.8}$$

By the similar way, we can also obtain the eigenenergy of A subbands. The Schrödinger equation of A subbands is the set of equation:

$$-\left(M + [B + D]\,\partial_y^2\right) A_1^i(y) + A\partial_y A_2^i(y) = E_i^A A_1^i(y). \tag{F.9a}$$

$$\left(M + [B - D]\,\partial_y^2\right) A_2^i(y) - A\partial_y A_1^i(y) = E_i^A A_2^i(y). \tag{F.9b}$$

Where E_i^A is the eigenenergy. $A_1^i(y)$ is odd and $A_2^i(y)$ is even. For the edge like A state, $A_1^i(y)$ and $A_2^i(y)$ are of the form:

$$A_1^i(y) = P_+ Q_+ \frac{\sinh\left[\lambda_+ y\right]}{\sinh\left[\lambda_+ w\right]} + P_- Q_- \frac{\sinh\left[\lambda_- y\right]}{\sinh\left[\lambda_- w\right]}. \tag{F.10a}$$

$$A_2^i(y) = P_+ \frac{\cosh\left[\lambda_+ y\right]}{\cosh\left[\lambda_+ w\right]} + P_- \frac{\cosh\left[\lambda_- y\right]}{\cosh\left[\lambda_- w\right]}. \tag{F.10b}$$

Taking this form into equation(F.9a), we obtain $Q_+ = \frac{1}{A\lambda_+}\left(M - E_i^A - \frac{\alpha-\beta}{B+D}\right)\tanh\left[\lambda_+ w\right]$ and $Q_- = \frac{1}{A\lambda_-}\left(M - E_i^A - \frac{\alpha+\beta}{B+D}\right)\tanh\left[\lambda_- w\right]$. The eigenenergy is determined by the equation.

$$Q_- = Q_+. \tag{F.11}$$

For bulk like state, $A_1^i(y)$ and $A_2^i(y)$ are of the forms:

$$A_1^i(y) = P_+ Q_+ \frac{\sinh\left[\lambda_+ y\right]}{\sinh\left[\lambda_+ w\right]} + P_- Q_- \sin\left[\lambda_- y\right]. \tag{F.12a}$$

$$A_2^i(y) = P_+ \frac{\cosh\left[\lambda_+ y\right]}{\cosh\left[\lambda_+ w\right]} + P_- \cos\left[\lambda_- y\right]. \tag{F.12b}$$

Where $\lambda_- = Im[\lambda_-]$, $Q_+ = \frac{1}{A\lambda_+}\left(M - E_i^A - \frac{\alpha-\beta}{B+D}\right)\tanh\left[\lambda_+ w\right]$ and $Q_- = \frac{1}{A\lambda_-}\left(M - E_i^A - \frac{\alpha+\beta}{B+D}\right)$. The eigenenergy is determined by the equation.

$$Q_- \sin\left[\lambda_- w\right] = Q_+ \cos\left[\lambda_- w\right]. \tag{F.13}$$

Appendix G

The analytical form of $\tilde{\gamma}_{MS}$

Consider a $N \times N$ matrix γ. Let vector $|i'\rangle$ is eigenvector of γ with eigenvalue g_i.

$$\gamma |i'\rangle = g_i |i'\rangle . \tag{G.1}$$

The set of vector $(|i'\rangle)$ contains N elements and it is linear independent.

The matrix γ is non-hermitian so the vectors $|i'\rangle$ are not orthonormal. We need an orthonormal set of vector so we define a orthonormal set of vector $(|\tilde{i}\rangle)$.

$$\left|\tilde{1}\right\rangle = |1'\rangle \qquad \qquad \text{for m} = 1. \tag{G.2a}$$

$$|\tilde{m}\rangle = N_m \left(|m'\rangle - \sum_{n=1}^{m-1} |\tilde{n}\rangle \langle \tilde{n} | m' \rangle \right) \text{ for m} > 1. \tag{G.2b}$$

The set of vector $(|i'\rangle)$ is linear independent so the subset of vector $(|j'\rangle; j \leq n')$ is linear independent and expands a n' dimension vector space V'. According to the definition of vector $|\tilde{i}\rangle$, we have

$$
\begin{aligned}
\left|\tilde{i}\right\rangle &= \tilde{N}_i |i'\rangle - \tilde{N}_i \sum_{j=1}^{i-1} C_{ij} \left|\tilde{j}\right\rangle \\
&= \tilde{N}_i |i'\rangle - \tilde{N}_i \sum_{j=1}^{i-1} C_{ij} \tilde{N}_j |j'\rangle + \tilde{N}_i \sum_{j=1}^{i-1} C_{ij} \tilde{N}_j \sum_{k=1}^{j-1} C_{jk} \left|\tilde{k}\right\rangle \\
&= \sum_{k=1}^{i} \tilde{C}_{ki} |k'\rangle.
\end{aligned}
\tag{G.3}
$$

The subset of vector $\left(\left|\tilde{j}\right\rangle ; j \leq n'\right)$ is linear independent and expands a n' dimension vector space $\tilde{V}$. From the equation (G.3), the vector space $\tilde{V}$ is equal to the vector space V'.

For $i > n'$, the vector $\left|\tilde{i}\right\rangle$ is orthogonal to the all elements of the subset of vector $\left(\left|\tilde{j}\right\rangle ; j \leq n'\right)$. So it is also orthogonal to the all elements of the subset of vector $(\left|j'\right\rangle ; j \leq n')$. The matrix γ doesn't change vector $\left|i'\right\rangle$. The vector $\gamma \left|\tilde{i}\right\rangle$ is of the form.

$$\gamma \left|\tilde{i}\right\rangle = \sum_{k=1}^{i} g_k \tilde{C}_{ki} \left|k'\right\rangle. \tag{G.4}$$

Therefore the matrix element $\left\langle\tilde{j}\right| \gamma \left|\tilde{i}\right\rangle$ is zero when $j > i$.
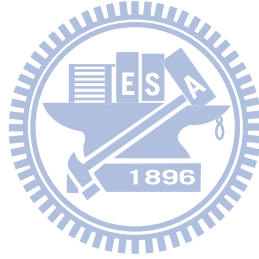
Bibliography

[1] B. Andrei Bernevig, Taylor L. Hughes, Shou-Cheng Zhang, Science **314**, 1757 (2006).

[2] Markus König, Steffen Wiedmann, Christoph Brüne, Andreas Roth, Hartmut Buhmann, Laurens W. Molenkamp, Xiao-Liang Qi, Shou-Cheng Zhang, Science **318**, 766 (2007)

[3] Hasan, M.Z. and C.L. Kane (2010). "Colloquium: Topological insulators," Reviews of Modern Physics. vol. 82, pp. 3045-3067.

[4] Bin Zhou, Hai-Zhou Lu, Rui-Lin Chu, Shun-Qing Shen and Qian Niu, Phys. Rev. Lett **101**, 246807 (2008).

[5] L. B. Zhang, Feng Zhai, and Kai Chang, Phys. Rev B **81**, 235323 (2010).

[6] Roland Winkler: *Spin-Orbital Coupling Effects in Two-Demensional Electron and Hole systems* (Springer, Berlin, Heidelberg, 2003).

[7] Markus König, Hartmut Buhmann, Laurens W. Molenkamp, Taylor Hughes, Chao-Xing Liu, Xiao-Liang Qi, and Shou-Cheng Zhang , J. Phys. Soc. Jpn. **77**, 031007 (2008).

[8] R. Winkler, L.Y. Wang, Y.H. Lin, C.S. Chu, Solid State Communications **152** 2096 (2012).

[9] Y. Takagaki, Phys. Rev B **85**, 155308 (2012).

[10] Y. Takagaki, J. Phys. Condens. Matter 24 (2012) 435301

[11] Viktor Krueckl and Klaus Richter, Phys. Rev. Lett **107**, 086803 (2011).

[12] E. G. Novik, A. Pfeuffer-Jeschke, T. Jungwirth, V. Latussek, C. R. Becker, G. Landwehr, H. Buhmann, and L. W. Molenkamp, Phys. Rev B **72**, 035321 (2005).

[13] M. Cardona, N. E. Christensen, and G. Fasol, Phys. Rev. B **38**, 1806 (1988).

[14] Wen Yu Shan, Hai Zhou Lu and Shun Qing Shen, New Journal of Physics 12 (2010) 043048.

[15] Xiao-Liang Qi, Taylor L. Hughes, Shou-Cheng Zhang, Phys. Rev B **78**, 195424 (2008).

[16] Emil Prodan, Phys. Rev B **80**, 125327 (2009).

[17] Huichao Li, L. Sheng, D.N. Sheng, and D.Y. Xing, Phys. Rev B **82**, 165104 (2010).

[18] J.J. Sakurai: *Advanced Quantum Mechanics* (Addison-Wesley, Reading, MA, 1967).

[19] Shuichi Murakami, arXiv1006.1188v3.